X-921-77-63
PREPRINT

TMX - 71337

THE SPECTRUM OF THE GEOID FROM ALTIMETER DATA

C. A. WAGNER

APRIL 1977

GSFC — GODDARD SPACE FLIGHT CENTER
GREENBELT, MARYLAND

X-921-77-63
Preprint

THE SPECTRUM OF THE GEOID FROM ALTIMETER DATA

C. A. Wagner

April 1977

GODDARD SPACE FLIGHT CENTER
Greenbelt, Maryland

CONTENTS

LIST OF ILLUSTRATIONS

LIST OF ILLUSTRATIONS (Continued)

LIST OF TABLES

APPENDICES

LIST OF ILLUSTRATIONS (Continued)

THE SPECTRUM OF THE GEOID FROM ALTIMETER DATA

C. A. Wagner
Geodynamics Branch, Goddard Space
Flight Center, Greenbelt, Md. 20771

ABSTRACT

A variety of sources of detailed information has been analyzed to arrive at a geoid power spectrum from global altimeter data. Using the equivalent of only two revolutions of data (mostly from GEOS-3) from all the major oceans, the high frequency geoid power (rms) is estimated (most simply) to be

$$80.7n^{-1.47} \text{ meters},$$

where n is in cycles/global revolutions. This law is valid for all frequencies above 19 cycles but includes sea state. The (simple) law has more power than predicted by Kaula's rule for the geopotential. However, the data shows significantly less power for frequencies below 100 cycles. A closer approximation to the altimetry accumulates 2.18m (rss) for all frequencies higher than 19 cycles/rev. (including sea state), somewhat less power than predicted by the rule. The data permits up to 1 1/4 (rms) non-gravitational departures from the high frequency marine geoid.

THE SPECTRUM OF THE GEOID FROM ALTIMETER DATA

INTRODUCTION

The earth and ocean dynamics application program of the National Aeronautics and Space Administration has as its ultimate goal, knowing ocean topography at the 10 cm level (with 50 km horizontal scale). With this understanding ocean currents can be detected and calculated as departures from the mean sea surface. The shape of this mean surface is due mainly to the Earth's gravity field (the geoid) but includes contributions on a very large scale (>1000 km) from luni-solar and atmospheric tides as well as any stable ocean current and wind systems. On a smaller scale there may also be stable non gravitational surface features which will be difficult to distinguish from the gravity field. But these small scale features may vary in time (meander) and be detectable by repetitive satellite altimetry. In any case the major contribution of the geoid to high frequency sea surface undulations (scale < 1000 km) should be known in order to judge the importance of small scale departures and their possibility of measurement.

With the advent of the satellite altimeter it is now possible to measure the spectrum of the ocean's surface to very high frequency and begin to assess these

departures from the global marine geoid. Unfortunately while the spectral analysis of the sea surface from altimetry has been relatively straightforward, the interpretation of that spectrum as the reflection of a marine geoid has been ambiguous. I have chosen to work out the interpretation in terms of the spherical harmonics of the geopotential for which much information is known. But without special restrictions, an infinite series of these will diverge on a surface interior to the sphere on which the harmonics are defined. However, it is already known that the spherical harmonics of gravity (defined on the bounding sphere) must decline at least as fast as ℓ^{-2} [Jeffreys, 1959; Cholshevnikof, 1965]. (Here ℓ is the harmonic degree.) This restriction follows from the mass integral representation of spherical harmonics and the (reasonable) existence of maximum bounds on density contrasts within the earth. Indeed, Morrison (1971), proposed (from intuition) that the harmonics decline as a^{ℓ} ($a < 1$) without specific justification.

Results from satellite tracking over the past decade have confirmed the earlier gravimetric results that $\sigma_{\ell_m} \doteq [b\ell^{-c}]^2$. ($\sigma^2_{\ell_m}$ is the variance of a fully normalized geopotential harmonic of degree ℓ and order m.) The constants are $b \sim 10^{-5}$ and $c \sim 2$ consistent with the theoretical expectation. The satellite results are global but extend only to about degree 20 [e.g. Gaposchkin, 1974]. The gravimetric statistics are far from global but are sensitive to degree 180 [e.g. Kaula, 1959]. The gravimetric data, however, have not been corrected for the depression of the geoid below the bounding sphere. Thus the

comparison with spherical harmonics must be severly distorted at degrees above 100. Of course the effects of 100 degree terms are small (~1mgal of anomalous gravity) and only a 30% change in these small anomalies of degree 100 would be expected from pole to equator. This change would be difficult to detect from the current distribution and quality of surface gravimetry. Nevertheless Morrison's suggestion seems essential to the interpretation (with bounding spherical harmonics) of all data on the geoid. Without an exponential decline attached to the conventional power law for bounding spherical harmonics, infinite gravity anomalies and geoid undulations would result on the earth's surface. At any rate I have interpreted the high frequency geoid data two ways:

1. Conventionally, as though the geoid were referenced to the sphere and
2. Differently, continuing the geopotential on the bounding sphere down to the ellipsoid.

It turns out that with either approach the data analysed here is probably dominated by non gravitational geoid departures below a scale of about 600 km (60 cycles/global revolution). Before the data was analysed I had hoped it would have been able to discriminate between the two approaches and extend the known degree variances of the gravity field to very small wavelengths. But the unexpectedly large departure power has precluded this.

It should be emphasized that what I am after in this study is a global geoid power law. Thus the departures found here may be a reflection of the limited

altimeter data analyzed. While all the major oceans have been covered, there is no more than a few passes in each. Strong ocean dynamics or rough gravitational features may have been emphasized. Nevertheless even this preliminary look at the sea's surface from satellite altimetry has profound implication for oceanography.

DATA ANALYSED

Eleven arcs of altimetry from Skylab and Geos 3 have been examined (Figure 1). They are all more than 10 minutes (4500 km) long. For Skylab, the 83-minute 'round the-world' pass of 31 January 1974 was used (McGoogan, Leiteo and Wells, 1975). However, since it was broken by 20 one minute operation pauses and a long pass over the United States, only 50 minutes of it represents actual sea-surface altimeter data. I have linearly interpolated for the data in the gaps. While this probably resoluts in excessive smoothness for the results, the major gap over the U. S. is known to have small geoidal undulations from gravimetry (Marsh & Vincent, 1974).

The Geos 3 altimetry (William Wells, private communications, 1976), as well as that for Skylab, was in the form of strip charts of sea surface height calculated from the high speed (>10 records/sec) data (e.g. Figure 2). Here the sea surface height was calculated from the orbit as the difference of the satellite's height above the ellipsoid and the measured altimeter height. Thus sea surface dynamics (e.g. tides & currents) as well as possible very long wave length orbit errors remain in this 'measurement'.

At the outset, I did not expect ocean dynamics to distort severly the gravity signal I sought from the altimetry. At low frequencies (< 20 cycles/global rev.) the altimeter spectrum should be dominated by the geopotential (the geoid) and orbit errors. At intermediate frequencies (20 to 600 cycles/rev.; 150 to 5 second wavelengths of altimetry record) the geoid should still dominate with an unknown (but probably small) amount of ocean dynamics. At greater frequencies, the noise of the instrument should begin to dominate.

Figure 2 shows a typical 20 second record of high speed (measured sea surface height) data from GEOS 3 over the North Atlantic. This record is from the 'global' (low intensity) mode of altimeter operation which averages the (weak) return pulse over a 'footprint' on the ocean of 8 km (~1 second). It is noted that a strong sinusoidal oscillation (~1 m rms) of about this period indeed exists in this data. It is probably due to the correlation of noisy return pulses overlapping (in successive records) from the same points on the ocean.

In this analysis I have (hand) drawn a smooth line through the mean of these 'highest' frequency oscillations. I have also tried to avoid (in the 'mean' line) too rapid fluctuation (> 5 m) over a 5 second interval which is probably due to sea state effects on the return signal. The result (sampled every 10 seconds for Skylab, 5 seconds for the 'noisiest' GEOS 3 arcs and 2-1/2 seconds for the quietest) is a smoothed sea surface height record to the nearest 0.5 m (1m for Skylab). The dominating noise in the 'smoothed' record is this strip chart

reading error. Extensive harmonic analysis has shown this residual error to be actually as low as 0.12 m (rms), about the same as in analysis of major frame average (2-3 second) data processed entirely by machine [see Harmonic Analysis of Altimeter Residuals; this report]. Brown, Masters & Kahn (personal communications, 1976) report similar residual noise figures for machine processed high speed data. There is also a good expectation for this low level of 'read error' (see Appendix C).

The smoothed altimeter derived sea surface heights were then compared to the GEM 7 geoid [Wagner, 1976], removing the effects of very low frequency orbit errors (mainly) at the same time. Residuals from that comparison, for the 11 altimeter arcs, are shown in Figure 3: the statistics are summarized in Table 1. Also analysed, for high frequency geopotential behaviour, was a profile along the 270° meridian of the Marsh and Vincent detailed gravimetric geoid (personal communication, 1975). This arc (also in Figure 3 & Table 1) was chosen to verify the method for the altimeter data inasmuch as the 1° × 1° gravimeter data (which this geoid reflects) is compatible with geopotential variances which are somewhat smaller than $(10^{-5}/\ell^2)^2$ at all degrees (ℓ) [see, e.g. Rapp (1972)]. This gravimetric arc is felt to be the longest (> 60°) most representative of the surface data. (The Marsh-Vincent geoid actually uses data from a much smoother (30, 30) satellite-surface geopotential to interpolate where no 1° × 1° gravimetric measurements are available.)

The Gem 7 residuals (in Figure 2) for the altimetry arcs show significant fluctuations across the mid ocean ridges, trenches and near island rises. Generally the ridges, plateaus and rises show positive residuals and the trenches and deep plains negative, being geoidal reflections of the obvious mass excess or deficit directly beneath the sea surface. But there are some notable exceptions: the Cocos Ridge off Central America (Figure 3a) shows as a negative geoid anomally perhaps because it is in an active zone carrying light material up from the mantle. On the other hand the Mid Atlantic Ridge off Iceland (Figure 3a) shows as a positive anomaly.

The overall comparisons of the altimetry with low frequency geopotential models are also revealing (Table 1). Gem 7 [Wagner, et. al., 1977] is a 400 coefficient satellite model complete to (16, 16) in spherical harmonics. Gem 8 (with 650 coefficients) combines the satellite data in Gem 7 with worldwide $5° \times 5°$ surface gravimetry strongly weighted in continental areas. It is complete to (25, 25). Surprisingly, the overall fit to altimetry is poorer with Gem 8 than with Gem 7. On the other hand, when the truncation effect (above 25th degree) is accounted for in the 5° data (downweighting the best continental anomalies) a solution far more favorable to ocean altimetry is achieved. This is the Gem 8N solution in Table 1.

Summarizing the residual statistics for Gem 7, the rms residual for the 12 long arcs here is 3.2m. 2.3m of this is estimated to be due to commission error in the Gem 7 coefficients, taken from the error geoid map in Wagner, 1976.

The omission error (for geopotential terms of degree > 20 and geoid departures) must therefore be about $(3.2^2 - 2.3^2)^{1/2} = 2.2$ m (rms). This is in excellent agreement with the harmonic analysis of these residuals (see 'Power Law Estimates', also Table 1: this report).

Recall that Chovitz (1973) showed that $64/\ell$ estimates the worldwide Geoid power (in meters) of all geopotential terms higher than degree ℓ. This fraction is based on Kaula's (1966) rule for geopotential decline ($\sigma_{\ell_m} = \pm 10^{-5}/\ell^2$). Thus the 2.2 m omission error figure appears to imply a decline considerably faster than Kaula's Rule. However the 2.2 m residual is not for a global arc but one which averages about 1/6 revolution. The power in these short arcs is expected to be less than in the global arc because some long wave power is absorbed in the bias & tilt terms used to adjust the data for 'orbit error'. The estimation. of those effects is made in Appendix B. I will return to these overall statistics in the section on 'Power Law Estimates'.

The residuals in Figure 3 were then subjected to an harmonic analysis in order to estimate the global power spectrum for altimeter data.

TECHNIQUE OF HARMONIC ANALYSIS

It might be supposed that the simple power spectrum of each sub orbital arc of geoid heights is a good estimate of the global spectrum with the frequencies scaled up by (N) the number of arc lengths in one revolution. A little thought will show that the power has to be scaled down for a proper global estimate.

Clearly, in the sub orbital arc (of a function nearly periodic in one revolution) the harmonic analysis will involve only 1/N of the global harmonics. But if the total power in the sub arc is to be a good estimate of the total global power, then the power in each sub arc frequency must absorb roughly N times the global power at the equivalent global frequency. In this paper I define power as the root mean square amplitude of an harmonic. Thus as a rule the global power (rms) at a given frequency is $\sqrt{N}$ times the power in the 1/N-th sub arc at the equivalent frequency.

In Appendix C I have analysed the estimation problem for pieces of periodic data. Both the theoretical expectation and the results of analysis of simulated data confirm the rule. In the simulations however the edge effects in the short arcs were controlled by analysing only the deviations of the data from a line fitting the end points. This creates a pseudo periodic (residual) data set with remarkable ability to estimate the power in the global arc on average. [It is analogous to using a tapered window function for computing the Fouier transform of segments of time series].

The simulations (in Appendix C) also included more realistic cases of short altimeter arcs from random geopotential fields to (100, 100). These arcs (on a rotating earth) were analysed in the same way as those from samples of strictly periodic (1 revolution) geoid profiles. [Some periodic profiles were altimeter samples on a non rotating earth (great circles). Others were of artificial functions]. The more realistic cases showed greater variance from the expected

altimeter power due to the given geopotential. But the power averages for the sub arcs were again remarkably close to the global expectation. Greater variance still was encountered when pseudo random noise was added to the observations.

The major lesson learned from the simulations was that considerable averaging of the power (in the short arcs) over many frequencies is necessary to reduce the power fluctuations caused by both limited geopotential sampling and 'altimeter noise'. Limited geopotential sampling causes wide variances from expectations at low frequencies (< 60 cycles/rev.). Altimeter noise at the GEOS 3 level of about 1/4 meter (after 2-5 second smoothing) causes difficulties in estimating geoid frequencies higher than about 250 cycles/rev.

These difficulties were compounded by even wider variability when the actual data was examined. Nevertheless the methods of averaging and noise estimation developed from the simulations gave reasonably smooth average power spectra for the individual arcs of the altimeter geoid. The averages showed evidence of geoid signals down to the sub centimeter level even in the presence of decimeter noise.

HARMONIC ANALYSIS OF ALTIMETER DATA

A convential Fourier analysis was applied to the equally spaced residual height data for all the arcs. A linear trend was further applied to match the end points and reduce remaining spurious 'edge effects'. The major difficulty with 'edge effects' had already been eliminated by the removal of trend and offset fit to the Gem 7 geoid). For Skylab and Geos 3, arcs 197, 301, 319, 324,

362, 416, 429, 538, 1962 and 1993, strip charts of altimeter derived sea-surface heights were the basic measurements.

In the Geos 3 arc 528, 2 second computer-averaged altimeter data (from high speed records) was used. This kind of data served as a check against the hand processed operation in the other arcs.

The power spectra of the residual geoid height data are the root mean square variation in each harmonic of the Fourier analysis

$$\Delta H(t) = \Delta c_0 + \sum_{n=1}^{n(max)} (\Delta c_n \cos nx + \Delta s_n \sin nx),$$

where $x = 2\pi t/T$, t being the time in the arc from the start and T the total arc time-length. Using a finite data set, n(max) is limited to half the number of data points.

From this definition the power spectrum is:

$$P_n(\Delta H) = [(\Delta c_n^2 + \Delta s_n^2)/2]^{1/2},$$

where

$$\Delta c_0 = \langle \Delta H \rangle$$

$$(\Delta c_n, \Delta s_n) = \frac{2}{T} \int_0^T \Delta H(t) \begin{Bmatrix} \cos 2\pi nt/T, \\ \sin 2\pi nt/T \end{Bmatrix} dt.$$

With the finite (sampled) data set I have replaced the integrals with simple sums. Using ΔT as the time spacing:

$$(\Delta c_n, \Delta s_n) \doteq \frac{2}{T} \sum_{n=1}^{n(max)} \Delta H(t) \begin{Bmatrix} \cos 2\pi nt/T, \\ \sin 2\pi nt/T \end{Bmatrix} \Delta T$$

The raw power spectra (so determined) for all the arcs are shown in Figure 4. Instead of the arc frequencies, n in Figure 4 are the equivalent global frequencies n(global) = n(arc) N, where, as before, N is the number of arc segments in a revolution. (For the Skylab round the world pass, N = 1.12, while for the Geos 3 arcs, N ranged from 3 to 10.)

The noise in each altimeter arc was estimated as the simple lower limit of the averaged power spectrum (leaving a small amount of signal). The averaging varied from 20 to 80 cycles/rev., the amount depending on the requirement for a smooth power 'tail' at high frequencies. In arc 429 (Figure 4g) the high estimated noise level (.32m) probably means that the 'smooth' geoid profile has inadvertantly picked up significant instrument noise as well as 'read error'. At any rate the use of the higher data rate in arcs 319 & 324 (as well as the 2 second computer-averaged data in 528) appears to give significant geoid information to a frequency of over 1000 cycles/rev. (< 20 km scale for a half wavelength).

Also shown in Figure 4 is the expected power law for the arcs due to a geopotential with degree variances following Kaula's rule. This law was calculated (in Appendix D) under the assumption that the altimeter data is given on the bounding earth sphere where the external geopotential is defined (e.g. Kaula, 1966, p. 31). The bounding sphere is chosen to ensure

convergence of the spherical harmonics for the potential (e.g. Hotine, 1969, pp. 159, 160) but other conventions and interpretations are possible (see Appendix D). However Lelgemann (1976, p. 6) asserts that to a level of 10 cm (frequencies as high as about 100 cycles/rev.) data on the geoid can be continued upward to the bounding sphere and only a small long wavelength correction needs to be made affecting low degree harmonics (mainly). If true to all levels than the simple expectations in Figure 3 (almost linear in log-log coordinates) calculated for the bounding sphere are also true to all frequencies on the lower geoid.

After the noise level was estimated for each arc a reduced signal was estimated for the power averages by subtracting the noise:

$$P_n(\text{reduced}) = [\langle P_n^2(\text{measured})\rangle - P^2(\text{noise})]^{1/2},$$

under the assumption that the noise is white or constant for all frequencies. (This assumption is valid for pseudo random noise averaged over a sufficient number of frequencies). The original and reduced averages are both shown in Figure 4.

The reduced averages were then converted to global power estimates [P_n (global) = P_n (arc) $\times N^{-1/2}$] and replotted in Figure 5. Also in Figure 5 I have shown the scatter in power averages from similar harmonic analysis of simulated data. Six 1/6 revolution arcs were analysed here from six different periodic (1 rev.) profiles generated from 600 pseudo-random harmonics according to the (global) power law:

$$P_n = 70n^{-1.5} \text{ meters},$$

with n in cycles/rev. This law is close to the expectation for Kaula's rule. The scatter lines in Figure 4 represent a 'random' sample of short arcs totaling 1 revolution in length. The actual data shows greater scatter but the short arcs total somewhat more than two revolutions. More interesting than the large scatter of the actual data are the systematic trends for almost all the arcs. The arcs tend to have high or low power consistently for all frequencies. There is also noticeably less power (compared to that expected from Kaula's rule) at low frequencies (< 80 cycles) and greater power for higher frequencies.

The reduced-global power estimates from all the arcs were then aggregated in 21 frequency groups spanning 14 to 1200 cycles/rev. The lowest group averaged all arc averages over 30 cycles from 10 to 40 cycles/rev. The next 14 groups aggregated averages over 40 cycles from 40 to 600 cycles/rev. The last groups considered only the 3 arcs with high data rates (319, 324 and 528) and the averages varied, being over approximately 100 cycles.

The data in each frequency group is independent except at the highest frequencies where data was used twice to achieve reasonably smooth statistics. The aggregate averages (with errors of the mean estimated from the sample variance) are listed in Table 2. They were then scaled down to 'point power' estimates accounting for the averaging spans. This scaling was based on the average power law $P_n = 70n^{-1.5}$ for which (rms) average power (over various

spans) was compared to mid point values (see Appendix D). The scaled down aggregates (and their likely deviations) are also listed in Table 2 and displayed in Figure 6.

GLOBAL POWER LAW ESTIMATES

Three power laws were calculated from the power averages in Table 2: they were all of the simple form.

$$P = An^{-B}$$

which seems sufficient to explain the nearly linear (log-log) decline of the data. (When more data is analysed and the variances are reduced, a more complicated law may be justified).

First, coefficients were estimated covering all the data. Then two laws were calculated, one for the data to 220 cycles and the other for the very high frequency averages. These two together gave a far more satisfactory representation of the total power in the residuals.

The power law An^{-B} is non linear in the unknown coefficient B. Thus, the linear model, fit to the data was:

$$\ln P = \ln A - Bn \pm \Delta(\ln P). \qquad (1)$$

But $\Delta \ln p = \Delta P/P$, the weight of each observation of ln P and n.

The least squares solution of (1) for best fitting values of ln A and B over the full set of observations in Table 2 was:

$$\begin{Bmatrix} \widehat{\ln I} \\ \widehat{B} \end{Bmatrix} = \begin{Bmatrix} 4.391 \pm 0.230 \\ 1.471 \pm 0.038 \end{Bmatrix},$$

with a correlation coefficient of -0.9927. Defining $\hat{A} = e^{\widehat{\ln A}}$, from which $\widehat{\Delta A} = \hat{A}\Delta(\widehat{\ln A})$;

$$\begin{pmatrix} \hat{A} \\ \hat{B} \end{pmatrix} = \begin{pmatrix} 80.72 \pm 19 \\ 1.471 \pm 0.038 \end{pmatrix} \qquad (2)$$

The wide fluctuation of A reflects the fact that it is best determined at n = 1, far from the data. The power expressed by (2) is shown as the full solid line in Figure 6. There is an obvious trend with the data to less power for $n < 100$. Nevertheless only 3 of the (21) power averages in Figure 6 are (slightly) more than 2σ away from the law expressed by (2).

More damaging to solution (2) is that it overestimates the total residual power in the data by allowing (essentially) equal weight at all frequencies. ,But the total power is dominated by the low frequencies. For example, the total global (rms) from 20 cycles is:

$$TP = \left[\sum_{n=20}^{\infty} (An^{-B})^2 \right]^{1/2} \doteq \frac{A}{[2(2B-1)]^{1/2}} [19^{-(2B-1)} + 20^{-(2B-1)}]^{1/2} \qquad (3)$$

In (3) I have approximated the sum by the average of the two covering integrals around the lower limit. Using solution (2):

$$TP \doteq 3.24m$$

But we know from the comparisons with Gem 7 (see Data Analysed) that the omission error (due to departures and terms $\ell > 20$) in these arcs must be about 2.2m. Furthermore some of this error goes into frequencies less than 20 cycles/rev. The error that goes into frequencies $0 \rightarrow 6$ is mostly absorbed in the offset and tilt for each arc. But from Figure B1 of Appendix B all geopotential terms of $\ell > 20$ contribute about $(.49)\ (14)^{1/2} = 1.83$ m to terms from $n = 6 \rightarrow 20$ leaving only $(2.2^2 - 1.8^2)^{1/2} = 1.3$ m for frequencies above $n = 20$. Of course I have assumed Kaula's (1966, p. 98) rule for geopotential effects and have allowed no ocean dynamics or departures. It is true that for the low degree geopotential Kaula's rule contains too much power. Nevertheless, even if all the omission error goes into frequencies above 20 this still leaves $[3.2^2 - 2.2^2]^{1/2} = 2.3$ m wholly unexplained. Indeed the harmonic analysis of the residuals themselves (see Table 1) gives the total power in the frequencies above $n = 20$ as 2.20 m (rms over all arcs). I conclude that the simple power law is probably too powerful and there is good reason to analyse the low end of the spectrum separately.

To this end the data in Table 2 was divided into two groups, the 6 averages to 220 cycles/rev. and those above that frequency. The least squares solution of (1) with the first six averages is [assuming $A = \exp(\ln A)$]:

$$\begin{Bmatrix} \hat{A} \\ \hat{B} \end{Bmatrix} = \begin{Bmatrix} 17.22 \pm 9 \\ 1.149 \pm 0.105 \end{Bmatrix}_{20 \rightarrow 220 \text{ cycles}} , \qquad (4)$$

with a correlation coefficient of -0.9923. The total power in this (low frequency) law over its range of validity is [using the integral approximation expressed in (3)]:

$$TP_{\substack{20\to 200\\ \text{cycles}}} \doteq \frac{17.22}{[2\times 1.298]^{1/2}}\left[19^{-1.298}+20^{-1.298}-2\times 220^{-1.298}\right]^{1/2} = 2.15\text{m}.$$

The corresponding high frequency solution is:

$$\begin{Bmatrix}\hat{A}\\ \hat{B}\end{Bmatrix} = \begin{Bmatrix}262.43 \pm 128\\ 1.659 \pm 0.078\end{Bmatrix}_{260\to 1100 \text{ cycles}}, \qquad (5)$$

with a correlation coefficient of -0.9927. The total power in this (high frequency) law from 220 cycles (where it makes a good closure with the low frequency law) to infinity is:

$$TP_{220 \text{ cycles}\to\infty} \doteq \frac{262.43}{[2\times 2.318]^{1/2}}\left[219^{-2.318}+220^{-2.318}\right]^{1/2} = 0.33\text{m}$$

[Note the small high frequency power compared to the low].

Using the separate power laws [(4) & (5)] the total power from 20 cycles to infinity is $[2.15^2 + .33^2]^{1/2} = 2.18$ m (rms), considerably reduced from the single (simple) law for all frequencies (3.24m). In fact it is now in agreement with the measured residual power above 19 cycles (2.20 m). This agreement is an excellent check on the many averaging procedures and the fitting technique used to derive the 'global' law.

In Figure 6 the three power laws are drawn against the aggregate data. The low power law fits especially well but the wide data variances allow for significant changes. These will be crucial to the separation of the gravitational geoid from sea state departures.

THE GEOID SPECTRUM FOR ALTIMETER DATA

The 'global' altimeter power spectrum in Figure 6 gains in significance when compared to values expected from the geopotential and other disturbing influences on the sea. The (time) frequencies of the tidal spectrum are well known but their amplitudes & phases in the open ocean are not [Apel, 1976, p. 618]. However values at island stations and theory give an upper bound of about 1-1/2 m for these with most of the power at low (spatial) frequencies ($n < 10$ cycles/rev.). Quasi-static geoid departures due to semi-permanent temperature-density anomalies also appear to have a similar (spatial) spectrum with (perhaps) more of its power at higher frequencies [Apel, 1976, p. 617]. The spectrum of dynamic topography from ocean currents, meanders & eddies is largely unknown though again, 1m is the estimated upper limit over short distances (across a few strong currents $\sim$ 200 km horizontally) [Kaula, 1970]. The gravitational spectrum alone seems most accessible to estimation since its high degree variances were first estimated by Kaula (1959) from gravimeter data.

The use of altimetry, of course, offers the prospect of a much denser and uniform data set for this purpose if the departures can be separated from the gravity 'signal'. The power spectrum of altimetry can serve to estimate the geopotential degree variances if in addition the gravitational spectrum can be estimated (for the altimeter geoid) in terms of its variances.

Rapp (1972b) first proposed as a rough rule that all the power of geopotential harmonics of degree ℓ goes into undulations of (spatial) frequency $n \equiv \ell$ cycles/ rev. If each normalized coefficient σ causes undulations of $|\sigma|$ R (rms - worldwide), the geoidal undulation power of all harmonics of degree ℓ is:

$$P_\ell = \left[\sum_{m=0}^{\ell} \sigma^2_{\ell,m} \right]^{1/2} R, \text{ (rms)} \qquad (6)$$

where R is the mean radius of the earth. Equation (6) assumes the geoidal undulations are on the bounding earth sphere where the geopotential coefficients are defined. (It is then a simple application of Bruns formula [Heiskanen & Moritz, 1967, p. 85] to compute this undulation from the disturbing potential. I will return later to the question of computing the undulation on the lower geoid). Accepting (6) and defining σ^2_ℓ as the mean square normalized geopotential coefficient of degree ℓ [the geopotential degree variance]:

$$P_\ell = R(2\ell + 1)^{1/2} \sigma_\ell .$$

Using Rapp's (1972b) proposal and Kaula's degree variances ($\sigma_\ell = \pm 10^{-5}/\ell^2$), the high frequency geoid power law is:

$$P_n \doteq 90.2\, n^{-1.5} \text{ meters (rms)} \tag{7}$$

However, even with the spherical approximation for the geoidal undulations, the detailed spectrum that the altimeter 'sees' is vastly more complicated than Rapp's proposal. Wagner (1976, Appendix B) showed that, approximating the altimeter track as a great circle, each harmonic ℓ has geoidal power at every frequency $n \leq \ell$ cycles/rev. of like parity. Summarizing that study, the expected power at each frequency ($n > 0$) was found to be:

$$E(P_n) = [E(P_n^2)]^{1/2} = R \sum_{\ell=n}^{\infty,\, n \text{ parity}} \sigma_\ell^2 \sum_{m=0}^{\ell} \left[F^2_{\ell,m,(\ell-n)/2}(I) + F^2_{\ell,m(\ell+n)/2}(I) \right]^{1/2}, \tag{8}$$

where σ_ℓ^2 is the expected degree variance of the geopotential coefficients (cross correlations are assumed to be zero) and the F(I) are fully normalized inclination functions. They are defined from Kaula's (1966) unnormalized inclination functions as: $F_{\ell m}(\text{norm}) = F_{\ell m}(\text{unnorm})\, N_{\ell m}$,

where:
$$N_{\ell m} = \left[\frac{(\ell - m)!\,(2\ell + 1)\,(2 - \delta_m)}{(\ell + m)!} \right]^{1/2},$$

$$\delta_m = 1, \; m = 0$$

$$0, \; m \neq 0 .$$

The inclination functions arise from the representation of a function of spherical harmonics rotated (transformed) from an equatorial system to a base plane of any inclination [Jeffreys, 1965]. Thus I had expected the power functions:

$$P^2_{\ell,n} = \sum_{m=0}^{\ell} \left[F^2_{\ell,m,(\ell-n)/2}(I) + F^2_{\ell,m,(\ell+n)/2}(I) \right]$$

to vary as widely with inclination as the individual inclination functions [see e.g. Allan, 1973].

Surprisingly, I found them (numerically) the same for all inclinations. These power functions of spherical harmonics are evidently invariant under rotation though no proof exists as far as I know.

Thus it is only necessary to evaluate the spectrum at the equator where the associated legendre polynomials are well known. For example, starting with Jahnke & Emde's (1945, p. 110) formula I find:

$$P^m_\ell(0) = 0, \ \ell - m \text{ odd}$$

$$= \frac{(-1)^{(\ell-m)/2} \cdot 1.3.5\ldots(2\ell-1)}{(\ell-m)(\ell-m-2)\ldots 2 \cdot (\ell+m+1)(\ell+m+3)\ldots(2\ell-1)}$$

$$= \frac{(-1)^{(\ell-m)/2}\,(\ell+m)!}{(\ell+m)(\ell+m-2)(\ell+m-4)\ldots(\ell-m+2)}, \ \ell - m \text{ even} \qquad (9)$$

Jahnke & Emde give:

$$P^\ell_\ell(0) = 1.3.5\ldots(2\ell-1) = \frac{(2\ell)!}{2^m m!} \qquad (10)$$

The P_ℓ^m's are unnormalized associated legendre polynomials of degree ℓ and order m. Since, on the equator, the spherical harmonics are merely

$$P_\ell^m(0)\begin{pmatrix}\cos m\lambda\\ \sin m\lambda\end{pmatrix}$$

where λ is the longitude, the unnormalized power functions for 'equatorial tracks' are merely the square of equations (9) or (10) with n substituting for m.

Introducing normalized legendre polynomials (on multiplying (9) & (10) by $N_{\ell,m}$) and identifying m with n, I find (after considerable manipulation):

$$E(P_n) = R\left[\sum_{\ell=n}^{\infty,\,n\ \text{parity}} P_{\ell,n}^2\right]^{1/2} = R\left\{\frac{(2n)![2n+1)/(2-\delta_n)]\sigma_n^2}{2^{2n}(n!)^2}\right. \qquad (11)$$

$$\left. + \sum_{\ell=n+2}^{\infty,\,n\ \text{parity}} \frac{(2-\delta_n)(2\ell+1)\ [(\ell+n)!]^2\ \sigma_\ell^2}{2^{2(\ell+n)}\ \{[(\ell+n)/2]!\}^4}\left[\frac{(\ell+n)(\ell+n-2)\ldots(\ell-n+2)}{(\ell+n-1)(\ell+n-3)\ldots(\ell-n+1)}\right]\right\}^{1/2}$$

From Equation (11) I can show that (assuming $\sigma_n^2 = 1$):

1. The first term on the right goes to infinity only as fast as $n^{1/2}$, and

2. For any finite n, the second term has an asymptote at $8/\pi$ as $\ell \to \infty$

[the terms of the infinite series themselves probably go to infinity as $n \to \infty$ but slower than $n^{1/2}$ (see Figure 7)]. Thus the convergence of (11) is assured as long as σ_ℓ^2 declines at least as fast as $(\ell^{-5/4})^2$ [to dominate the n infinite series giving the total power over all frequencies]. But this is a relatively mild restriction compared to the requirement that σ_ℓ^2 decline faster than $(\ell^{-2})^2$ to avoid infinite point gravity anomalies [Rapp, 1972a].

To show the asymptotic behaviour of the first term of (11) I use Stirling's approximation for large factorials [for a proof, see Hyslop, 1959, pp. 51-54]:

$$X! = (2\pi)^{1/2} X^{X+1/2} e^{-X} \left[1 + 0\left(\frac{1}{X}\right)\right].$$

Thus the first term of (11) for large n is:

$$P^2_{n,n} \doteq R^2 \left\{ \frac{(2\pi)^{1/2} (2n^{2n+1/2}) (2n+1) (2-\delta_n) e^{-2n}}{2^{2n} [(2\pi)^{1/2} n^{n+1/2} e^{-n}]^2} \right\} \sigma_n^2$$

$$= \frac{\left[2n^{1/2} + \frac{1}{n^{1/2}}\right] \left[2 - \delta_n\right] \sigma_n^2}{\pi^{1/2}},$$

which behaves as $n^{1/2} \sigma_n^2$ as $n \to \infty$.

Similarly, for finite n the asymptotic behavior of the other terms is (using Stirling's approximation):

$$P^2_{\ell >> n,n} \doteq R^2 \frac{(2-\delta_\ell)\, 2(2\ell+1) \{(2\pi)^{1/2} (\ell+n)^{\ell+n+1/2} e^{-(\ell+n)}\}^2}{2^{2(\ell+n)} \left\{(2\pi)^{1/2} [(\ell+n)/2]^{(\ell+n)/2+1/2} e^{-(\ell+n)/2}\right\}^4} \cdot$$

$$\cdot \frac{\left[\left(1+\frac{n}{\ell}\right)\left(1+\frac{n-2}{\ell}\right) \cdots \left(1-\frac{n-2}{\ell}\right)\right]}{\left[\left(1+\frac{n-1}{\ell}\right)\left(1+\frac{n-3}{\ell}\right) \cdots \left(1-\frac{n-1}{\ell}\right)\right]} \qquad (12)$$

The n products in the numerator and denominator of (12) all approach 1 as ℓ goes to infinity while the other factors reduce to:

$$P^2_{\ell>>n,n} \doteq R^2 \sigma^2_\ell (2 - \delta_\ell) \frac{4}{\pi} \frac{\left(2 + \frac{1}{\ell}\right)}{\left(1 + \frac{n}{\ell}\right)},$$

$$= R^2 \sigma^2_\ell (2 - \delta_\ell) \frac{8}{\pi}, \quad \ell \to \infty$$

The behaviour of the ensemble of terms in (11) is shown in Figure 7 for $\sigma^2_\ell = 1$ and R = 1. The dominant power function (for each frequency) is always $P^2_{\ell,\ell}$ where the geopotential is strongest also. But at all degrees a substantial amount of power goes into frequencies lower than the degree. The proportion that does grows with higher degree as more and more (lower) frequencies become available to share the power. This is in spite of the fact that the dominant power functions also grow with the geopotential degree. Using Kaula's rule, the expected altimeter geoid spectrum by degree is shown in Figure 8. The total power at each degree agrees with the worldwide average undulation (rms).

To arrive at an expected power for each (high) frequency, the power series [Equation (11)] must be summed to very high degree since the geopotential decline is slow. Full power spectra for two degree-variance laws have already been shown in Figure 6. They were calculated by summing equation (11) to degree 500 and using the integral approximation for the remaining power [e.g. equation (3)]. For example, Kaula's rule results in a power law $P = 70.8n^{-1.52}$, considerably less power at each frequency than from Rapp's simple proposal [equation (7)].

How important are the two critical assumptions made in arriving at these spectra?

1. Are equipotential undulations on the bounding earth sphere essentially the same as those on the lower geoid?

2. Does the fact that altimeter tracks are not great circles alter the interpretation of the spectrum significantly?

The second question is easier to answer but harder to explain in detail. The answer is no, the average spectrum does not change significantly. Some of the details are given in Appendix E. Essentially, the rotation of the Earth splits the power into many more frequencies than n = 1, 2, 3, ... cycles/rev, and the expected power in each depends on the inclination. But for the high frequency altimeter geoid the short period terms (ignoring the Earth's rotation) still dominate the spectrum.

The first question has been answered by Lelgemann (1976) in the affirmative. He claims the undulations on the geoid (to a level of 10 cm) are essentially the same as those on the bounding Earth sphere. But his result depends on ignoring contributions from the higher order terms (in ℓ) which may cause divergence of the potential series in its continuation down from the bounding sphere.

Consider the Earth's geopotential function at P outside the bounding sphere (Figure 9):

$$V_P = \frac{GM}{R} \left\{ 1 + \sum_{\ell=2}^{\infty} \sum_{m=0}^{\ell} \left(\frac{R}{r}\right)^{\ell} \bar{P}_{\ell}^{m} (\sin \phi) \left[\bar{C}_{\ell m} \cos m\lambda + \bar{S}_{\ell m} \sin m\lambda \right] \right\}, \quad (13)$$

where GM is the mass (μ) of the Earth, ϕ is the latitude, the $\bar{P}_{\ell}^{m}$ are fully normalized associated legendre polynomials and the $\bar{C}_{\ell_m}$ & $\bar{S}_{\ell_m}$ are fully normalized coefficients. The role of the radius R is somewhat arbitrary in equation (13). The Earth's external potential satisfies Laplaces equation as do all the spherical harmonics of (13). Thus the only mathematical requirement on R (other than to make the arbitrary coefficients dimensionless) is that the resulting series converge everywhere outside the Earth. Traditionally (e.g. Hotine, 1969, pp. 159-160), the scale R has been chosen as the maximum (i.e. the equatorial) radius of the Earth to insure the convergence (and the validity) of the mass integral representation for the spherical harmonics. Unfortunately it leaves the possibility of divergence of the series almost everywhere on the ellipsoid. Of course the mass integral representation of the harmonic coefficients can be given up by using R' (the polar radius) as the scale and insuring the convergence of (13) everywhere on the ellipsoid. But (short of abandoning spherical harmonics) convergence on the ellipsoid with R scale for the potential can also be insured by requiring an exponential decline for the harmonic coefficients. While this downward continuation converges it still does not represent the true potential on the geoid which requires an additional harmonic series in r^{ℓ}. However Cook (1967) shows the error to be negligible.

The traditional potential [equation (13)] downward continued at the pole has a radial factor

$$\left[\frac{R}{R-\Delta}\right]^{\ell} = (1-\Delta/R)^{-\ell} = (1-1/298.255)^{-\ell}$$

$$= .996647^{-\ell}.$$

If a counter factor of $.996647^{\ell}$ (close to 1 for low degree, decreasing rapidly for $\ell >> 100$) controls the high degree coefficients the series would converge everywhere. For example the degree variances of the geopotential (defined on the outer sphere) might be close to:

$$\sigma_{\ell}^2 = \left\{(10^{-5}/\ell^2)(.996647)^{\ell}\right\}^2. \qquad (14)$$

[e.g. Morrison, 1971].

Applying this rule to the geopotential [Equation (13)] continued down to the geoid results in high frequency undulations (and gravity anomalies) always less than that expected for Kaula's rule (away from the poles) and considerably less for lower latitudes and higher degrees (see Table 3).

Referring to Table 3 the values at the equator ($\phi = 0°$) reflect the geopotential variances which are known to be from 90% to 80% less than Kaula's rule from degree 5 to 25. The rule of equation (14) is a bit high in this range but (as Figure 6 implies) are probably too low in the range $25 < \ell < 100$ to explain the altimeter spectrum. It probably also has low gravity anomaly variances in this range compared to surface data (e.g. Rapp, 1972a, p. 7).

The second rule in Table 3 attempts to remedy these discrepancies by providing less power in the range $5 < \ell < 25$ but more for $25 < \ell < 100$. However point gravity anomalies in the vicinity of the poles will be infinite with this role. (The undulations, on the other hand, still converge). Figure 10 shows how the measured high frequency altimeter-sea surface power ($20 < n < 220$) compares to that calculated for the geoid by these two rules continued to the ellipsoid at 30° latitude (the average for the data examined). The power for two other simple variance laws are also shown assuming that the undulations are on the bounding sphere. The first is from Kaula's rule, the second from a modification of it which seems to fit satellite geopotential data and surface gravimetry quite well. None can accommodate the measurements, especially the slope of power spectrum. Probably the best overall match is obtained with a model due to Rapp (1972a, Model 6) which has slightly more power than $10^{-5}/\ell^2$ above 30 cycles and slightly less below.

Clearly the data analysed so far is not compatible with any simple degree variance rule for the geopotential. Of course, more complicated rules can be devised which provide the extra power above 20 cycles at the required rate. For example Bruce Marsh (private conversation, 1977) suggests that even the (seemingly simple) variances below degree 25 may actually be the result of the superposition of power laws from density anomalies in more than a few layers within the Earth. [Allan, 1972, had shown how the geopotential variances can be interpreted as reflecting density anomalies in one or more layers]. Thus

the initial slow decline of power in the high frequency altimeter geoid spectrum may reflect unusually large density anomalies in or just below the crust. A horizontal scale for these of a few hundred kilometers suggests tectonic plate fragments but the altimeter data is far too sparse to speculate further. In fact, sea state and ocean dynamics may well account for a large part of the extra power.

THE SPECTRUM OF GEOID DEPARTURES

The horizontal spectrum of all the departures from the geoid has never studied in detail, but much is known about the individual components [e.g. Rapp, 1975, and Apel, 1976]. For example, Hendershott, (1972) has given a simplified global solution for the principal lunar tide with maximum amplitudes of 1 meter requiring surface harmonics only up to (12, 12). Higher surface harmonics for the full tidal function seem to have significantly smaller amplitudes [e.g. Musen and Estes, personal communication, 1977]. Significant geoid departures with short wavelengths ($n > 20$ cycles/rev.) seem to be associated with ocean current systems. These would include effects from salinity and density differences (along vertical profiles) as well as from the movement of the currents themselves. Figure 11 is a horizontal departure profile (along the track of (Geos 3, Revolution 197) for the average sea surface topography in the North Atlantic estimated from density measurements [by Defant, 1961; shown in Apel, 1976]. The rise over the warm (light) waters of the Gulf Stream is clearly seen. The

high frequency spectrum for this track (after subtracting an end-matching trend) is shown in Figure 12. The estimated effects are a full order of magnitude below the power from Kaula's rule for the geoid. However these departures are long term averages and may underestimate the profile at the time of the altimeter pass. Furthermore, this underestimate is more likely at higher frequencies ($n > 40$ cycles) which must be considerably smoothed using 'average' sea-density data.

ESTIMATE OF DEPARTURE SPECTRUM FROM GLOBAL ALTIMETRY

The extra power (above 25 cycles) in the measured altimeter (sea surface) spectrum, above that predicted for the geoid, can be interpreted as departure power. In doing so I recognize:

1. The measured 'global' spectrum is still subject to considerable uncertainty from sparse coverage (just the 'formal' error bounds of the 'law' are shown in Figure 10).

2. The theoretical spectrum for the geoid is perhaps even more uncertain. Not only are the high frequency degree variances of gravity unknown (over the oceans) but the spectral interpretation (on the geoid) is controversial.

Nevertheless the calculation is interesting and a fairly reasonable result is achieved. When considerably more data is analysed this calculation may serve to estimate the geopotential degree variances on removal of 'known' sea state effects.

In estimating the departure power I take for the geopotential variances $\sigma_\ell^2 = [0.95 \times 10^{-5}/\ell^{2.06}]^2$. This rule gives a good fit to recent geopotential's from satellite data and smoothed (5° mean) surface gravimetry. It is also fairly representative of the high frequency surface data to degree 75 [Chovitz et. al., 1972]. Figure 13 shows the agreement. In addition this rule gives a reasonable point value for gravity anomalies [evaluated on the bounding sphere] of $[1250]^{1/2}$ mgals (rms), while a $(1/\ell^2)$ rule has infinite 'point power' for anomalies. I assume (with Lelgemann, 1976) that the high frequency geoid undulations are essentially the same as those calculated for the bounding sphere. (There is certainly no significant decline in actual power after 100 cycles as predicted by downward continuation, especially at low latitudes, with a uniform rule for geopotential variances).

With these assumptions the expected power on the geoid is given [from equation (11)] as:

$$P = 66.8n^{-1.58}, \qquad (15)$$

(see Figure 6). The departure power is given by $[P^2(\text{sea-surface}) - P^2(\text{geoid})]^{1/2}$. As Figure 6 shows, the departures are significant even at 25 cycles. They reach a peak [16 cm (rms)] at 35 cycles but (while declining) actually dominate the sea-surface topography at higher frequencies.

It should be emphasized however that this judgement is very sensitive to both the sea surface measurements and the assumptions, in estimating geoid

undulations. It is interesting though that the global estimate of sea surface power begins (at 25 cycles) almost at the geoid estimate using the best geopotential variances known (from satellite & gravimetry data). The measured sea surface power thus confirms the earlier results that the low frequency variances of gravity are significantly smaller than Kaula's rule. At higher frequencies however the surface gravimetry shows a strong tendency to move back closer to the rule (see Figure 13 and Rapp, 1972a, Figure 1). But it is not yet clear when this movement back begins. The altimetry suggests the geopotential variances may start back at 25th degree though the best evidence from gravimetry is that this movement is delayed till at least 50th degree. Thus the geoid departure estimate in Figure 6 may be too high. On the other hand Rapp (personal communication, 1977) has shown that 1° mean-gravity anomalies in ocean areas are significantly less than over the continents (reduced by the greater distance to the 'bottom' topography). No significant statistics are yet available for larger block means. The power of the ocean geoid therefore remains an open question. It is likely to remain so until the departures are much better known.

SUMMARY AND CONCLUSIONS

Preliminary estimates of the global spectrum of the sea-surface and geoid has been made using altimeter data from the Geos 3 and Skylab spacecraft. An 'altimetry' pass over a detailed gravimetric geoid has also been used. In all,

the equivalent of 3 revolutions of data has served for the 'global' estimates. The total power in the sea surface topography at and above 20 cycles/revolution (< 1000 km half wavelength) is 2.18 m (rms). The power above 220 cycles (< 91 km half wavelength) is 0.33 m (rms). The sea surface power departs noticeably above the best estimate of the geoid power at all frequencies higher than 25 cycles. Some of this departure is probably due to an underestimate of the geoid power at higher degrees. Some may be due to the sparsity of the data analysed. Accepting the data and the estimate of the geoid power, the total departure power above 20 cycles is $[2.18^2$ (sea surface) $- 1.84^2$ (geoid)$]^{1/2} =$ 1.17 m (rms). The peak power is 0.16 m at 35 cycles.

The geoid power above 20 cycles from Kaula's rule is 2.38m (rms). Thus the altimeter residuals overall, are compatible with geopotential variances somewhat less than $(10^{-5}/\ell^2)$. Above 200 cycles (< 100 km have wavelength) the sea surface topography seems certain to be dominated by sea state departures. This preliminary measurement places the cross over (where the departures begin to dominate the spectrum) at $n = 50$ cycles corresponding (roughly) to 50th degree geopotential harmonics.

This interpretation of the measured sea surface power spectrum is based on a uniform (simple) rule for geopotential variances. It also assumes the geoid undulations are (essentially) the same as potential variations on the bounding sphere. One or both assumptions can be criticized. If the geoid undulations can be represented by downward continuation of the spherical disturbing potential

(inside its sphere of convergence) than at some point that potential (on the sphere) must have an exponentially declining factor. This factor (if applied uniformly) would cause a rapid decline in geoid undulation power at frequencies higher than 100 cycles and for low latitudes. With the present data, this behaviour is not evident, but the latitude sampling is small and the sea state seems to dominate above 100 cycles. On the other hand detailed surface gravimetry shows that the geopotential variances may move from a decline faster than $1/\ell^2$ below degree 20 towards $1/\ell^2$ above. An empirical rule is not yet available for this behaviour.

In any case the use of altimeter data for geopotential determination beyond degree 50 will demand a greater knowledge of sea state than is now available.

ACKNOWLEDGEMENT

I thank Jeanne Roy for many of the harmonic analyses and the calculation of data residuals. The detailed calibration and verification of the method of analysis benefitted greatly from stimulating discussions with Francis J. Lerch.

REFERENCES

Allan, R. R., Change of Inclination in passing through resonance, In: Recent Advances in Dynamical Astronomy (Topley & Szebehely Eds.), pp. 338-339, Reidel Publishing Co., Holland, 1973.

Allan, R. R., Depth of sources of gravity anomalies, Nature, Physical Science 236, 22-23, 1972.

Apel, J. R., Ocean science from space, EOS (Transactions of the American Geophysical Union) 57; 612, 1976.

Cholshevnikov, K. V., On the values of the tesseral harmonic coefficients; Vest, Univ. Leningrad, No. 13, 1965.

Chovitz, B. H., Downward continuation of the potential from satellite altitudes, Bollettino Di Geodesia E. Sienze Affini, No. 2 (In English), p. 85, 1973.

Chovitz, B., J. Lucas and F. Morrison, Gravity Gradients at Satellite Altitudes, NOAA, Rockville, Md., 1972.

Cook, A. H., The determination of the external gravity field of the earth from observations of artificial satellites, Geophys. J. R. Astr. Soc., 13, 310 (1967).

Defant, A., Physical Oceanography, Vol. 1, Pergamon, N.Y., 1961.

Gaposchkin, E. M., Earth's gravity field to the eighteenth degree and geocentric coordinates for 104 stations from satellite and terrestrial data, Journal of Geophysical Research 79, 5377, 1974.

Hendershott, M. C., The effects of solid earth deformation on global ocean tides, Geophys. J. Royal Astron. Soc., 29, 389-403, 1972.

Hotine, M., Mathematical Geodesy, ESSA Monograph 2, U. S. Gov't. Printing Office, Washington, D. C., 1969.

Hyslop, J. M., Infinite Serves (5th Ed.), Interscience Publishers, N.Y.C., 1959.

Jahnke, E., and F. Emde, Tables of Functions (4th Ed.), Dover Press, 1945.

Jeffreys, B., Transformation of tesseral harmonics under rotation, Geophysical Journal; 10, 141-145, 1965.

Jeffreys, H., The Earth, 4th Edition, Comb. Univ. press, 1959.

Kaula, W. M. (Ed.), The Terrestrial Environment: Solid Earth and Ocean Physics, MIT Press, Camb., Mass., 1970.

Kaula, W. M., Theory of Satellite Geodesy, Blaisdell Press, Waltham, Mass., 1966.

Kaula, W. M., Statistical and harmonic analysis of gravity, J. Geophys. Res. 64, 2401-2422, 1959.

Lelgemann, D., Some problems concerned with the geodetic use of high precision altimeter data, Ohio State Dept. of Geodetic Science Report No. 237; Columbus, Ohio, 1976.

Marsh, J. G. and S. Vincent, Global detailed gravimetric geoid computation and model analysis, Geophysical Surveys 1, 481-511, 1974.

McGoogan, J. T., C. D. Leitao and W. T. Wells, Summary of Skylab S-193 altimeter altitude results, NASA TM X-69355, pp. 207-228, Wash. D. C., 1975.

Morrison, F., Density layer models for the geopotential; Bull, Geodesique, No. 101, 1971.

Rapp, R. H., The geoid: definition and determination, In: Proceedings of the geodesy/solid earth and ocean physics Research Conferences, p. 69-77, Ohio State Dept. of Geodetic Sciences Report No. 231; Columbus, Ohio, 1975.

Rapp, R. H., Geopotential coefficient behaviour to high degree, Ohio State Dept. of Geodetic Science Report 180, p. 12, Columbus, Ohio, 1972a.

Rapp, R. H., Geoid information by wavelength, Ohio State, Dept. of Geodetic Science Report 180; p. 18, Columbus, Ohio, 1972b.

Wagner, C. A., F. J. Lerch, J. E. Brownd and J. A. Richardson, Improvement in the geopotential derived from satellite and surface data (GEM 7 and 8), J. Geophys. Res., 82, 901, 1977.

Wagner, C. A., The accuracy of goddard earth models, NASA-GSFC Document X-921-76-187, pp. 191, 193; greenbelt, Md., 1976.

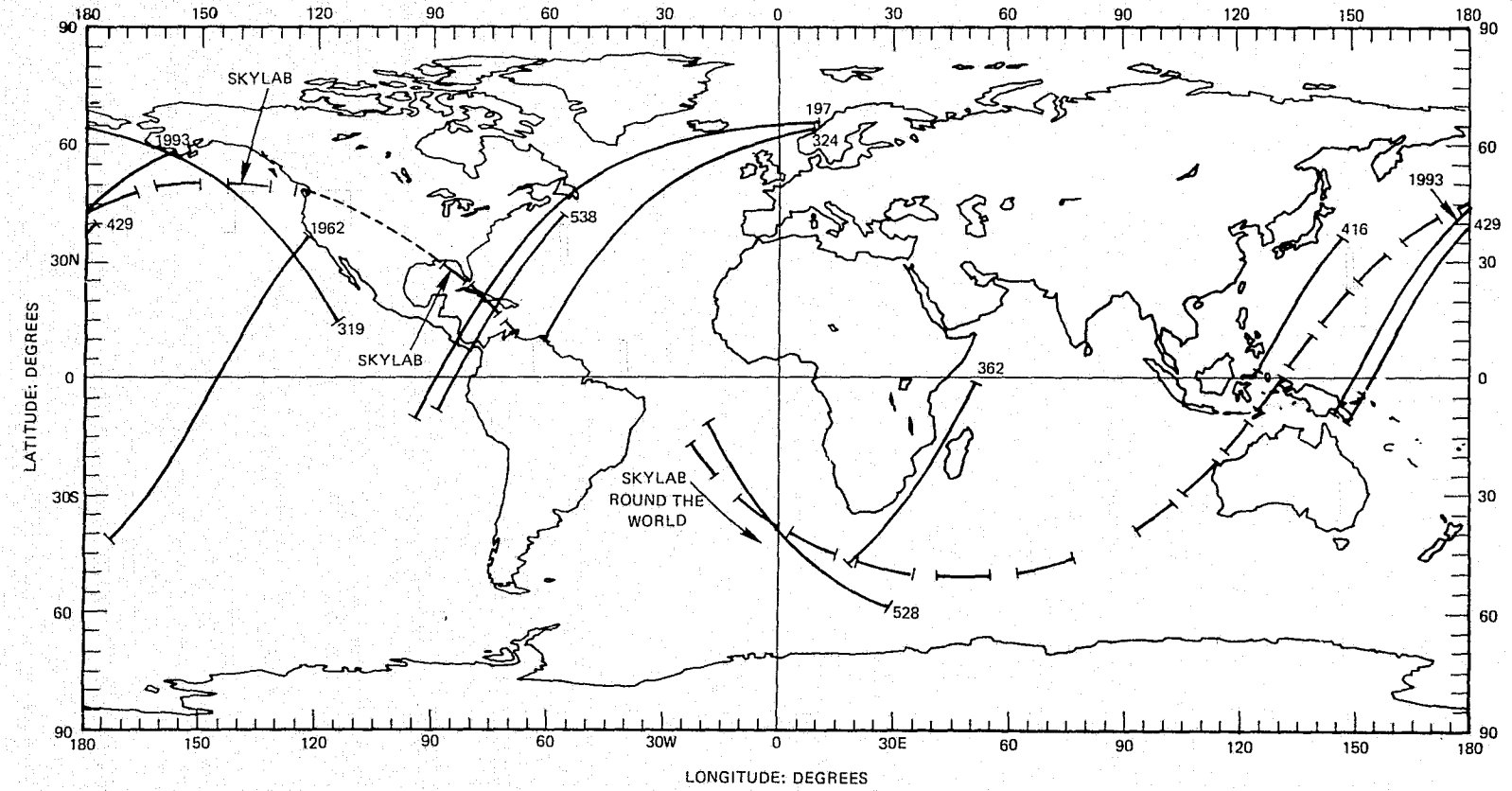

Figure 1. Distribution of Altimetry Arcs

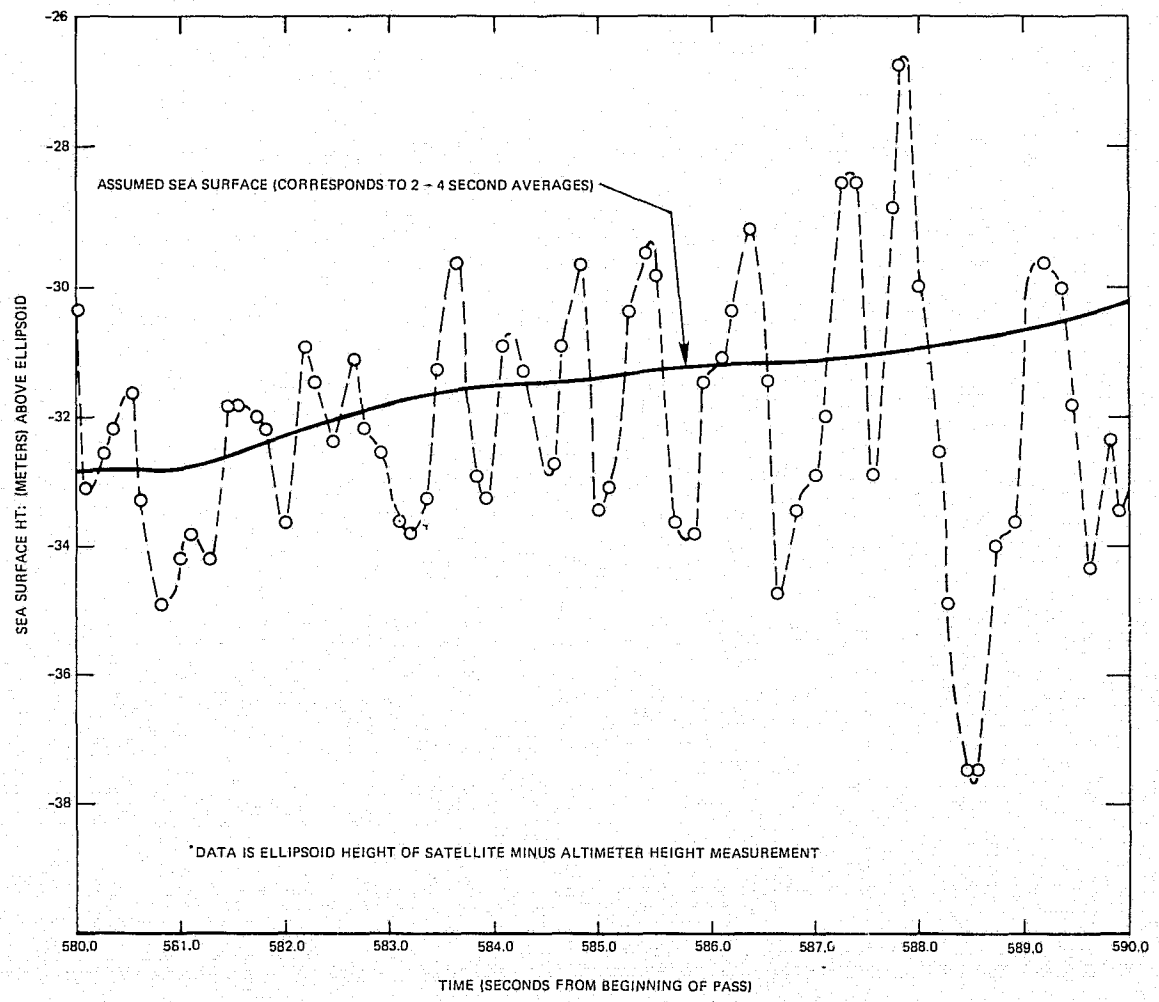

Figure 2. Sea Surface Heights over the North Atlantic from 'High Speed' GEOS 3 Altimetry*

*DATA IS: SATELLITE HEIGHT ABOVE ELLIPSOID–ALTIMETER HEIGHT–GEM 7 GEOID HEIGHT
(THE SATELLITE HEIGHT/ALTIMETER HEIGHT HAS BEEN CORRECTED FOR A BIAS AND ORBIT ERROR SLOPE IN AN ADJUSTMENT TO THE RESIDUAL HEIGHTS WITH GEM 7. THIS CORRECTION MAY ALSO ABSORB LONG WAVELENGTH ERROR IN GEM 7)

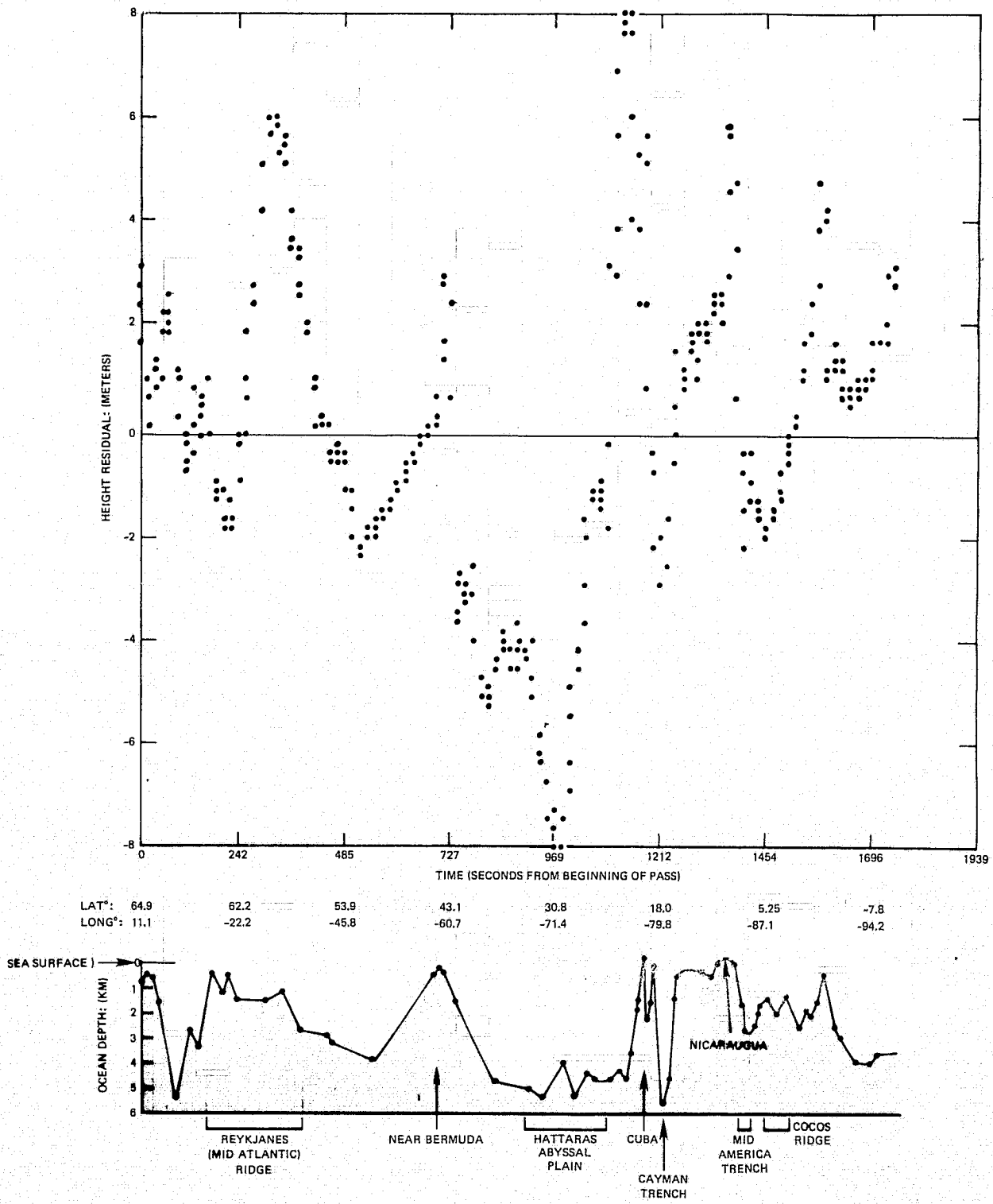

Figure 3a. Sea Surface Height Residuals of Satellite Altimetry with GEM 7: GEOS 3, Rev. 197*

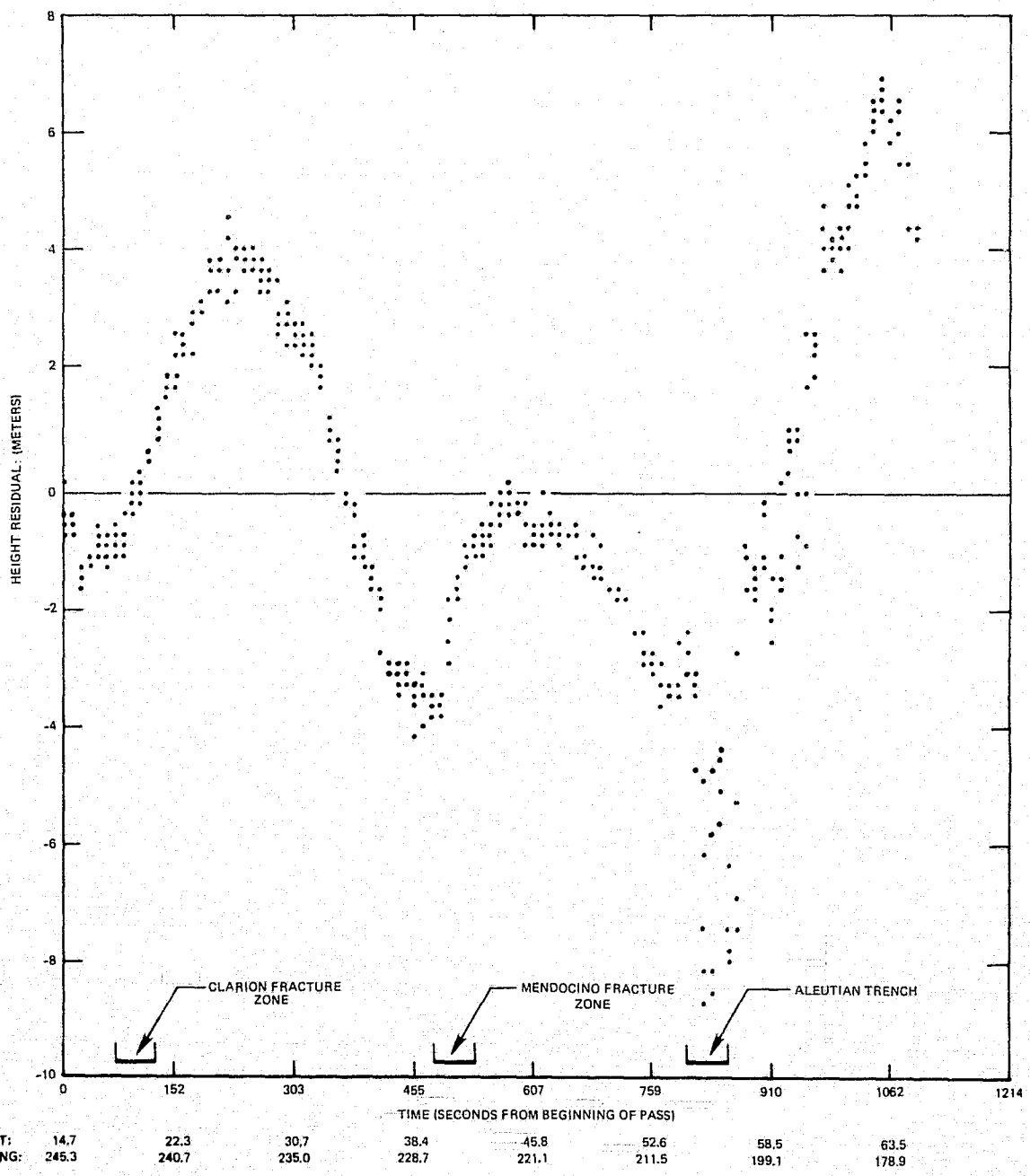

Figure 3c. Sea Surface Residuals of Satellite Altimetry with GEM 7: GEOS 3, Rev. 319

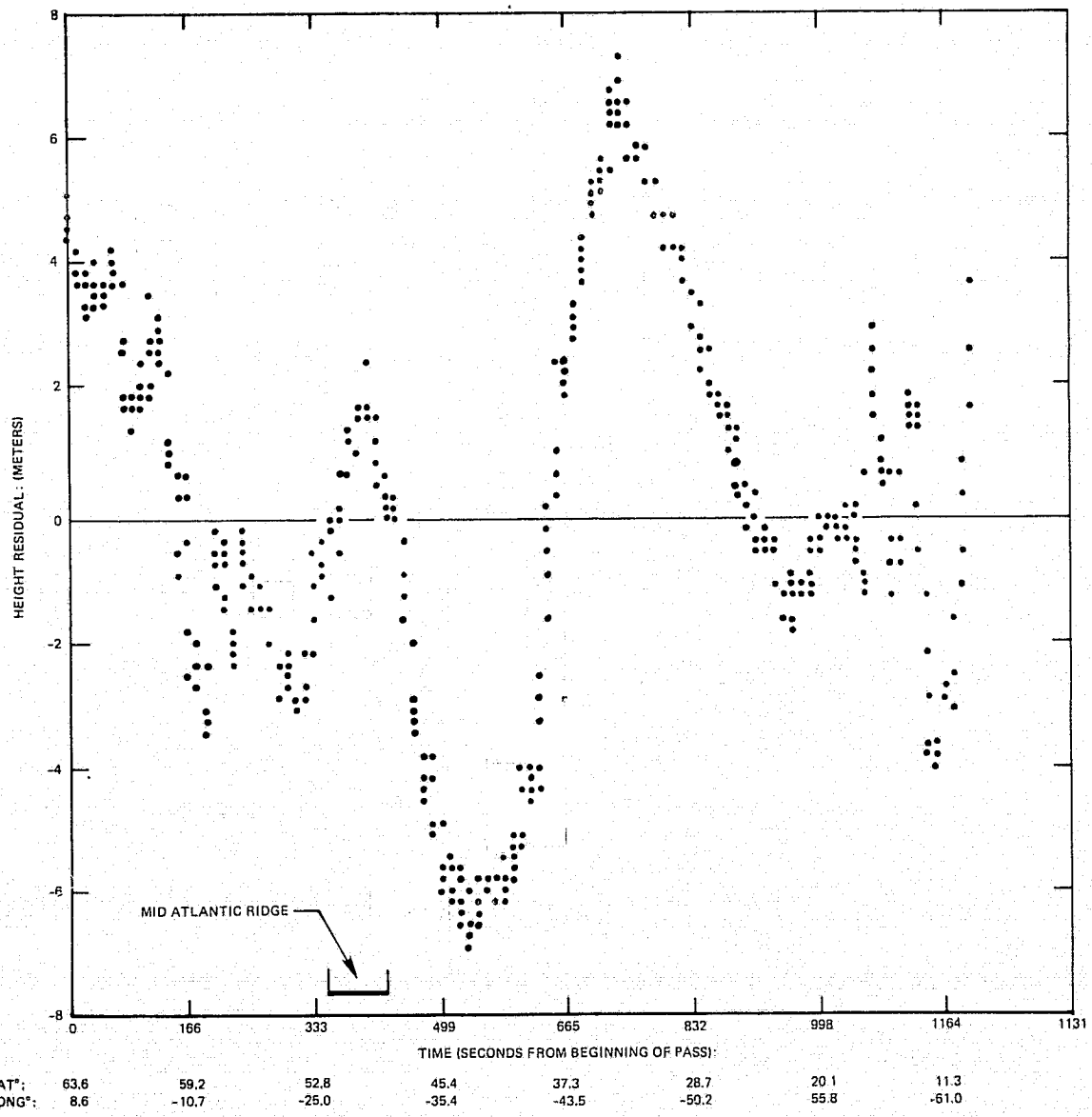

Figure 3d. Sea Surface Height Residuals of Satellite Altimetry with GEM 7: GEOS 3, Rev. 324

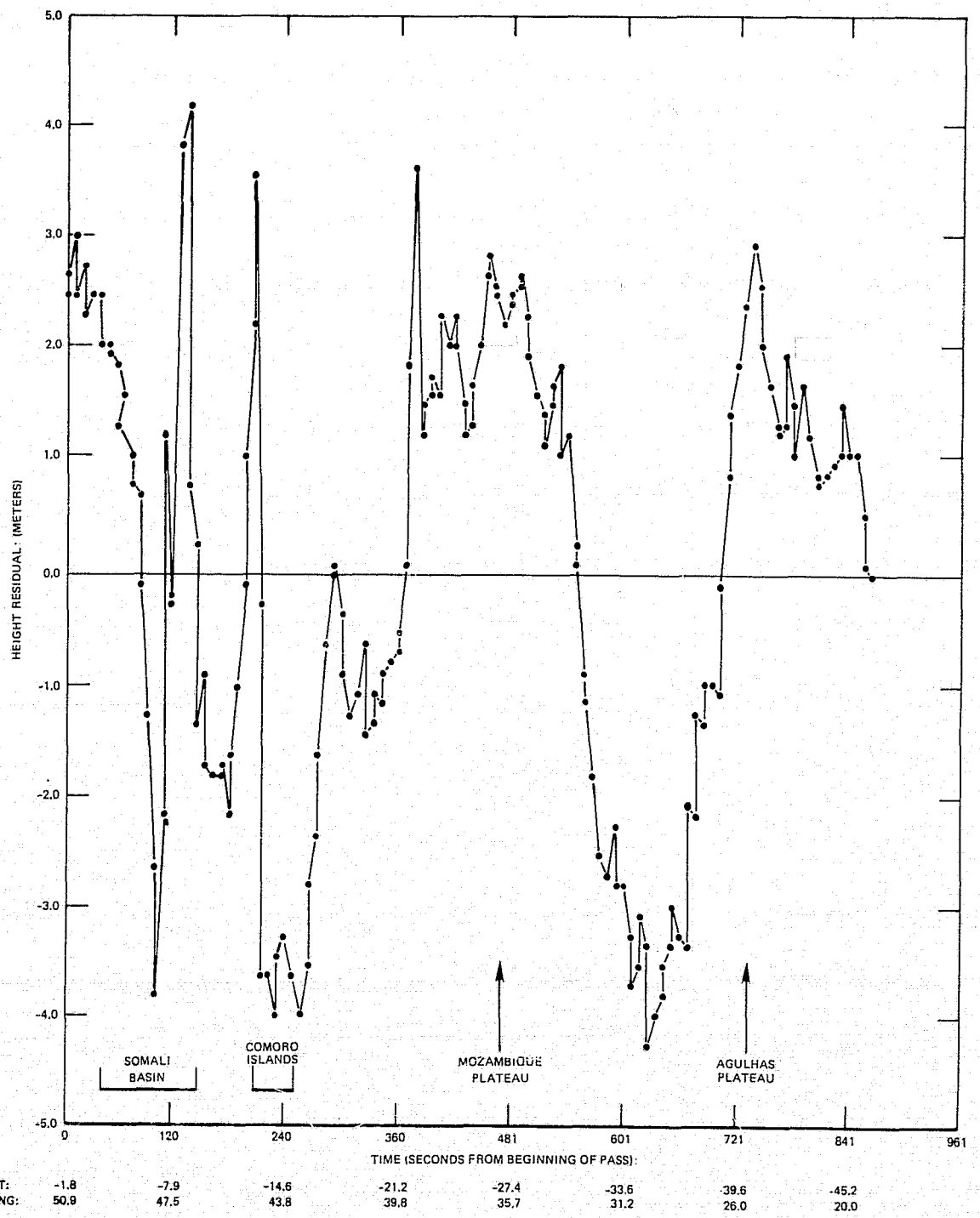

Figure 3e. Sea Surface Height Residuals of Satellite Altimetry with GEM 7: GEOS 3, Rev. 362

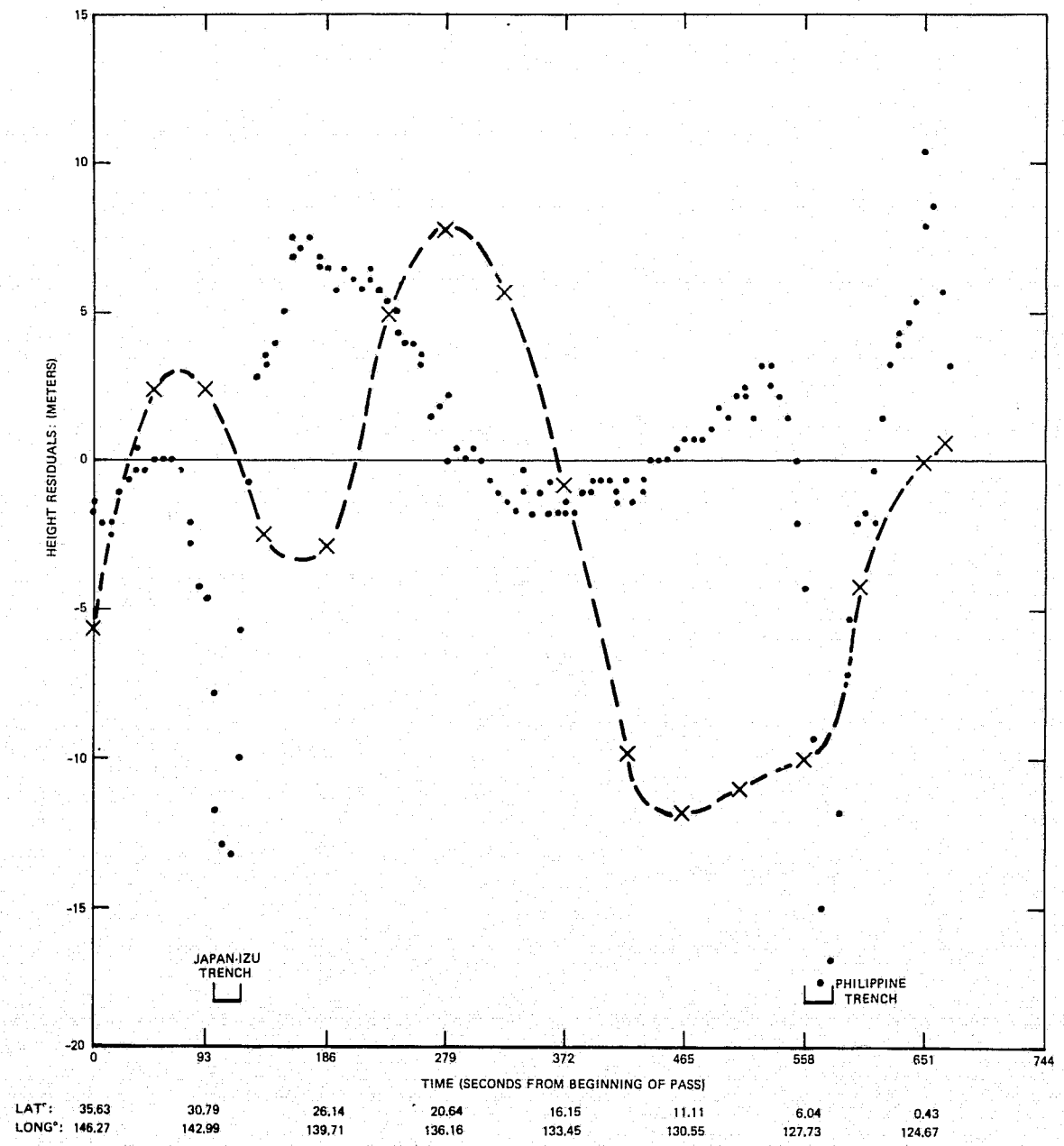

FIRST 670 SECONDS OF SIMULATED GEOID DATA FROM ARC 1 [USING THE GEOS 3 ORBIT, A ROTATING EARTH AND A RANDOM FIELD $13 < \ell < 100$, $\sigma^2_{\ell m} = (10^{-5}/\ell^2)^2$]; SEE FIGURE C8 FOR SPECTRUM. NOTE: THE HEIGHT RESIDUALS HAVE SUFFICIENT SCALE BUT LACK THE 'SHARPNESS' (VERY HIGH FREQUENCY POWER) OF THE REAL DATA OVER THE TWO TRENCHES.

Figure 3f. Sea Surface Height Residuals of Satellite Altimetry with GEM 7: GEOS 3, Rev. 416

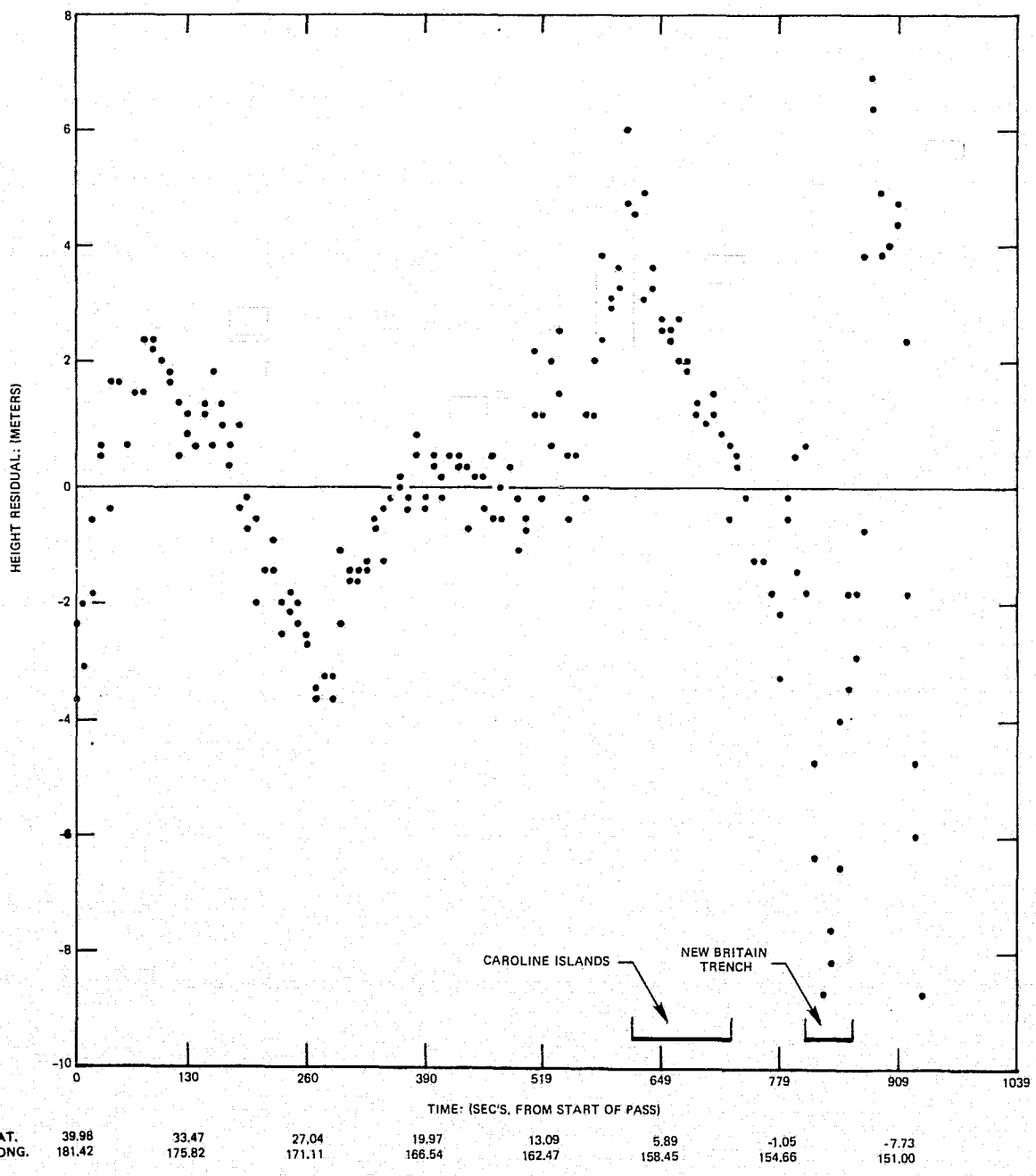

Figure 3g. Sea Surface Height Residuals of Satellite Altimetry with GEM 7: GEOS 3, Rev. 429

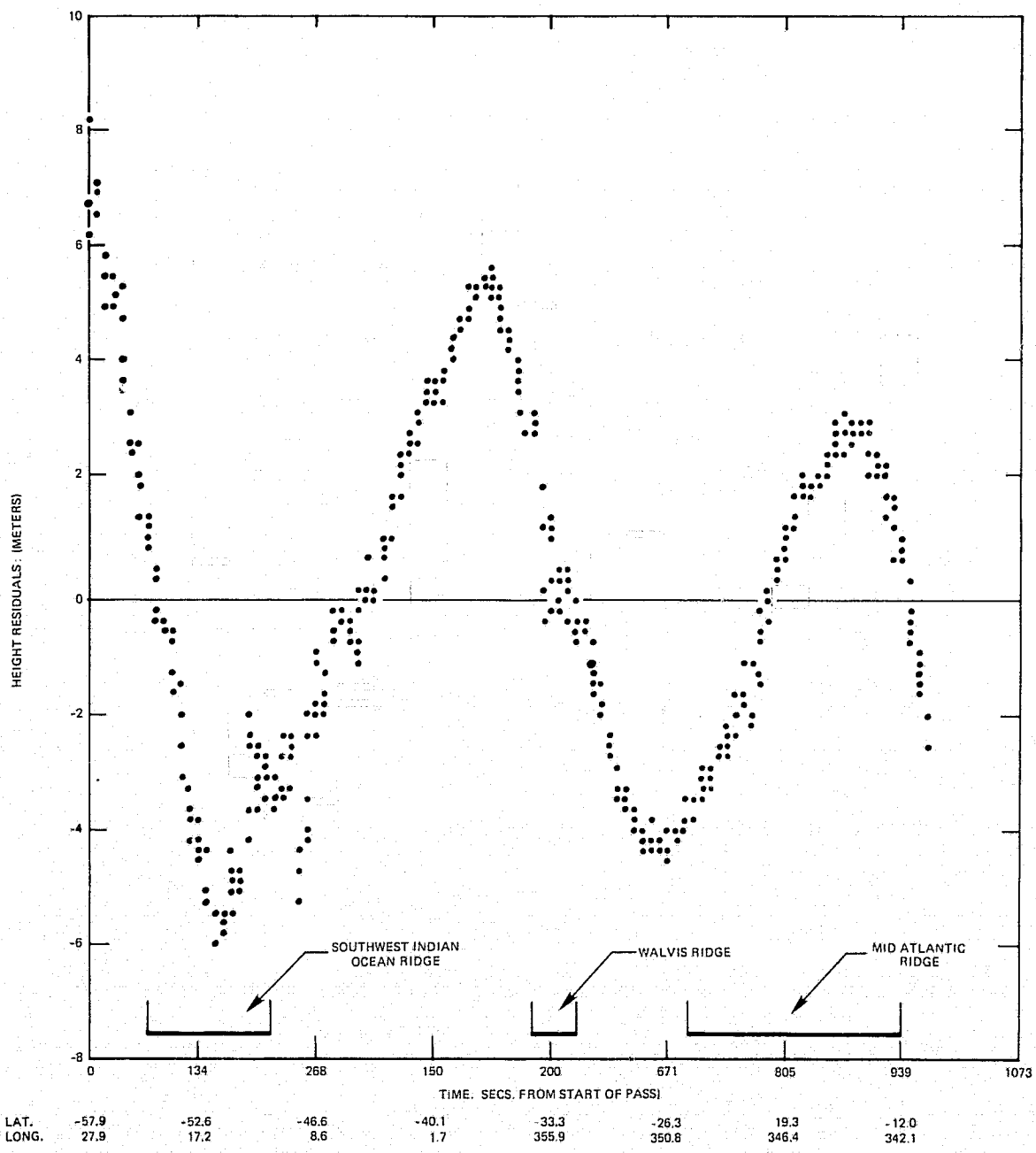

Figure 3h. Sea Surface Height Residuals of Satellite Altimetry with GEM 7: GEOS 3, Rev. 528

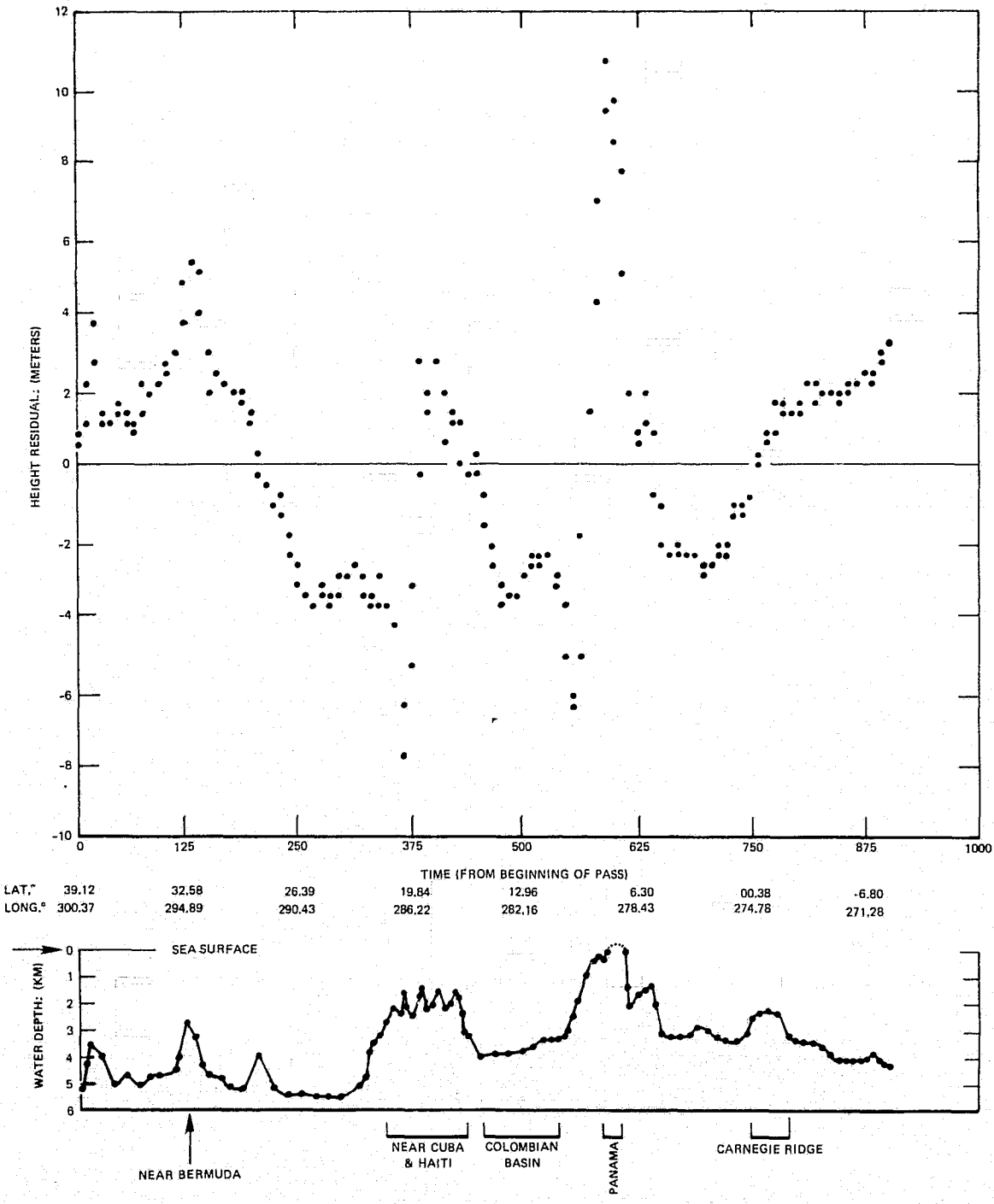

Figure 3i. Sea Surface Height Residuals of Satellite Altimetry with GEM 7: GEOS 3, Rev. 538

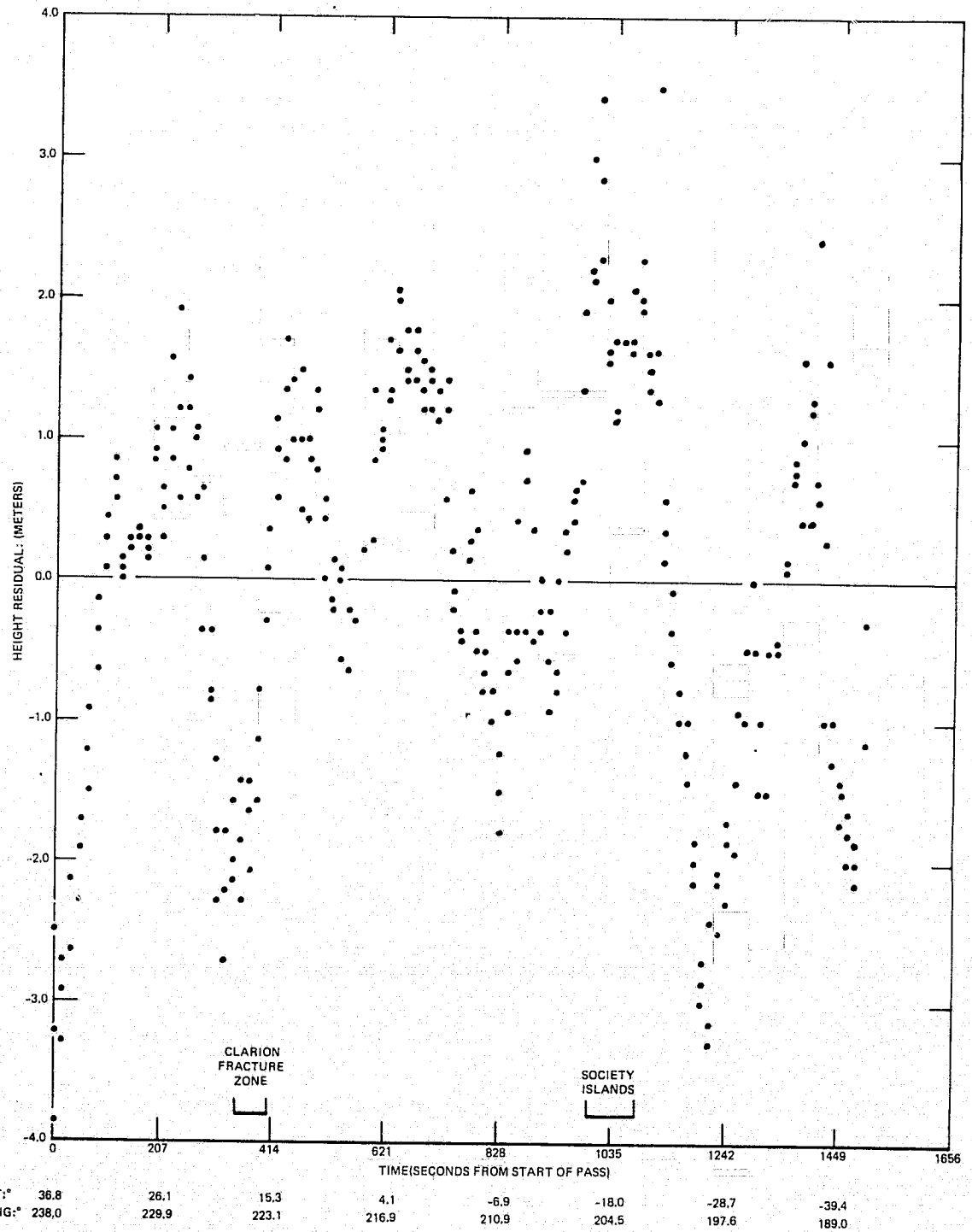

Figure 3j. Sea Surface Height Residuals of Satellite Altimetry with GEM 7: GEOS 3, Rev. 1962

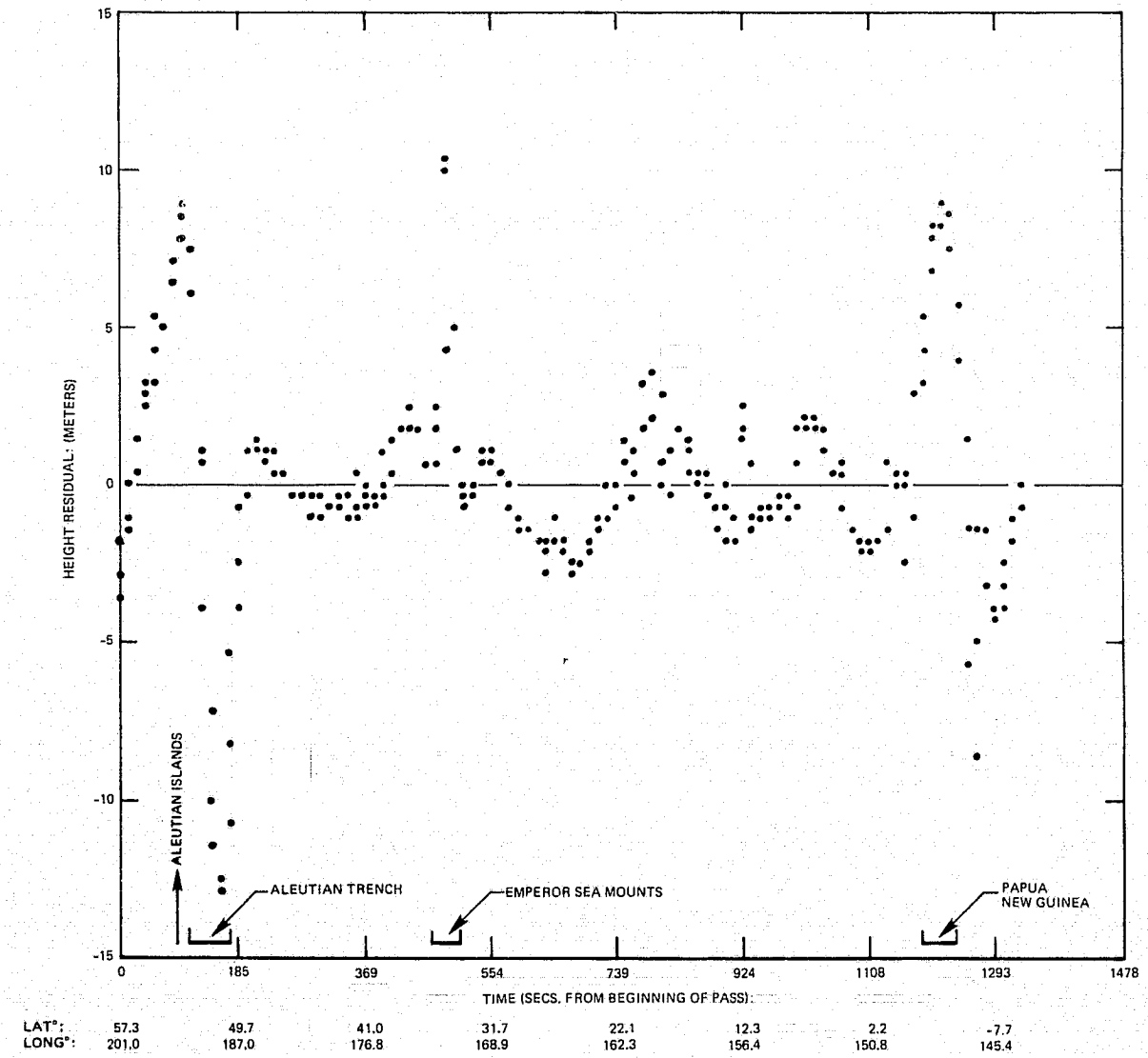

Figure 3k. Sea Surface Height Residuals of Altimetry with GEM 7: GEOS 3, Rev. 1993

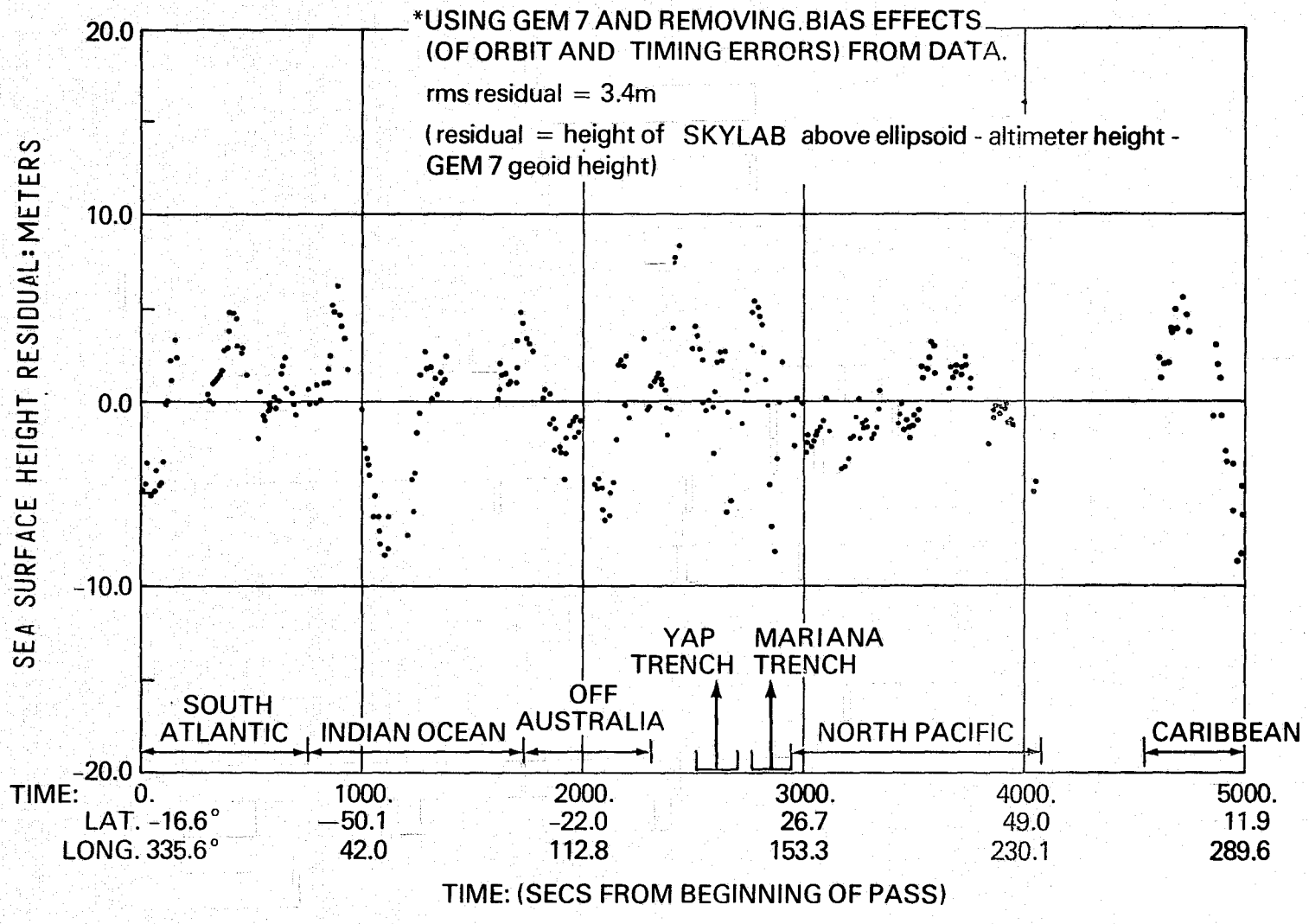

Figure 31. Sea Surface Height Residuals of Satellite Altimetry with GEM 7: Skylab Round-The-World Pass

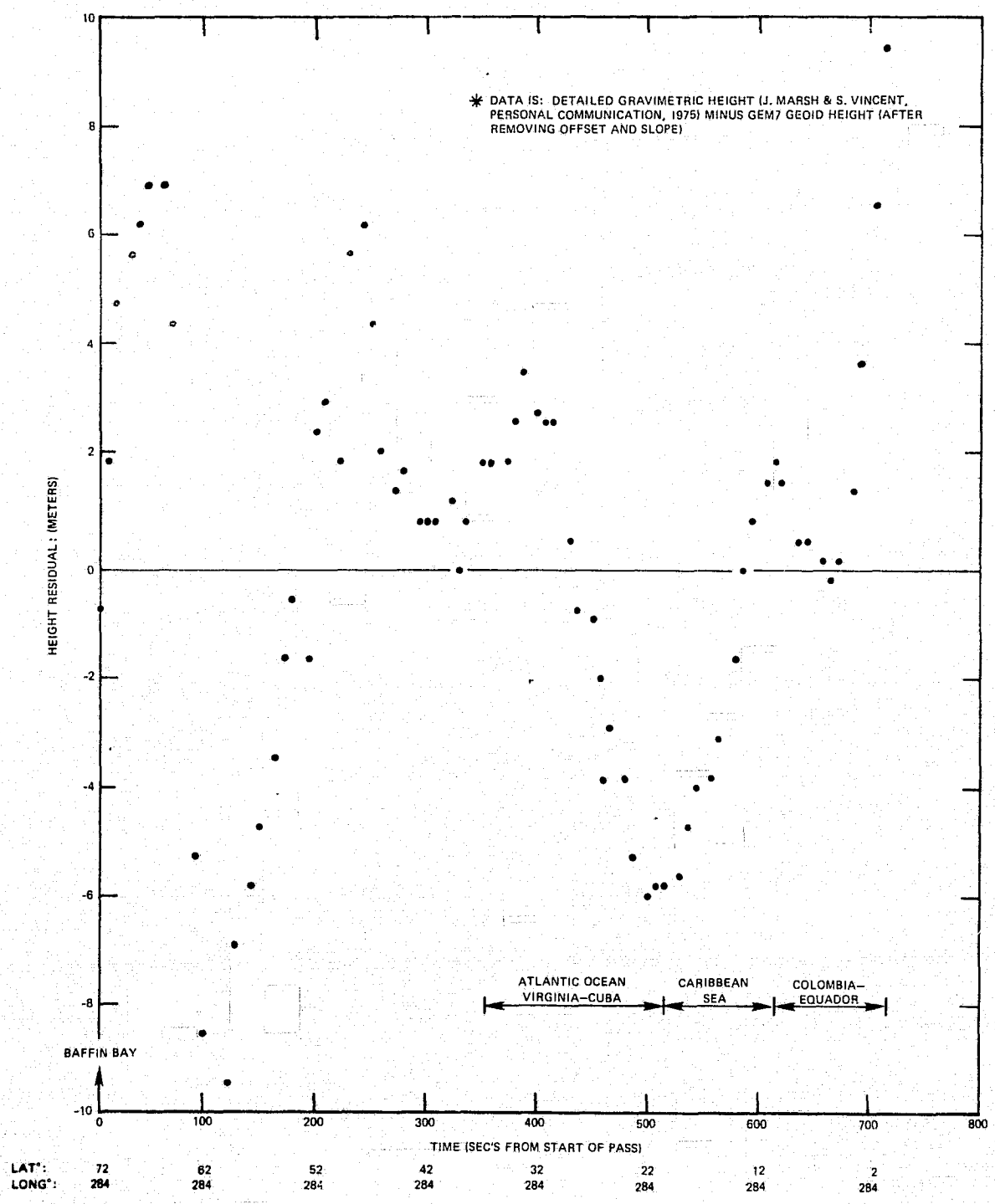

Figure 3m. Height Residuals of Detailed Gravimetric Geoid Residuals with GEM 7* (Simulating a Satellite Altimeter Pass)

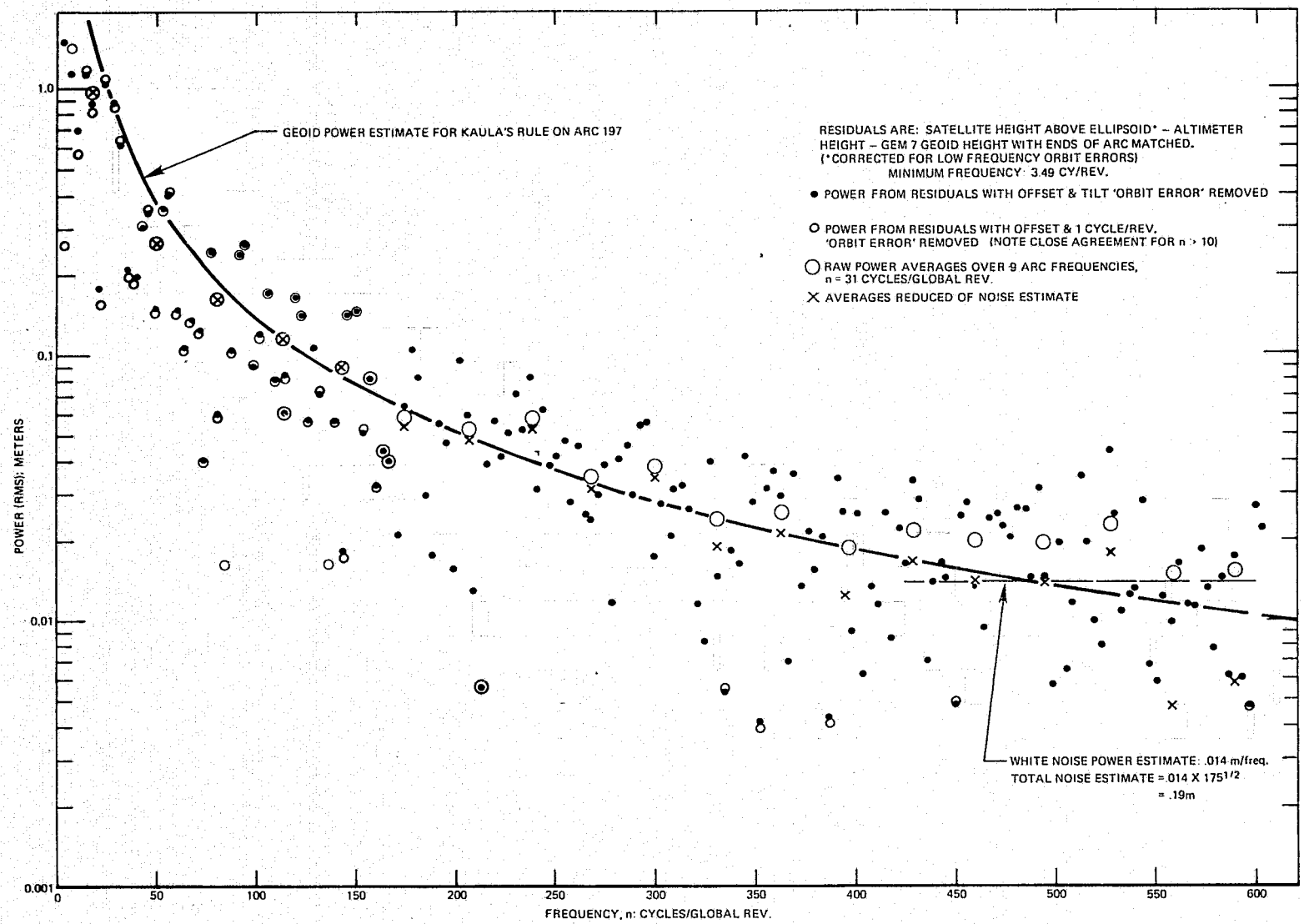

Figure 4a. Power Spectra for Sea Surface Height Residuals from Satellite Altimetry – GEOS 3, Rev. 197

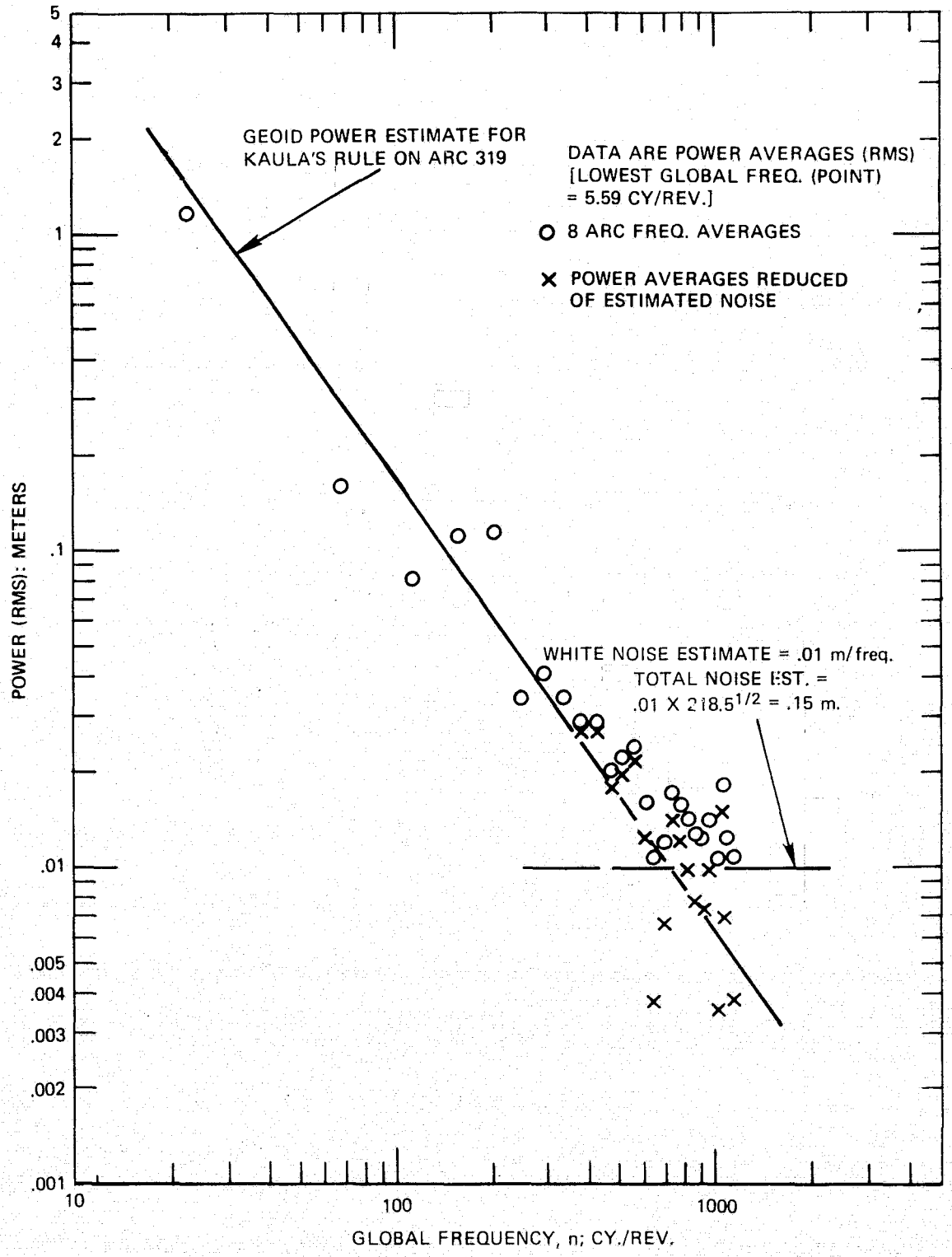

Figure 4c. Power Spectrum for Altimeter Height Residuals: GEOS 3, Rev. 319

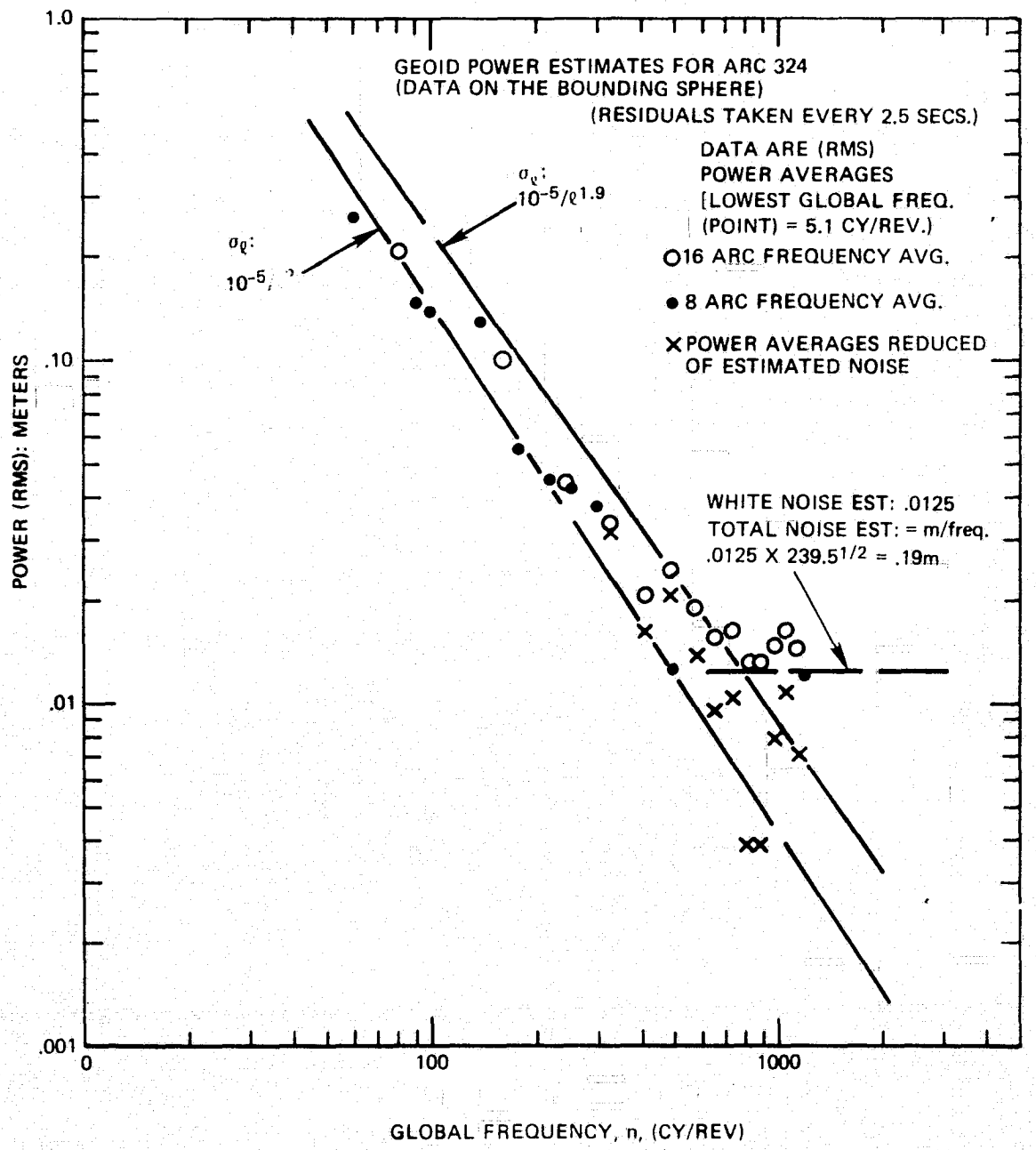

Figure 4d. Power Spectrum for Altimeter Height Residuals: GEOS 3, Rev. 324

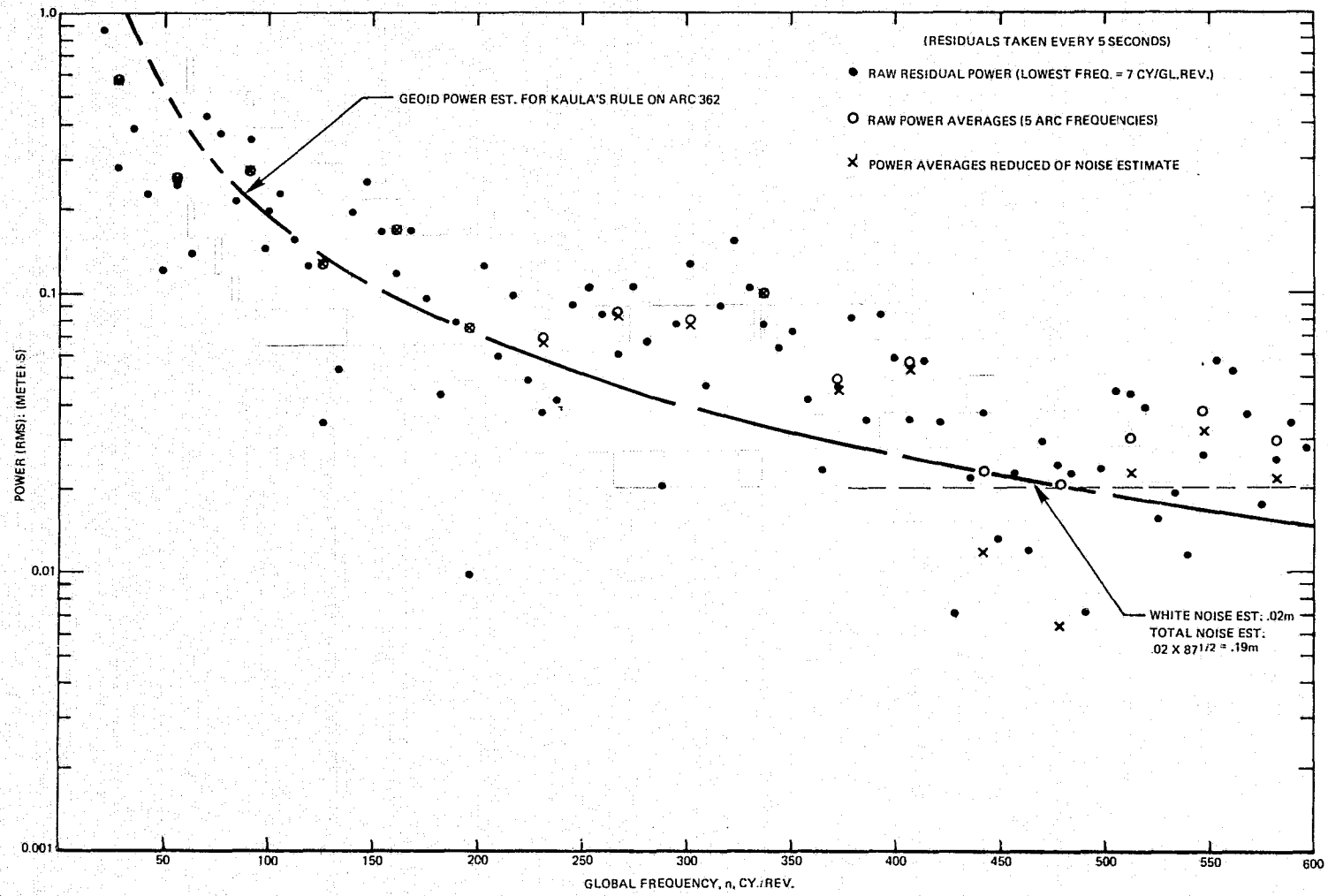

Figure 4e. Power Spectra for Altimeter Height Residuals: GEOS 3, Rev. 362

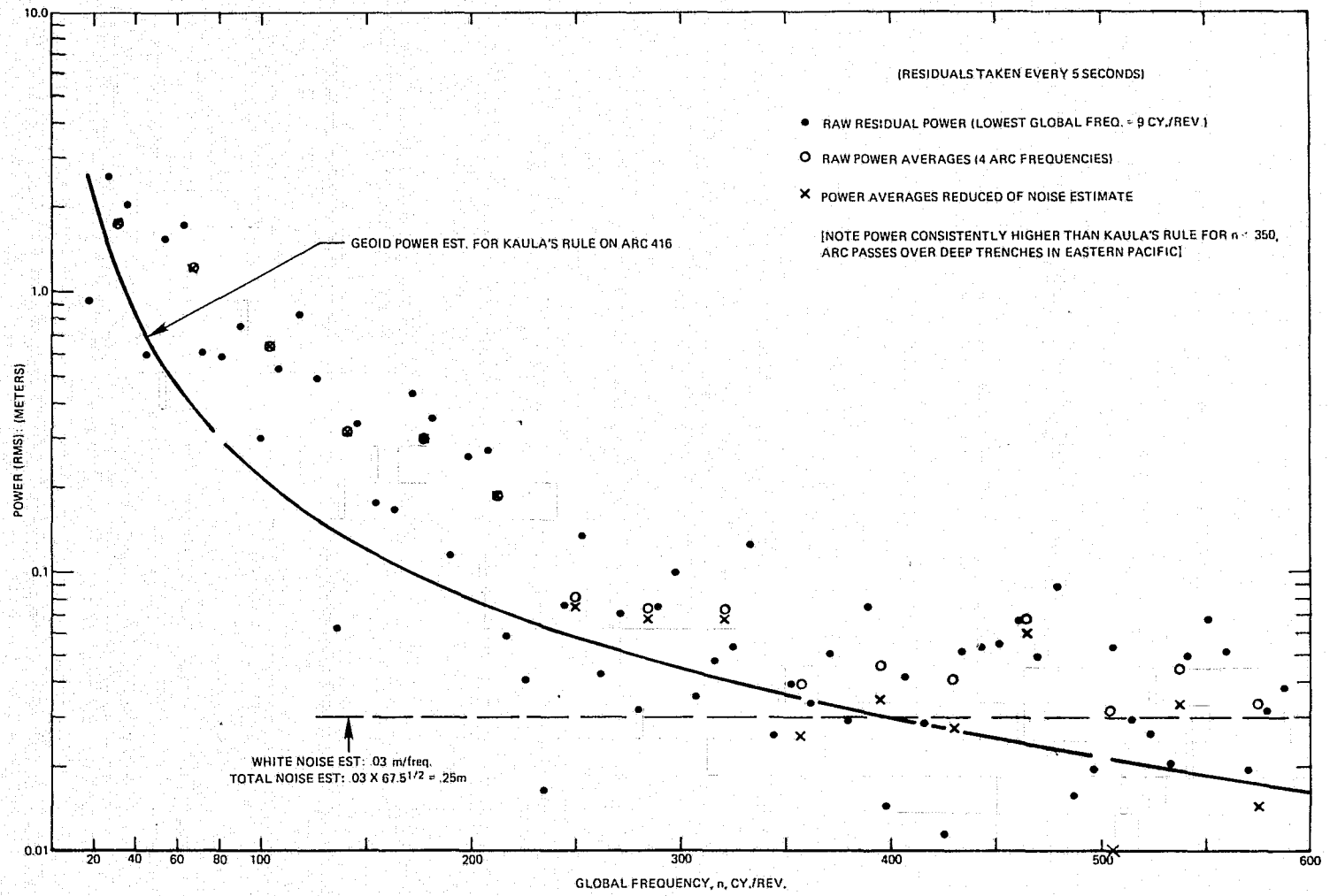

Figure 4f. Power Spectra for Altimeter Height Residuals: GEOS 3, Rev. 416

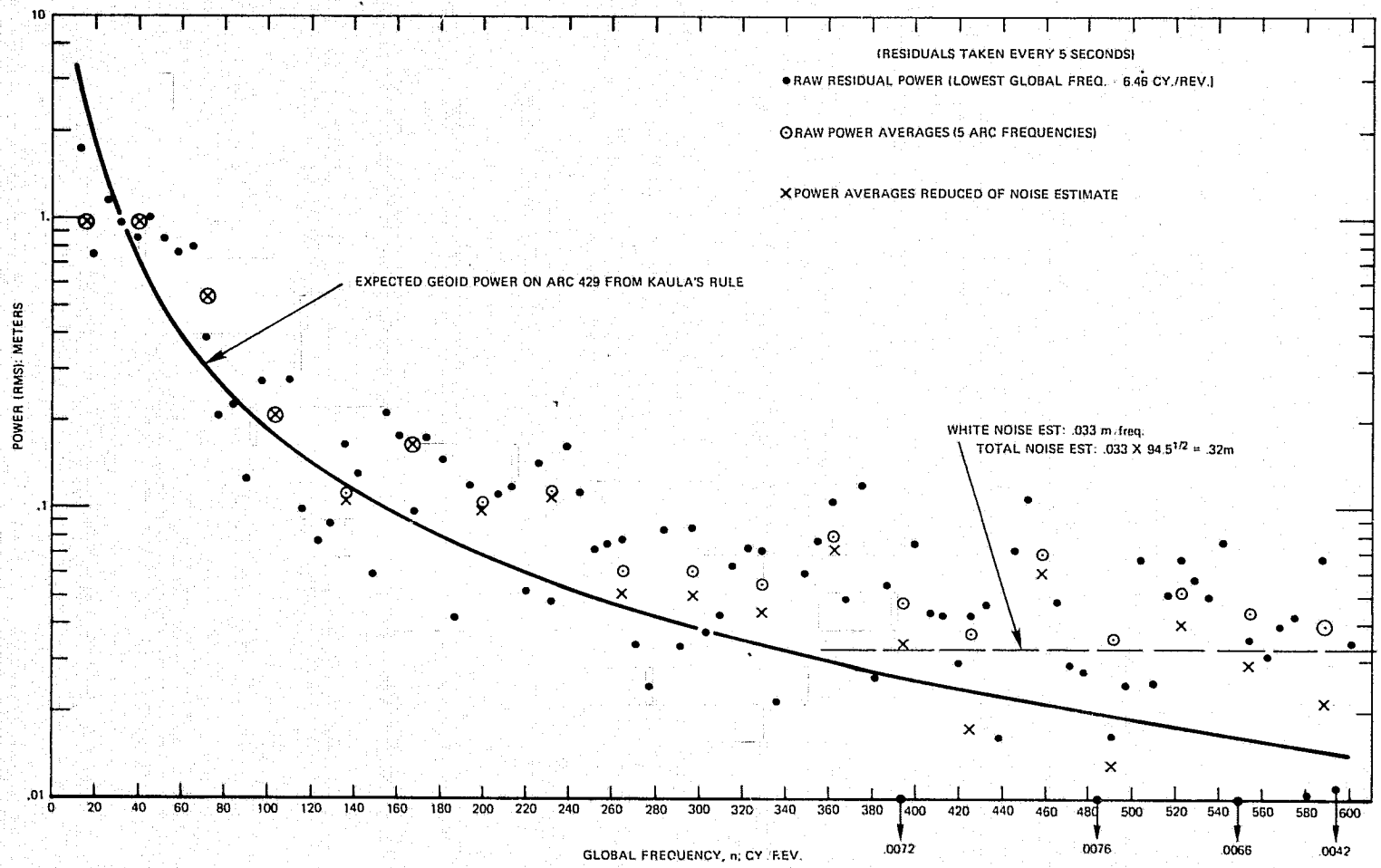

Figure 4g. Power Spectra for Altimeter Height Residuals: GEOS 3, Rev. 429

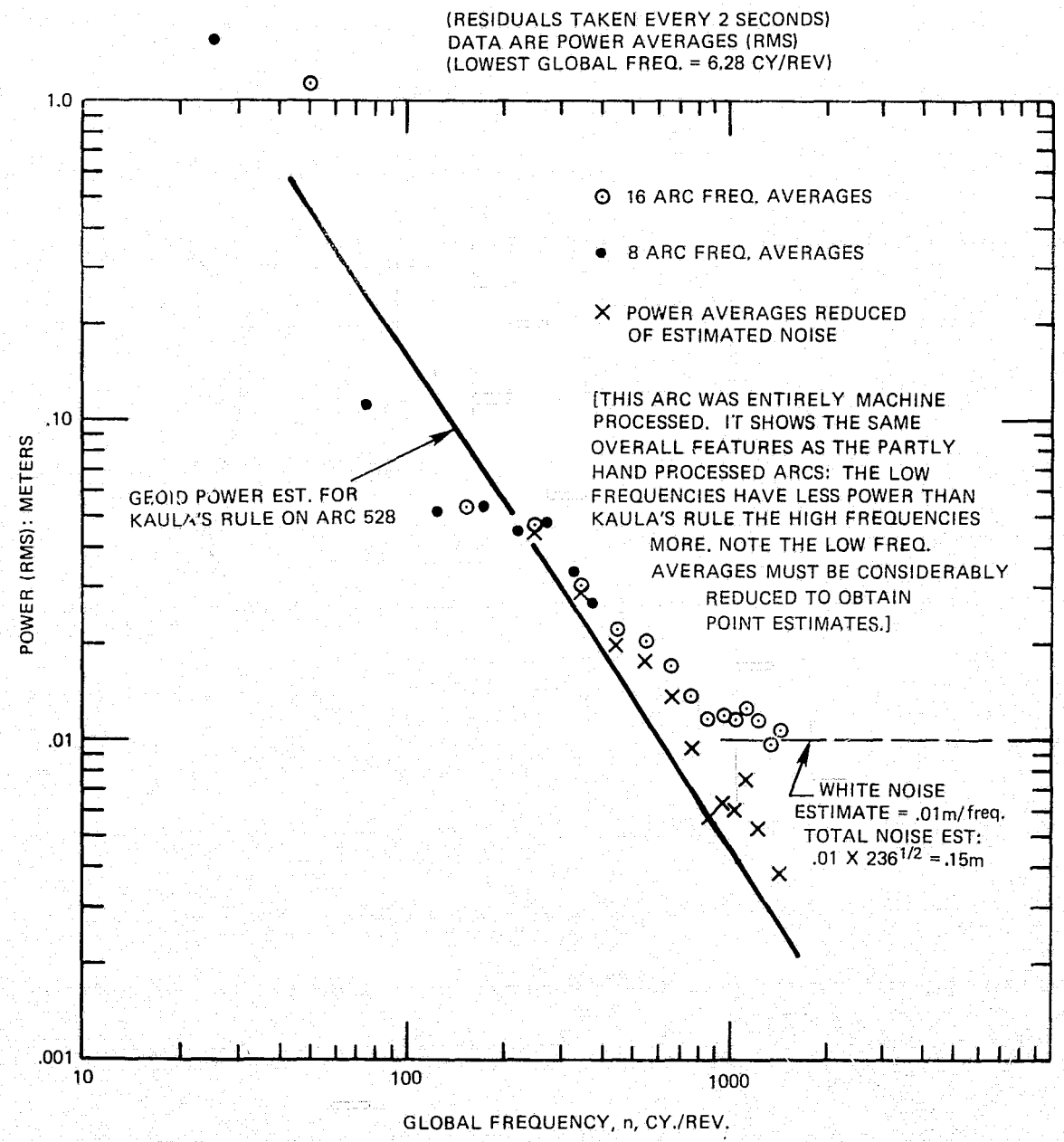

Figure 4h. Power Spectra for Altimeter Height Residuals: GEOS 3, Rev. 528

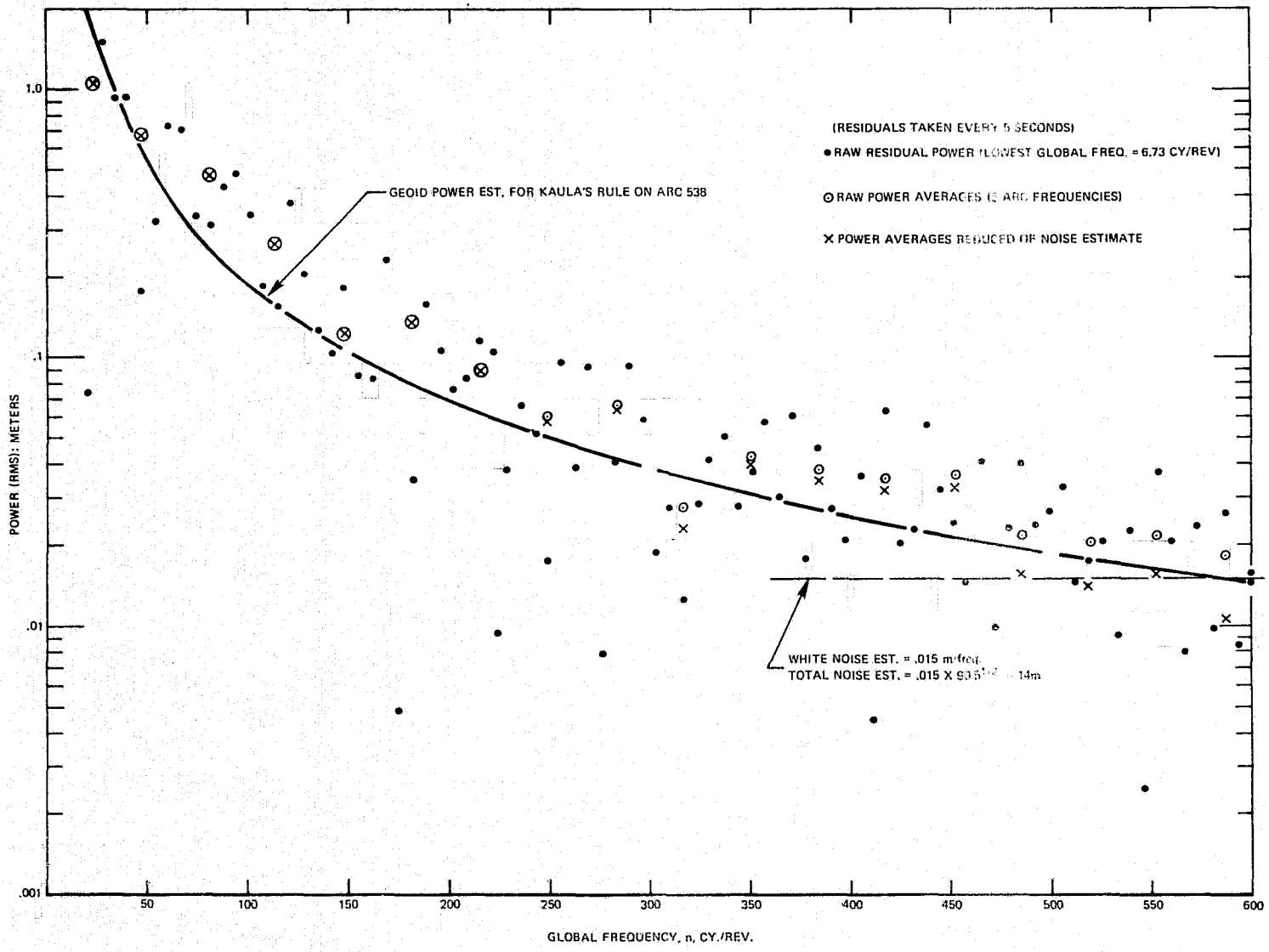

Figure 4i. Power Spectra for Altimeter Height Residuals: GEOS 3, Rev. 538

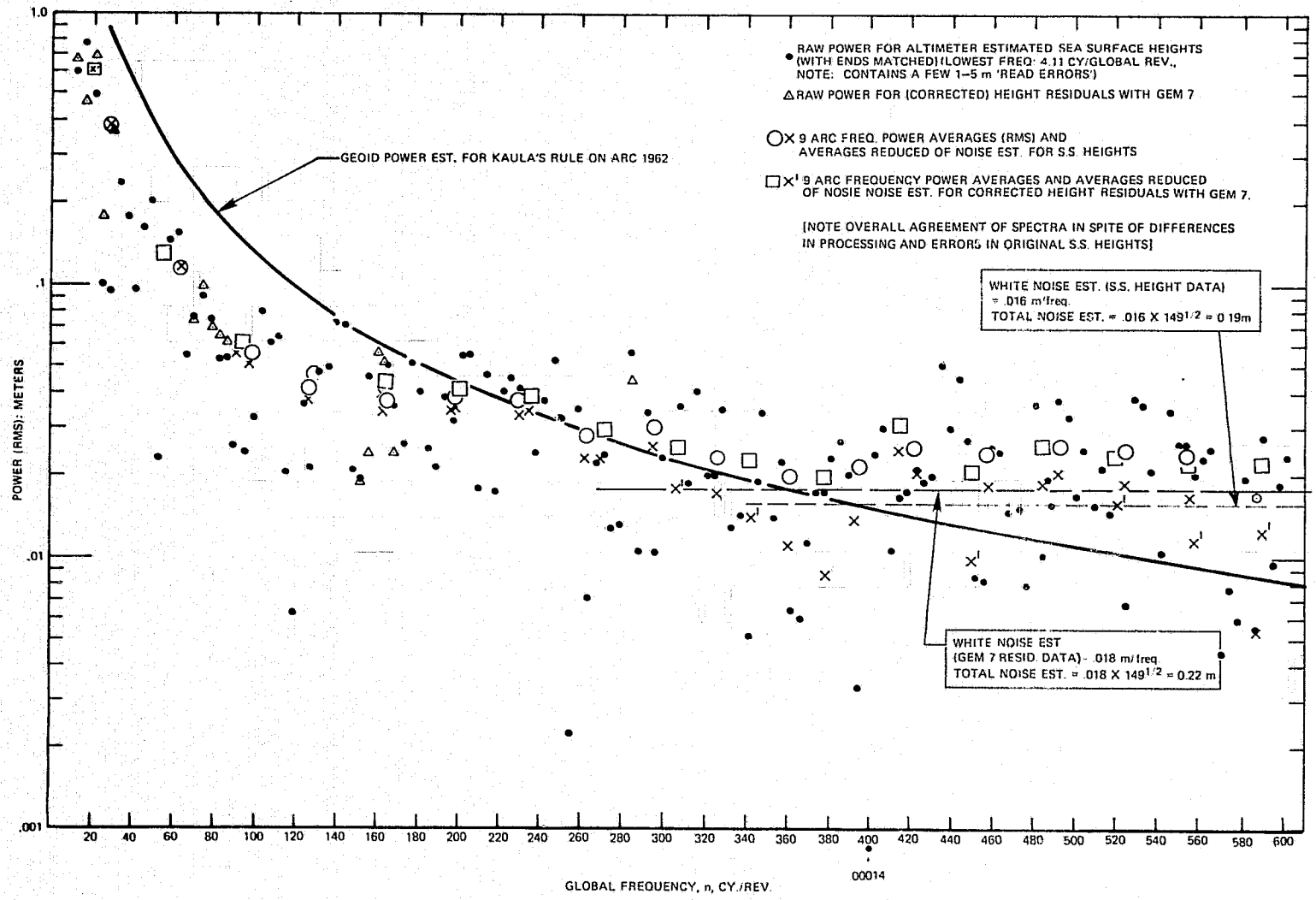

Figure 4j. Power Spectra for Altimeter Height Residuals: GEOS 3, Rev. 1962

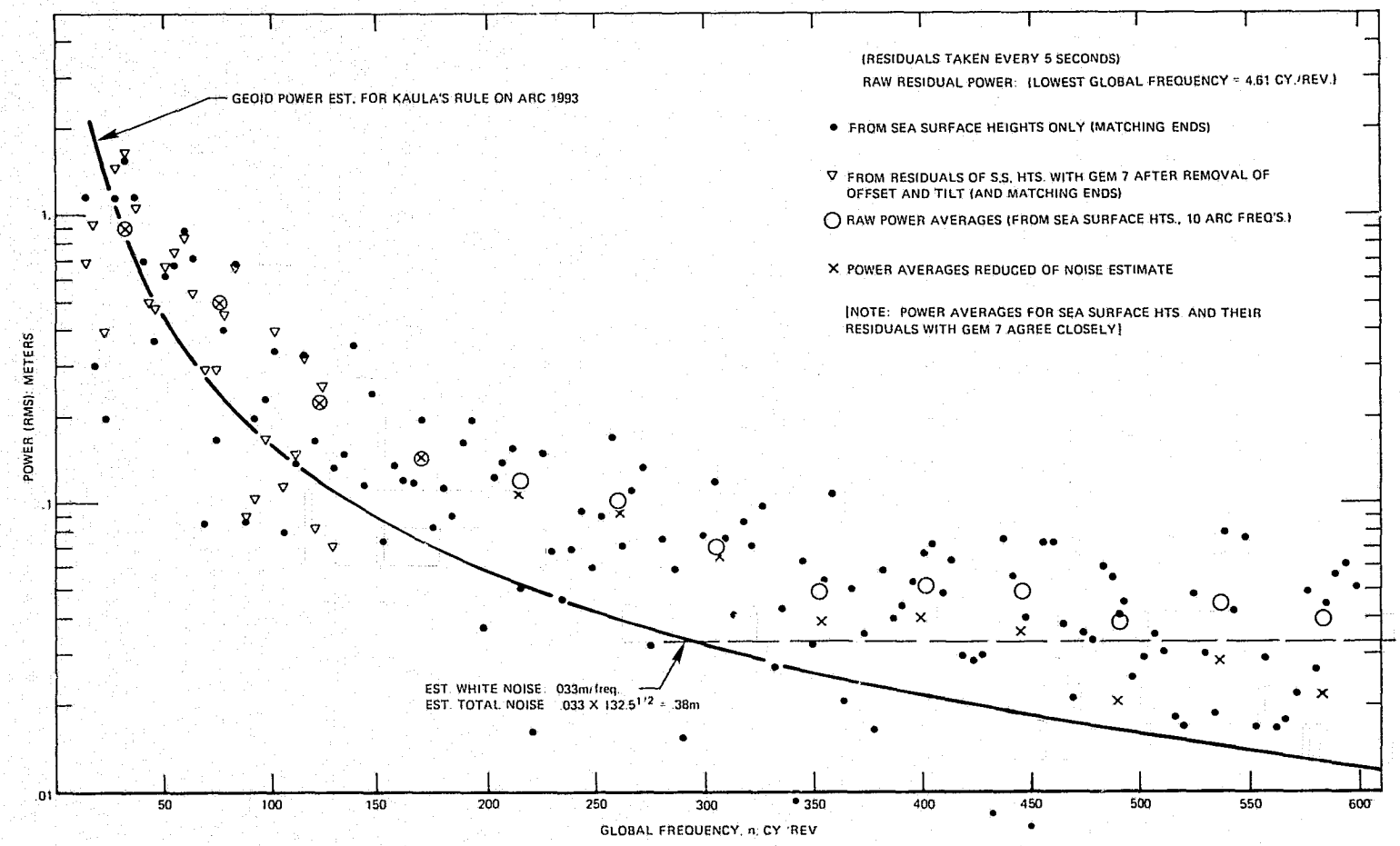

Figure 4k. Power Spectra for Altimeter Height Residuals: GEOS 3, Rev. 1993

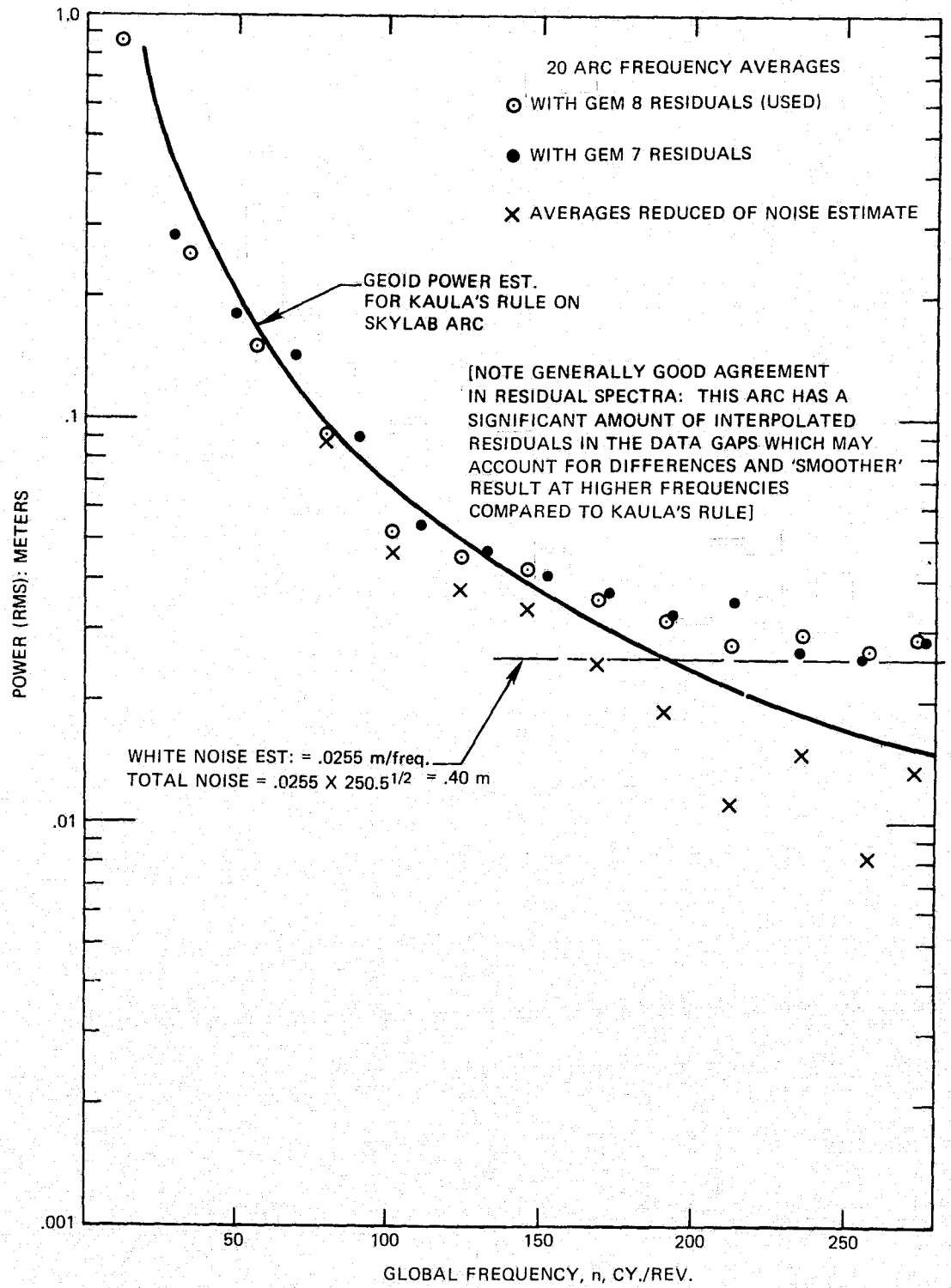

Figure 41. Power Spectrum (Averages) for Altimeter Height Residuals: Skylab: Round-The-World

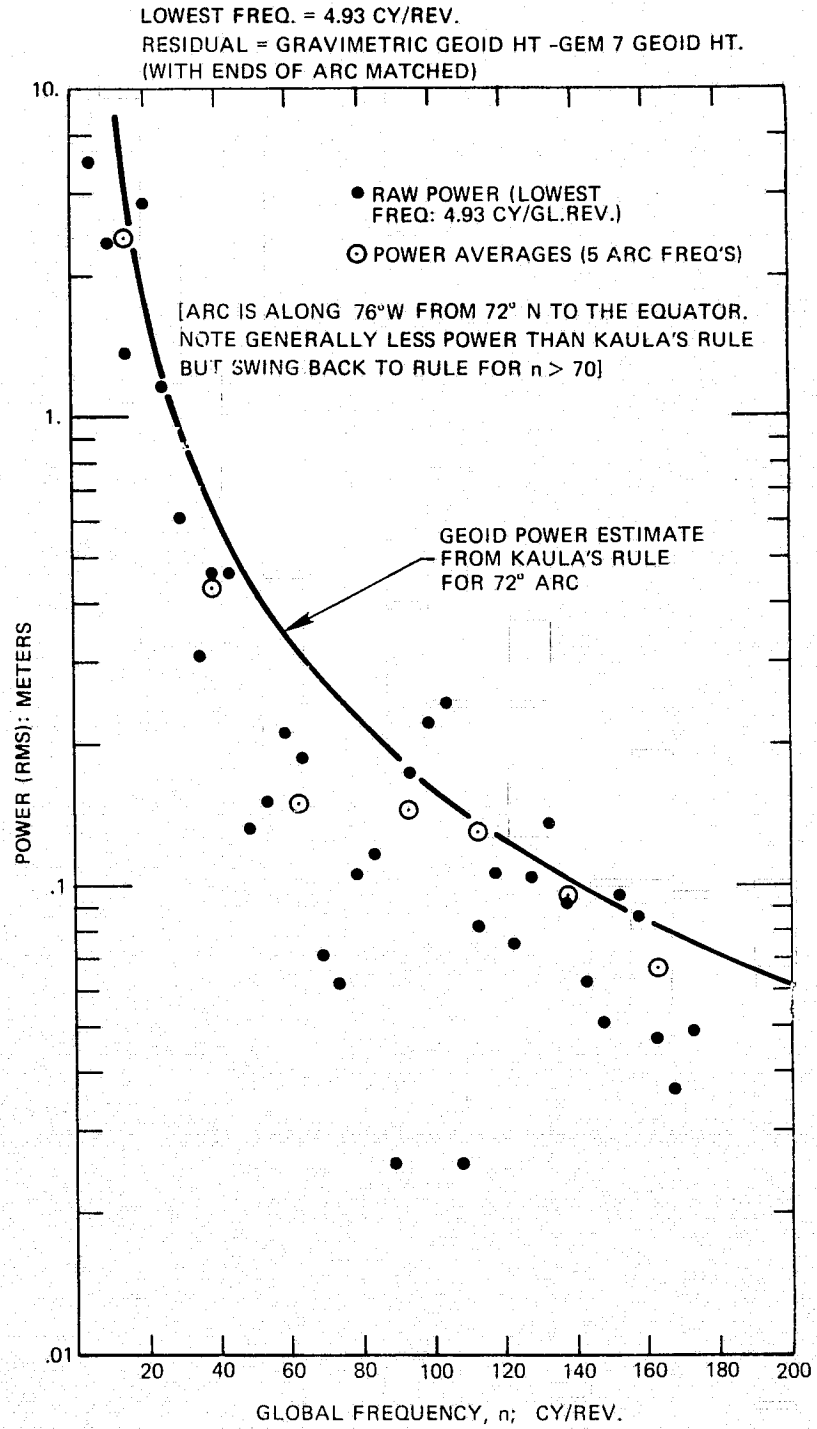

Figure 4m. Power Spectra for Height Residuals from the Gravimetric Geoid Arc (Canada-Equador)

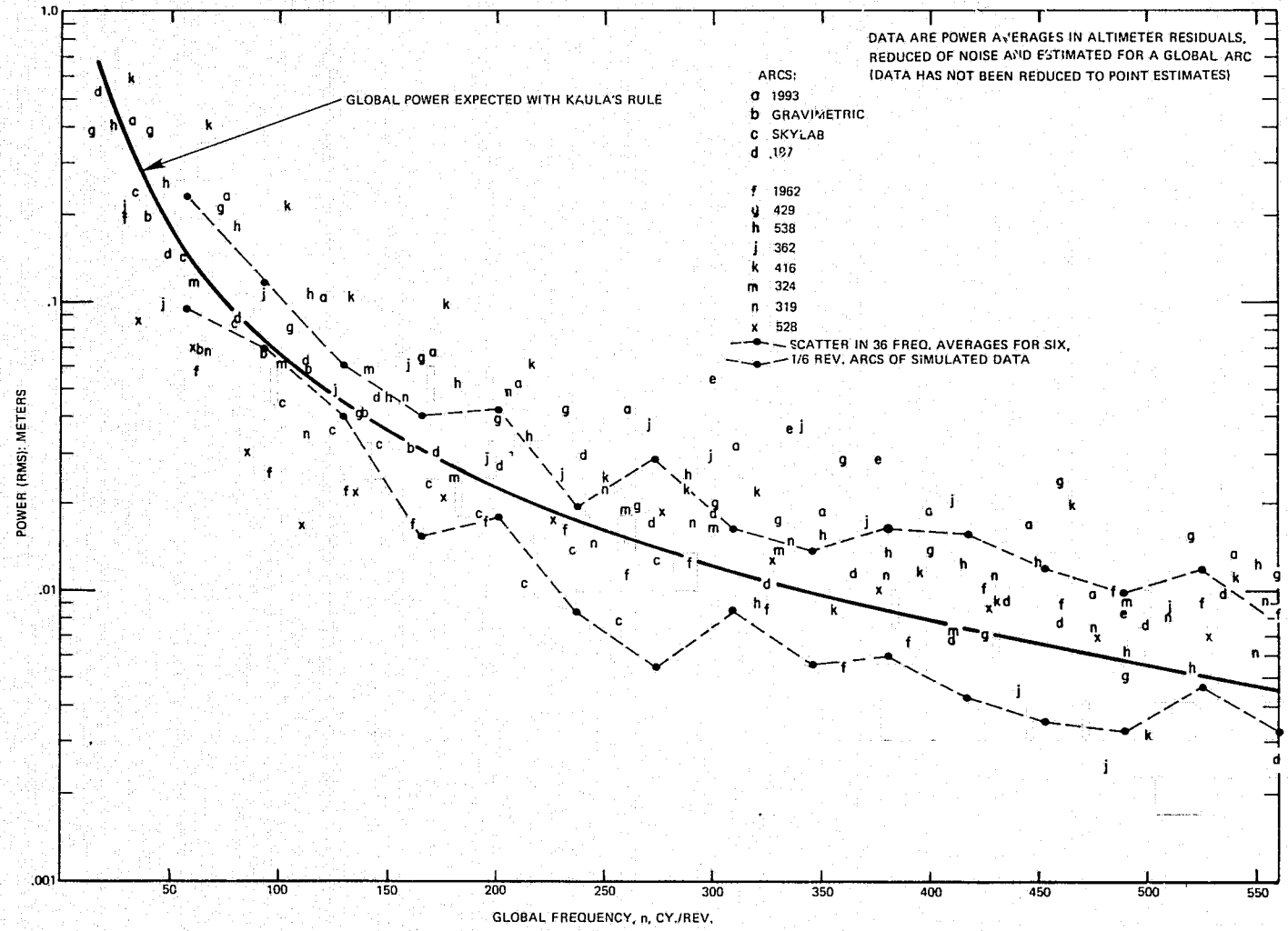

Figure 5. Global Sea Surface-Geoid Power Estimates from Satellite Altimetry Arcs

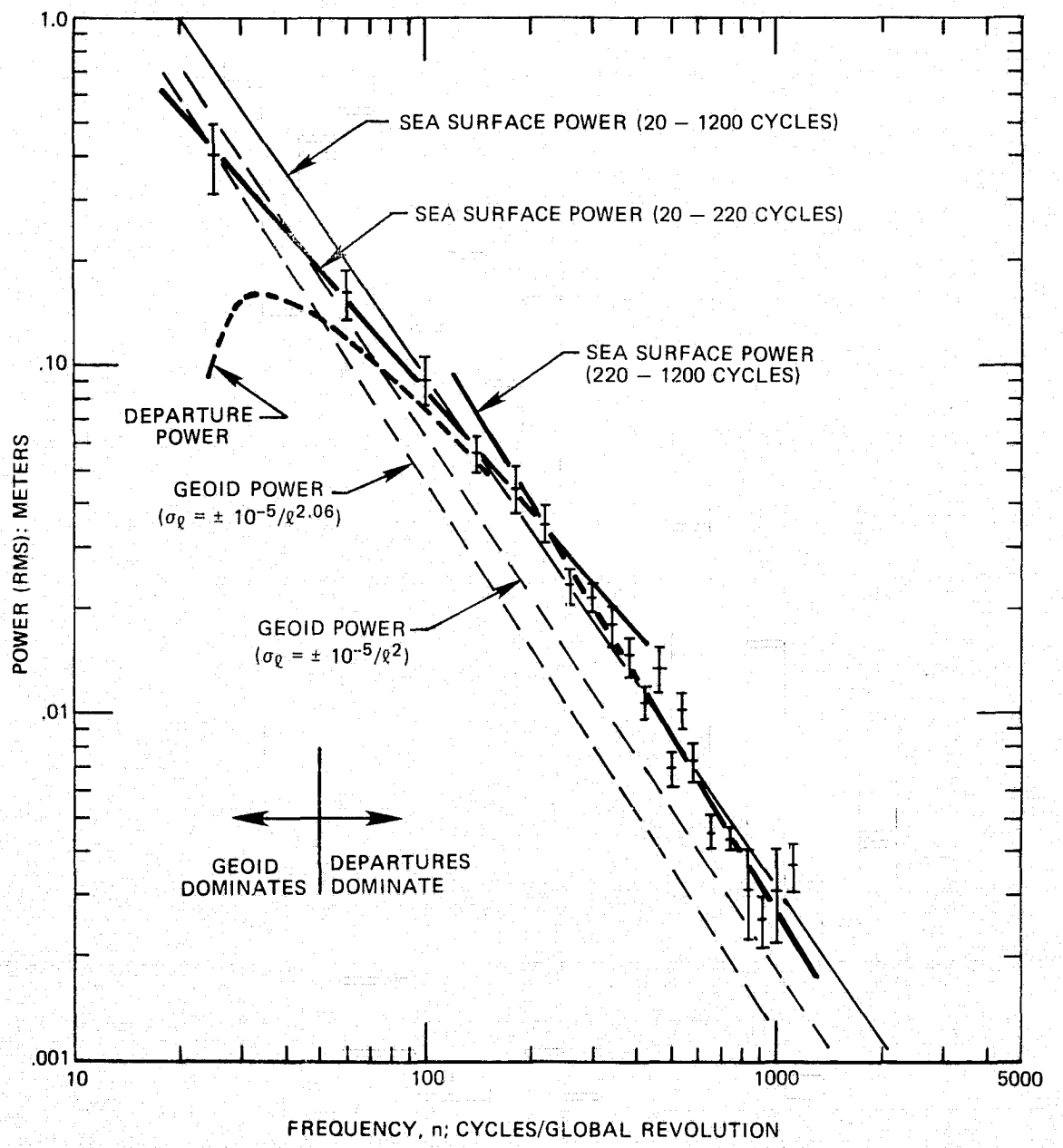

Figure 6. Sea Surface, Geoid and Departure Power for Altimeter Data

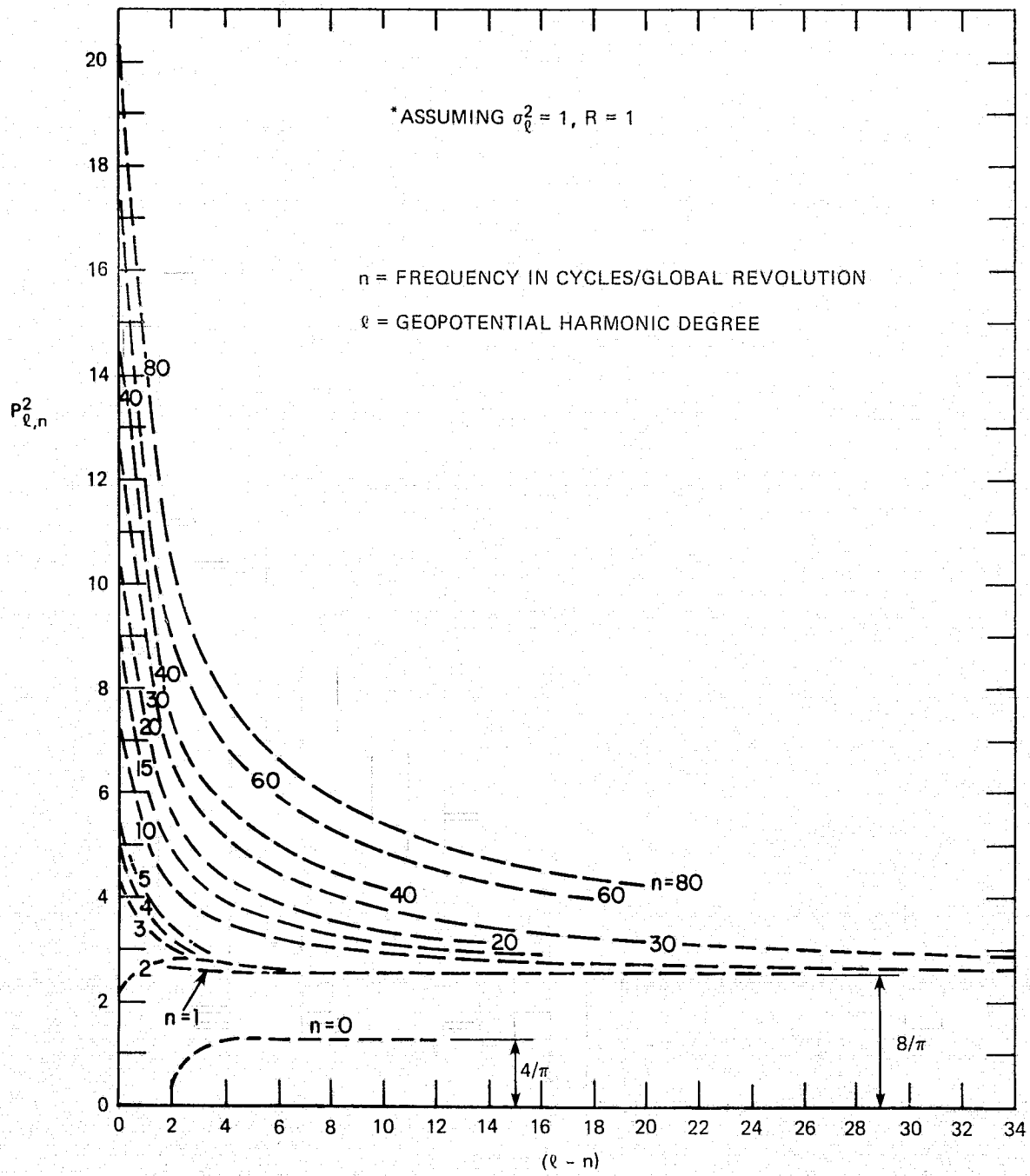

Figure 7. Power Functions for the Altimeter Geoid*

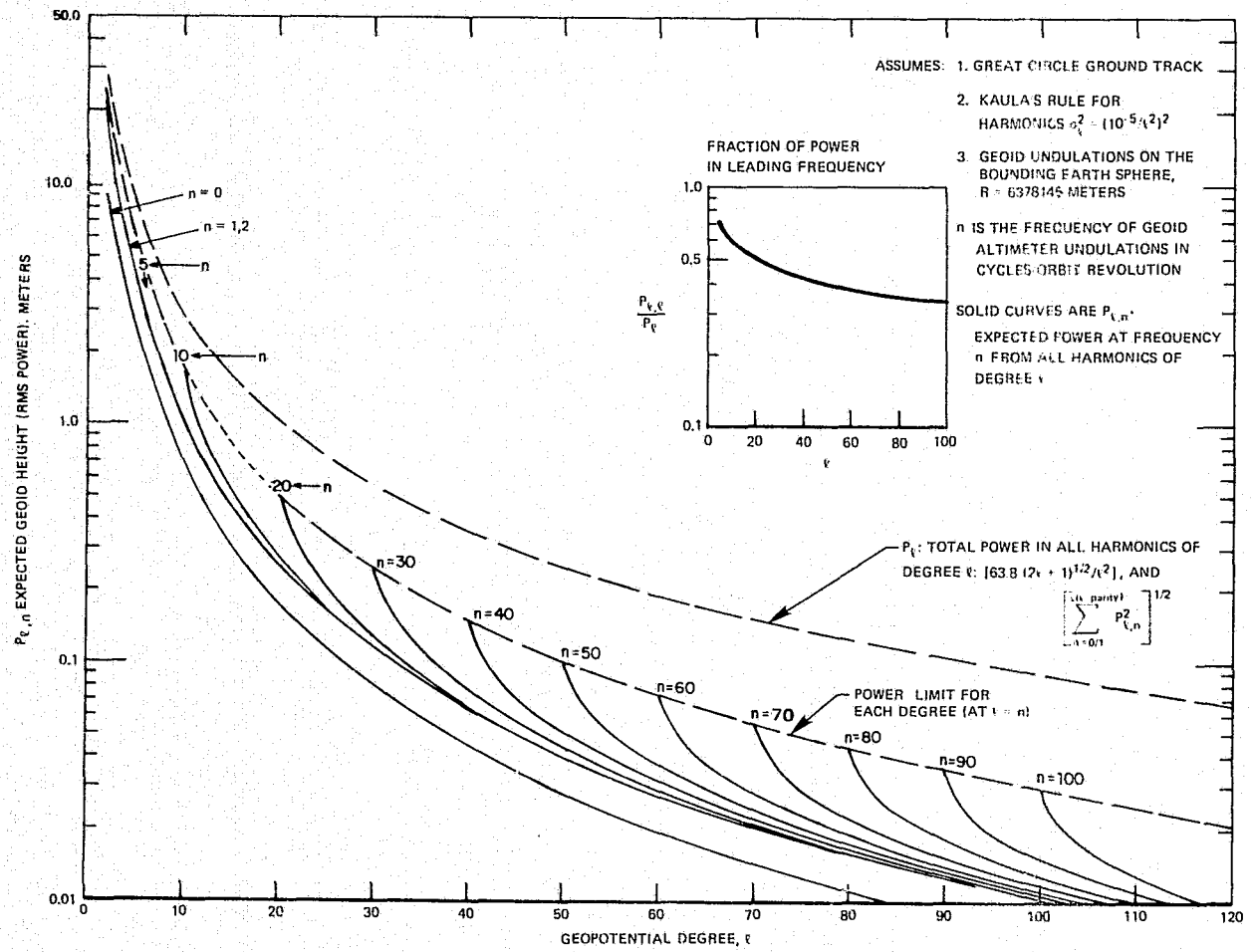

Figure 8. Expected Power Spectrum for the Altimeter Geoid from Geopotential Harmonics

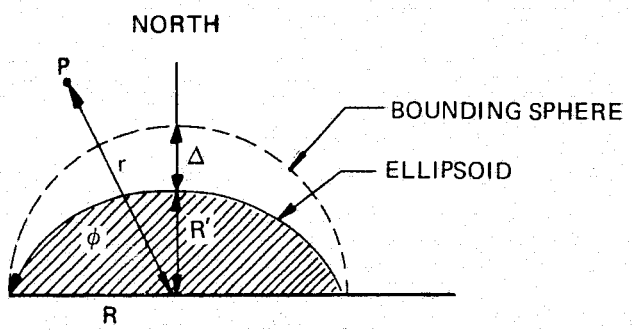

Figure 9. Earth Ellipsoid and Bounding Sphere

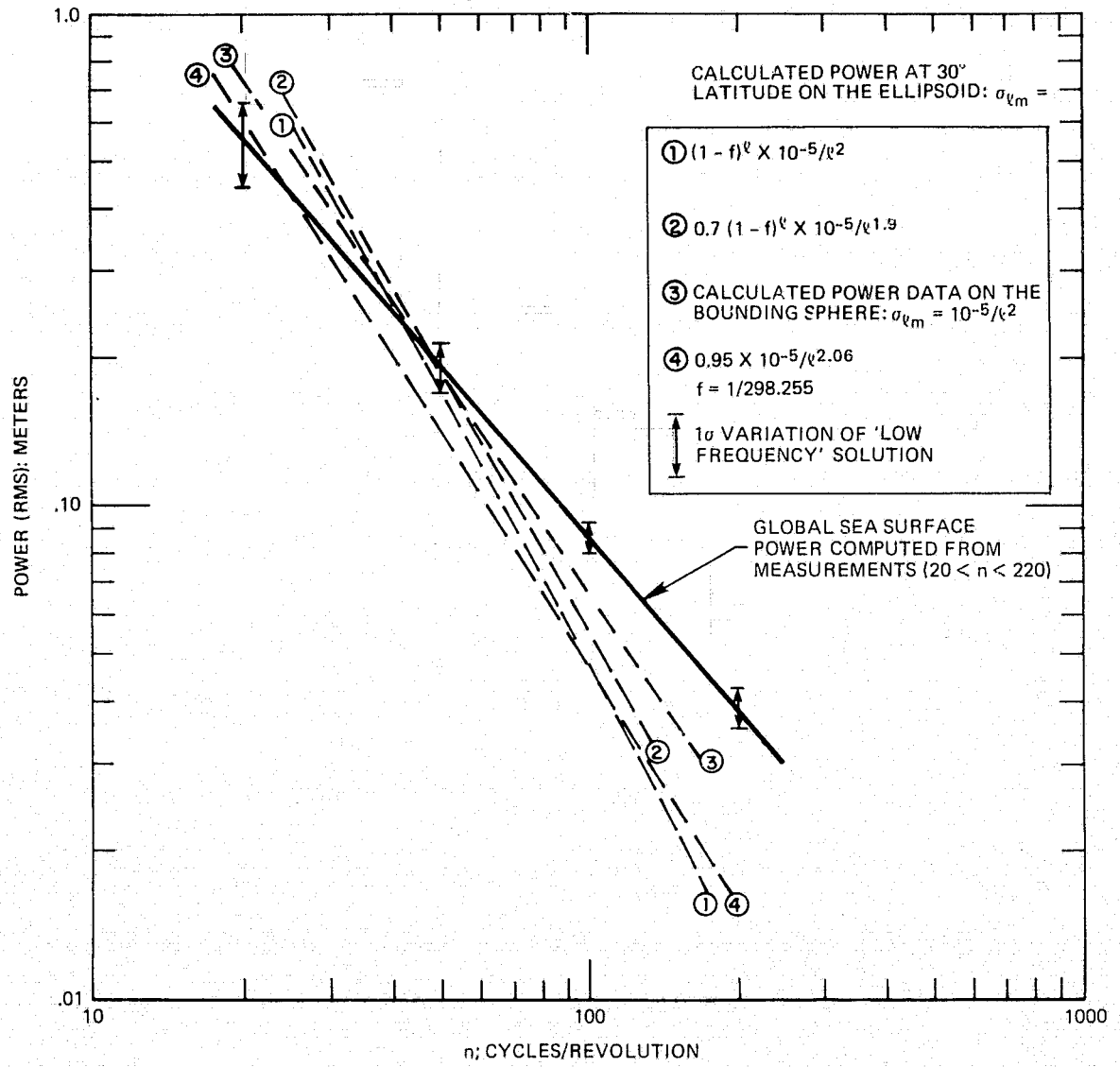

Figure 10. Global Sea Surface and Geoid Power at 'Low Frequencies'

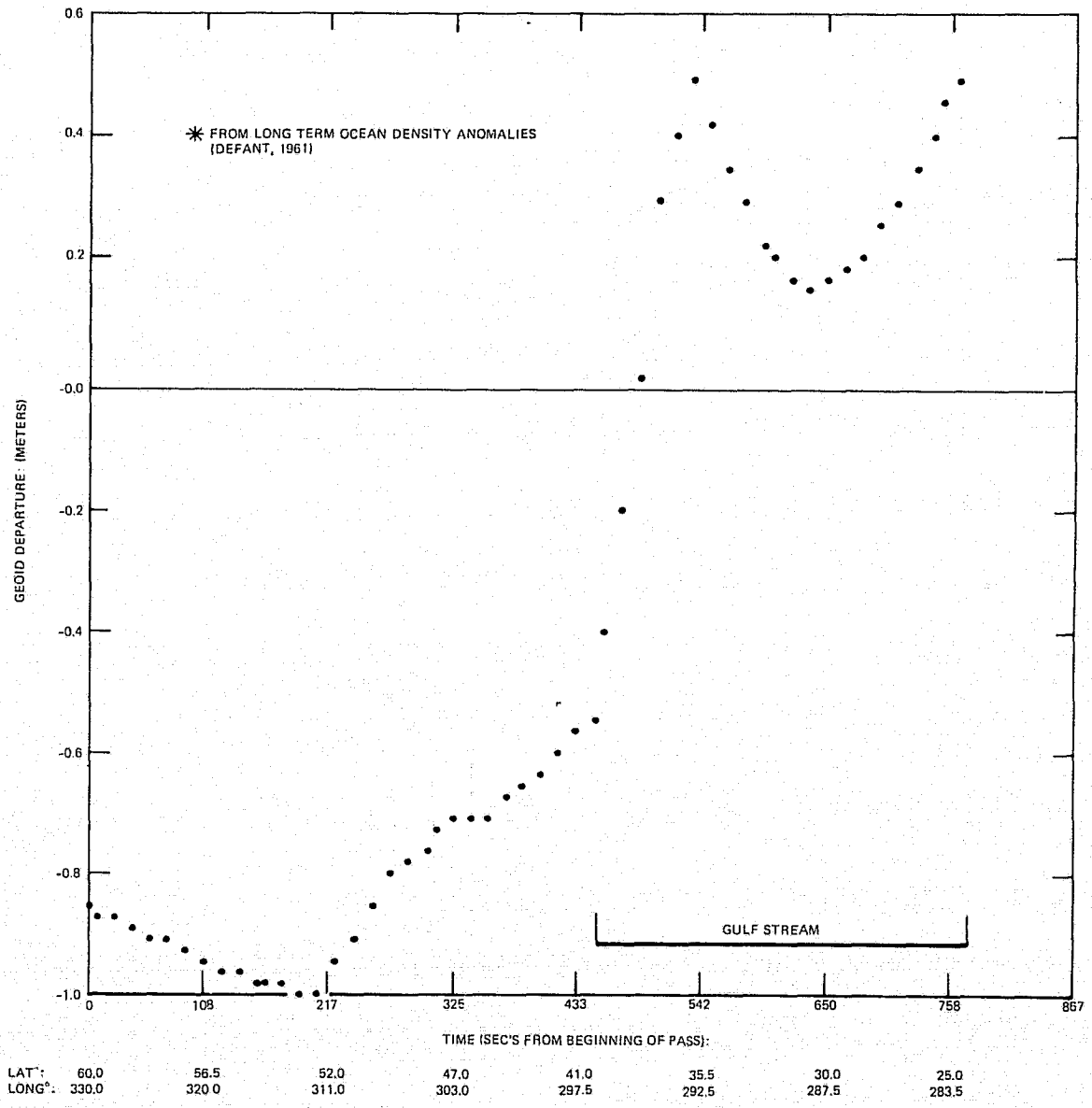

Figure 11. Estimated Geoid Departures Along the Track of GEOS 3, Rev. 197*

ORIGINAL DATA (ALONG GEOS 3 TRACK REV. 197):
MEAN SEA SURFACE TOPOGRAPHY FROM DENSITY
DIFFERENCES (DEFANT, 1961). SEE FIGURE 11

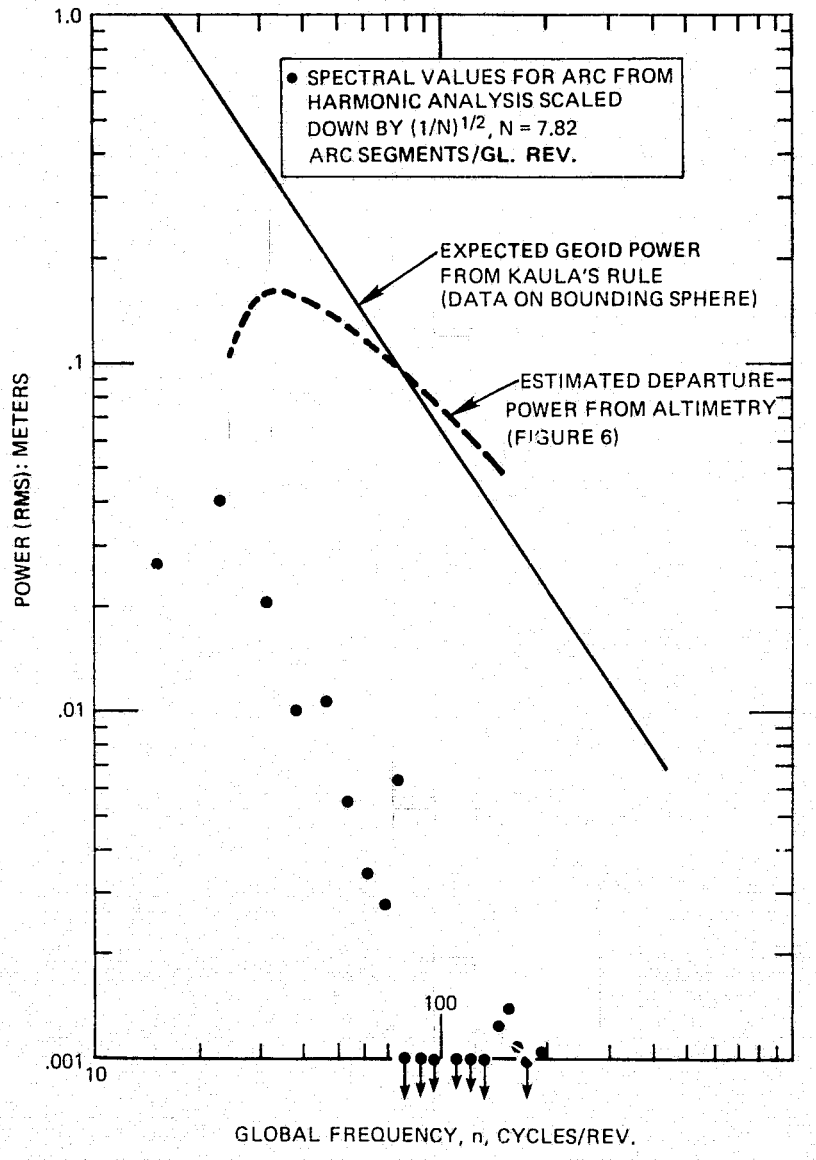

Figure 12. Global Spectrum for Estimated Geoid Departures Along One Arc

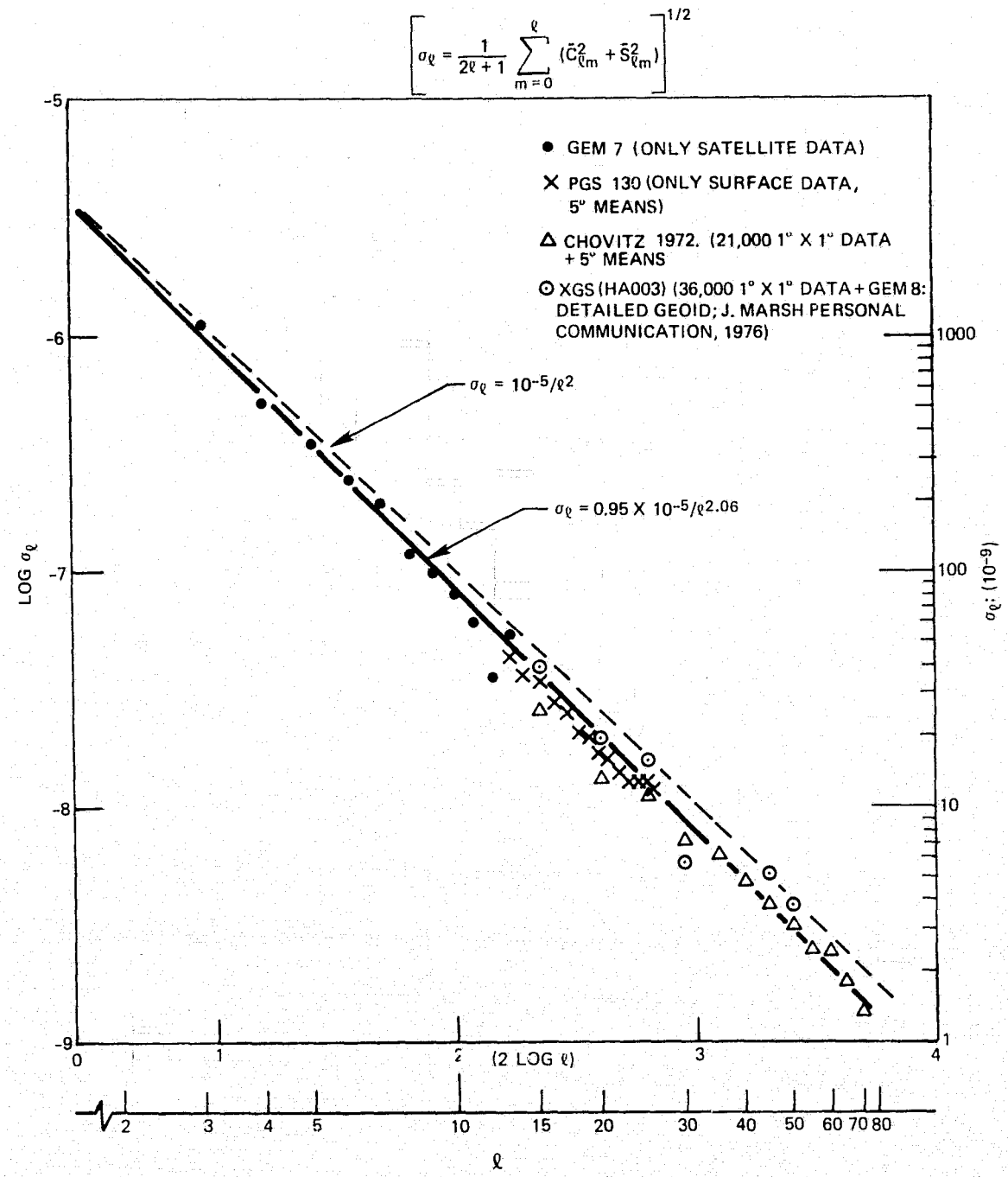

Figure 13. Mean Potential Coefficient by Degree from Satellite and Gravimetry Data

Table 1
Statistics of Altimeter Data and Arcs Used

Arc (Rev. #)	Length (Min.)	n ≥ 20 Cy/Global Rev. – From Harmonic Analysis of Residuals	Rms Sea Surface Ht. Residual (| Max Residual |) (m)			Comment (All GEOS 3 arcs except as noted are reduced with bias & tilt orbit error removed)
			GEM 7	GEM 8	GEM 8N	
416	11.2	4.00	4.87 (17.8)	6.68 (24.4)	5.40	Japan – Celebes, over deep west pacific trenches
197	29.1	1.88	2.96 (9.2)	3.61 (9.3)	3.04	Norway – Equador over Puerto Rico trench
1962	24.8	0.79	7.37 (3.5)	1.85 (4.6)	1.56	California – New Zeland
1993	22.2	3.11	3.32 (13.1)	4.72 (12.8)	3.55	Alaska – New Guinea
429	15.6	2.48	2.58 (8.7)	4.96 (14.6)	3.44	North Pacific – New Guinea
362	14.4	1.47	2.12 (4.2)	1.91 (5.9)	2.10	Kenya – Cape of Good Hope (Indian Ocean)
Gravimetric	20.3	2.38	4.07 (9.9)	3.21 (9.0)	3.26	Canada – Equador (from detailed geoid, 1975)
538	15.1	2.55	3.09 (10.8)	3.12	3.03	Nova Scotia – Equador
528	16.1	0.68	3.18 (8.1)	2.92 (6.9)		South Atlantic – Antartic over Mid Atlantic and Antartic Ridges
Skylab (Round-the-World)	83.3	1.80	3.24 (9.8)	4.7 (10.5)	3.8	'Round the World', South Atlantic - Indian Ocean - Pacific Trenches - Caribbean
324	19.9	1.81	3.22 (7.7)	2.59 (6.7)	2.06	North Atlantic: Norway-Venezuela
319	18.2	0.98	3.07 (8.7)	2.79 (6.6)	1.69	West Coast of North America - Mexico - Siberia
Totals	290.2	2.20 (rms)	3.20	3.84	3.18	

Table 2
Aggregate Sea Surface-Geoid Power Estimates from Altimetry

Frequency (Cy./Rev.)		Number of Arcs Contributing (All from Table 1)	Raw Mean Power (rms) m	Estimated Point Power [(rms): Mean Power Reduced for Range of Frequencies - See Appendix D] m
Mid Point	Range			
25	10-40	12	.63 ± .15	.403 ± .096
60	40-80	13	.181 ± .030	.161 ± .027
100	80-120	15	.095 ± .015	.091 ± .014
140	120-160	14	.057 ± .007	.056 ± .007
180	160-200	13	.045 ± .0073	.0444 ± .0072
220	200-240	13	.0351 ± .0046	.0350 ± .0046
260	240-280	13	.0234 ± .0028	.0233 ± .0028
300	280-320	10	.0215 ± .0019	.0215 ± .0019
340	320-360	11	.0180 ± .0024	.0180 ± .0024
380	360-400	11	.0148 ± .0019	.0148 ± .0019
420	400-440	10	.0108 ± .0012	.0108 ± .0012
460	440-480	10	.0134 ± .0021	.0134 ± .0021
500	480-520	10	.0070 ± .0008	.0070 ± .0008
540	520-560	10	.0102 ± .0012	.0102 ± .0012
580	560-600	11	.0073 ± .0009	.0073 ± .0009
647	600-700	3	.00456 ± .00045	.00456 ± .00045
740	700-800	3	.00436 ± .00030	.00436 ± .00030
822	775-875	3	.00314 ± .00091	.00314 ± .00091
912	875-975	3	.00256 ± .00043	.00256 ± .00043
1005	950-1050	3	.00313 ± .00093	.00313 ± .00093
1120	1050-1175	5	.00371 ± .00063	.00371 ± .00063

Table 3
Characteristics of Potential (or Undulation)
Variances* on the Geoid

	σ_ℓ^2:					
	$(1-f)^\ell \times 10^{-5}/\ell^2$**			$.7(1-f)^\ell \times 10^{-5}/\ell^{1.9}$		
	$\phi = 90°$	$\phi = 45°$	$\phi = 0°$	$\phi = 90°$	$\phi = 45°$	$\phi = 0°$
5	1	.992	.983	.822	.816	.809
10	1	.983	.967	.881	.867	.852
25	1	.958	.919	.966	.926	.888
100	1	.845	.715	1.109	.938	.793
200	1	.715	.511	1.189	.850	.608
300	1	.604	.365	1.238	.748	.452
500	1	.432	.187	1.303	.564	.244
1000	1	.186	.035	1.397	.260	.049

*In Units of the value for $\sigma_\ell^2 = [10^{-5}/\ell^2]^2$.
**f = 1/298.255 = .996647

APPENDIX A

EXPECTATION OF 'READ ERROR' FROM ALTIMETER STRIP CHARTS

A major source of error in the data reduction scheme was the height estimation read from the 'smoothed' sea surface line on the strip charts [e.g. Figure 1] . These heights could only be read to the nearest 0.5m (1m for Skylab). While this may seem to sacrifice the excellent quality of the 'sea surface' line, the standard error of this truncating process is actually considerably smaller than the discrimination interval.

Referring to Figure A1, let ϵ be the maximum read error. Assume it is equally probable for the correct sea height to fall within the discrimination interval. That interval will be 2ϵ and the probability distribution will be rectangular (gray area). The constant probability (a) is $1/2\epsilon$ since

$$\int_{-\epsilon}^{\epsilon} a\,d\delta = 1 .$$

The variance of the error with this distribution is:

$$VAR(\delta) = \int_{-\epsilon}^{\epsilon} \delta^2 p(\delta)\,d\delta = \frac{1}{2\epsilon}\left[\frac{\epsilon^3}{3} + \frac{\epsilon^3}{3}\right] = \frac{\epsilon^2}{3} .$$

Thus, for Skylab the minimum standard 'read error' should be $(1/2)/\sqrt{3} = 0.289$m, surprisingly small for a discrimination interval of 1m. For GEOS 3 the corresponding minimum error is 0.144m.

The actual noise estimate for the Skylab record was 0.4m (Figure 4-1) but a few GEOS arcs appear to approach the minimum figure (e.g. Figure 4c). However there is a general tendency to underestimate the noise since it is always taken as the lower bound of all the averaged data. (This tendency can be minimized with sufficient averaging. But then the resolution of the 'signal' is compromised.) In fact a good number of GEOS 3 noise estimates are 2 to 3 times this minimum. These do not seem to reflect actual signal. In none of these high noise spectra do the averages continue to decline significantly at the highest frequencies.

The high noise arcs probably contain more than a few 'points' read with an error greater than ϵ. It is very unlikely (in this circumstance) that an error greater than 2ϵ can be made. This would involve reading more than one interval 'off'. [Such gross blunders will be discussed shortly]. However, errors between $|\epsilon|$ and $|2\epsilon|$ should happen occasionally. I simplify the likely distribution of errors as including the dashed 'tails' in Figure A1. The analysis of this (more realistic) 'small blunders' distribution is straightforward. The standard error is given as:

$$\text{STD ERROR} = \epsilon\,[5/6]^{1/2}.$$

For Skylab the result is 0.456m. For GEOS 3 this maximum reasonable (standard) error should be 0.228 m. The fact that a fair number of spectra exceed this figure

(and even more would with sufficient averaging) indicates that a few gross blunders ($|\epsilon| > 0.5$m) were probably made in reading the strip charts.

What would be the effects of a few gross blunders (say ϵ = 1m for the GEOS arcs)? The spectrum of an impulse function is flat. This can be seen most simply for discrete sampling where

$$(c_n, s_n) \doteq \frac{1}{\pi} \sum_{i=1}^{N} f_i \Delta \{\cos[n(i\Delta)], \sin[n(i\Delta)]\}. \qquad \text{(A1)}$$

In equation (A1) N (equally spaced) points of f are sampled at intervals of Δ. But $\Delta = 2\pi/N$, so that (A1) becomes:

$$(c_n, s_n) \doteq \frac{2}{N} \sum_{i=1}^{N} f_i \{\cos(2\pi in/N), \sin(2\pi in/N)\}. \qquad \text{(A2)}$$

If the 'impulse' (f = h) occurs at $i\Delta = T$, only one term of the right side of (A2) remains (f = 0 everywhere else) and:

$$(c_n, s_n)_{\text{IMPULSE}} \doteq \frac{2h}{N} (\cos Tn, \sin Tn). \qquad \text{(A3)}$$

Thus the power is constant and independent of T:

$$P_n \doteq \sqrt{2}\ h/N. \qquad \text{(A4)}$$

For example, a typical GEOS 3 arc has 150 residual 'points' so that with h = 1m, P_n (blunder) $\doteq$ .01m/freq. This level could be a significant contribution to the 'noise' figures for all the GEOS arcs (see Figures 4).

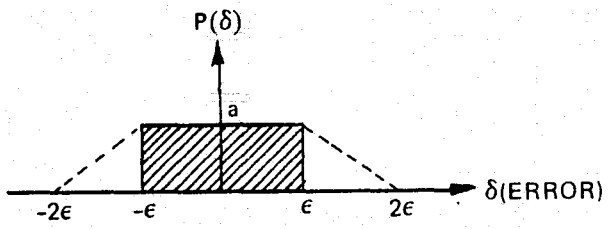

Figure A1. Probability Distributions for 'Read' Error

APPENDIX B

ESTIMATION OF TRUNCATION ERROR IN THE ALTIMETER GEOID SPECTRUM

It is a common misconception that low frequency effects in altimeter data arise solely from correspondingly low degree geopotential terms. As equation (11) shows there is power at each frequency n from all terms $\ell \geq n$ of like parity. This power arises from the order (m) of the spherical harmonic which is always less than (or equal to) the degree. In Figure 8 it is seen that for degrees past 20 the major part of the power in the harmonics of degree ℓ radiates to frequencies (n) less than ℓ. The result is that the truncation error of geopotential solutions using altimeter data becomes more serious as the degree at truncation rises (see also Figure B1 - continued). Thus the aliasing in the high degree terms of the solution can be expected to rise proportionately. Wagner (1976) showed that all the terms above degree 16 could be expected to accumulate errors of about 0.5 m even in the bias ($n = 0$) and other very low frequency altimeter effects.

In the present study (Appendix E) I used simulations of a high degree field to confirm the interpretation of results of harmonic analysis of actual altimeter data. Since I analysed residual altimeter sea surface heights with respect to a low degree field, I began these simulations at degree 13. The 'random' fields used stopped at degree 100. An estimate of truncation effect at both ends was

necessary to compute the more-complicated (expected) power spectrum for such fields. Evaluations of equation (11) using Kaula's rule (with the geoid interpreted on the bounding sphere) are displayed in Figures B1 and B2, showing the truncation effect two ways. In Figure B1 the effect on the frequencies is given from all terms less than (or equal to) a given degree. Here the truncation effects are well discriminated for terms ℓ near the frequency n. In Figure B2 the effects are shown of all terms greater than a certain degree. When the truncation is far from the frequency the discrimination of this Figure is superior.

The rather complicated spectrum of the random field [$\sigma^2_{\ell_m}$ = normal (0, $10^{-5}/\ell^2$) for all terms $13 \leq \ell \leq 100$ derived from this truncation data, is shown in Figure C8. (It has been scaled up by $\sqrt{6}$ in this figure to compare to the spectra in the six simulated 1/6 revolution arcs.) The jagged structure for $n < 13$ is due to the lack of harmonics of degree less than 13, the (low) even frequencies suffering more because they are further from their nearest contributor ($\ell = 14$) than the odd frequencies (from $\ell = 13$).

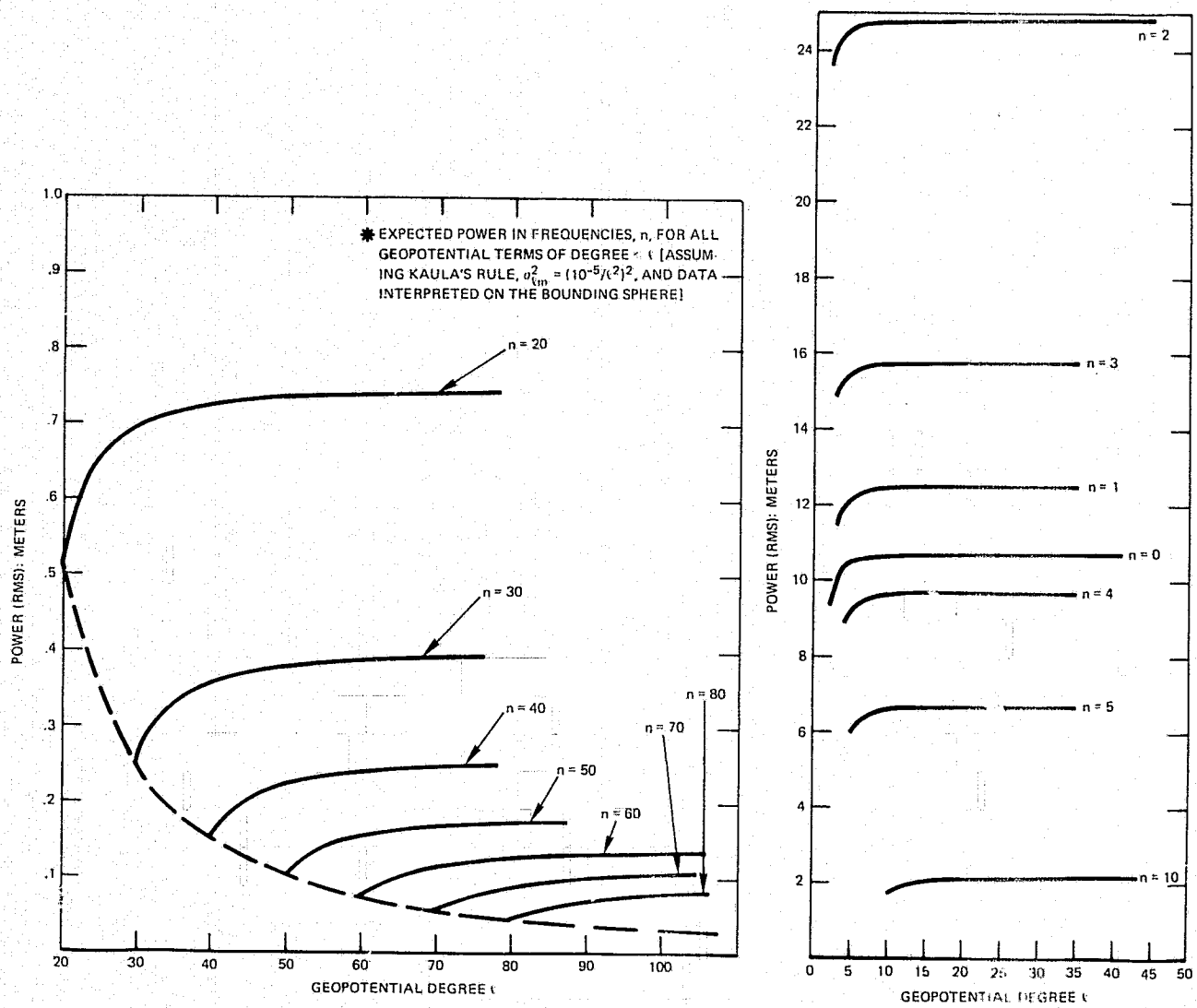

Figure B1. Accumulation Power Spectrum* of the Altimeter Geoid

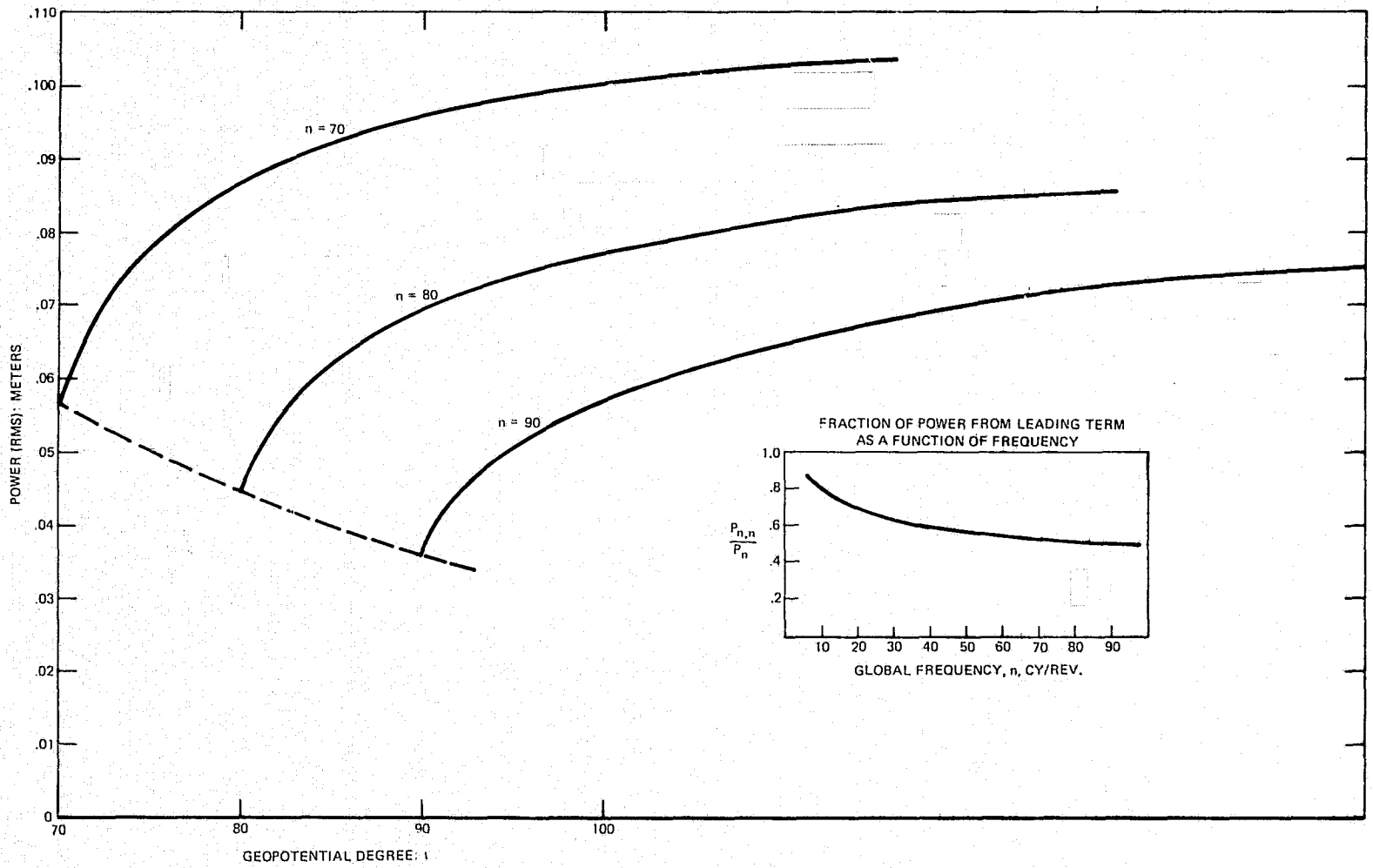

Figure B1 (Continued). Accumulation Power Spectrum* of the Altimeter Geoid

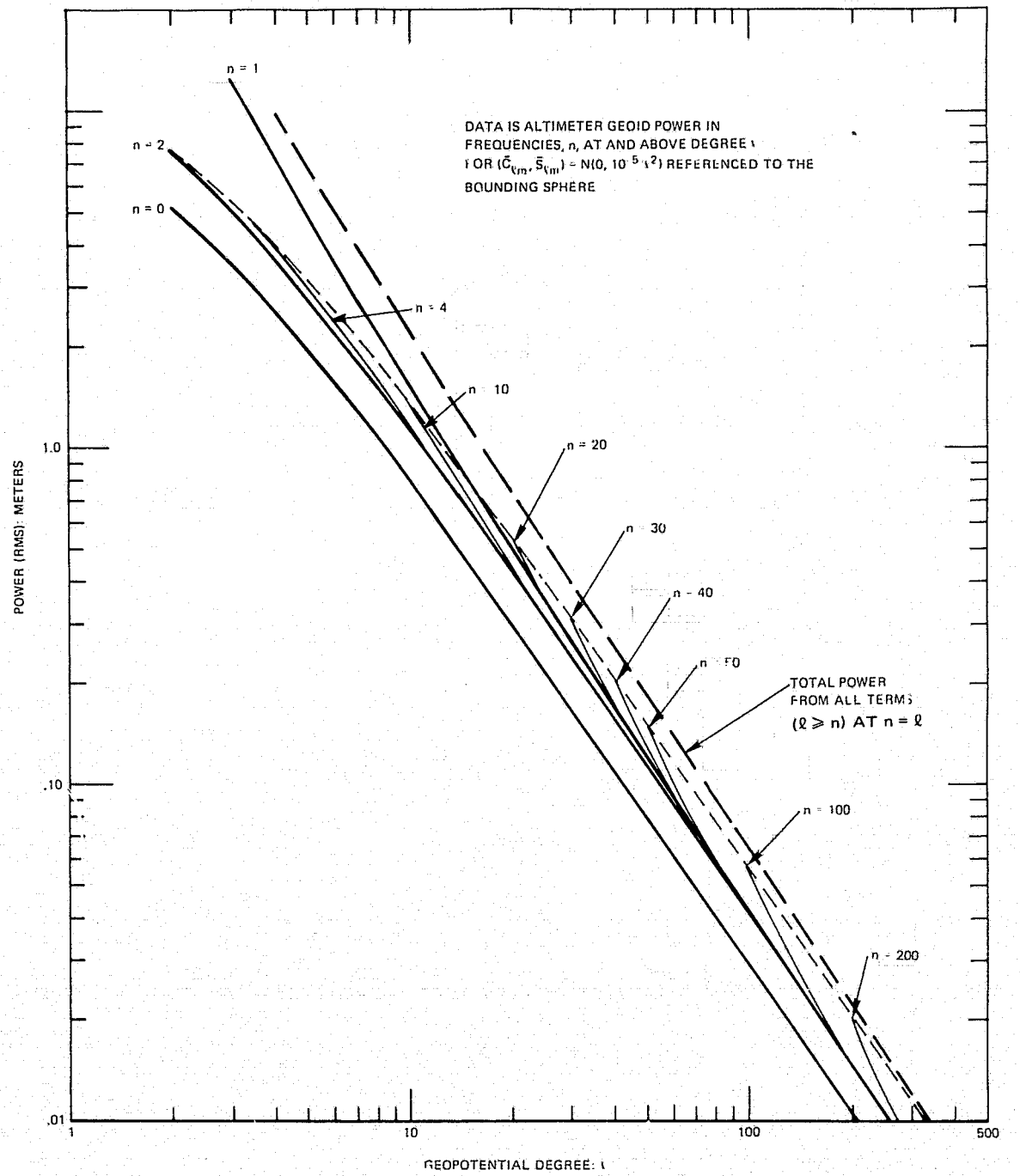

Figure B2. Altimeter Geoid Truncation Power Spectra by Geopotential Degree ℓ

APPENDIX C

ESTIMATE OF GLOBAL POWER FROM NON GLOBAL DATA

The original intention of this study was to derive the high degree ($\ell > 20$) geopotential variances from altimeter sea surface height measurements. Broadly speaking this could be accomplished if high frequency sea state departures were negligible and the data was global. Ironically the (unknown) sea state did not worry me initially (but see 'Summary and Conclusions'). The inherent non global nature of satellite altimetry was an immediate problem. Even the celebrated round-the-world Skylab altimetry pass (Figure 1) contained 'geoid' data for only 2/3 revolution due to operation breaks and over-land flight. The GEOS 3 altimetry has been even more episodic due to power limitations in the ATS-GEOS 3 link and the lack of an on-board storage device. No GEOS 3 arc has been found which is more than 1/4 rev. and very few more than 10 minutes.

In fact early simulations of truly global (1 revolution) altimetry data showed wide fluctuations of (low frequency) power from worldwide expectations. Figure C1 shows the results of harmonic analysis of 4 great circle profiles of the geoid height calculated from Goddard Earth Model 8 [Wagner et.al., 1977]. The results confirm what is known; that GEM 8 has geopotential variances generally smaller than Kaula's rule [Wagner, 1976, p. 196]. But the variability of the spectra is large, even for these global profiles. Harmonic analysis of shorter

arcs might be expected to show even greater variations. Furthermore I did not know the exact relation between the expected power in the short (non periodic) data arcs and the global ones.

It might be thought that a satisfactory solution could be found for global power in short arcs by forcing the data to fit the (known and non-orthogonal) global frequencies. However this process (e.g. using least squares estimation) introduced severe correlation between the determined power at close frequencies (even for the 2/3-complete Skylab round-the-world pass). In fact the solution was essentially singular for more than 30 global frequencies. It is true this defect might be overcome by assigning appriori constraints to the power (according to their global expectations). But this procedure can be criticized as both introducing an arbitrary amount of smoothing and prejudging the answer. On the other hand least squares estimation with appriori constraints is a well known process that provides error estimates for the power. These estimates can be viewed as showing the 'improvement' of the solution from the apriori assumption of variability. But the formation and solution of full (correlated) 'power' matrices is far more time consuming than simple harmonic analysis of the short arcs. Furthermore, as will be seen, there is justification for a simple interpretation of the short arc harmonic power in terms of global power.

Consider a periodic function h(x) defined between 0 and 2π with the natural frequencies (in cycles/rev.) given in Figure C2.

The harmonic analysis of h(x) yields:

$$h(x) = h_0 + \sum_{n=1}^{\infty} c_n \cos nx + \sum_{n=1}^{\infty} s_n \sin nx \qquad \text{(C1)}$$

The same analysis of the $1/N^{th}$ segment of the same function gives:

$$h'(x') = h'_0 + \sum_{n'=1}^{\infty} c_{n'} \cos n'x' + \sum_{n'=1}^{\infty} s_{n'} \sin n' x', \qquad \text{(C2)}$$

where $x' = Nx$ and $h(x') \equiv h(x)$, $o \leq x \leq 2\pi/N$.

What is the relation between the (c_n, s_n) and the $(c_{n'}, s_{n'})$ or their expectations? The harmonics of h(x') are:

$$(c_{n'}, s_{n'}) = \frac{1}{\pi} \int_0^{2\pi} h(x') (\cos n'x', \sin n'x') \, dx'$$

$$= \frac{N}{\pi} \int_0^{2\pi/N} h(x) (\cos n' nx, \sin n'Nx) \, dx \qquad \text{(C3)}$$

Substituting the right side of (C1) for h(x) in (C3) and integrating, the harmonics of the $1/N^{th}$ segment are:

$$\{c_{n'}, s_{n'}\} = \frac{N}{\pi} \sum_{n=1}^{\infty} \left\{ \frac{n c_n \sin 2\pi n/N}{n^2 - (n'N)^2} + \frac{n s_n (1 - \cos 2\pi n/N)}{n^2 - (n'N)^2} \right.$$

$$\left. \frac{n' N c_n (\cos 2\pi n/N - 1)}{n^2 - (n'N)^2} + \frac{n' N s_n \sin 2\pi n/N}{n^2 - (n'N)^2} \right\} \qquad \text{(C4)}$$

The constant term is:

$$h'_0 = h_0 + \frac{N}{2\pi} \sum_{n=1}^{\infty} [c_n \sin 2\pi n/N + s_n(1 - \cos 2\pi n/N)] \qquad \text{(C5)}$$

Since the (h_0, c_n, s_n) for a geoid profile arise as linear combinations of the geopotential harmonics, their expected value (over all global profiles) are zero. But their variances are not zero. Assume that the global profile harmonics (h_0, c_n, s_n) are uncorrelated with zero mean and variances $\sigma_0^2, \sigma_n^2, \sigma_n^2$. Then the expectation of the squares of the right sides of (C4) & (C5) yields:

$$E(h'_0)^2 = \sigma_0^2 + \left(\frac{N}{2\pi}\right)^2 \sum_{n=1}^{\infty} 2\sigma_n^2 (1 - \cos 2\pi n/N)$$

$$\sigma^2(P_{n'}) = E\left[\frac{1}{2}(c_{n'}^2 + s_{n'}^2)\right]$$

$$= \left(\frac{N}{\pi}\right)^2 \sum_{n=1}^{\infty} \sigma_n^2 \frac{(1 - \cos 2\pi n/N)\,[n^2 + (n'N)^2]}{[n^2 - (n'N)^2]^2}, \qquad \text{(C6)}$$

where σ_n^2 is also equal to $\sigma^2 P_n$, the variance of global power. Equation (C6) is singular when $n = n'N$. But it is easy to show from the integrals in (C3) that for this term ($n = n'N$) the right side of (C4) is simply (c_n, s_n). Thus equation (C6) is ammended:

$$\sigma^2(P_{n'}) = \sigma^2 P_{n=n'N} + \left(\frac{N}{\pi}\right)^2 \left\{ \sum_{n=1}^{\infty (n \neq n'N)} \frac{\sigma^2 P_n (1 - \cos 2\pi n/N)\,[n^2 + (n'N)^2]}{[n^2 - (n'N)^2]^2} \right\} \quad \text{(C7)}$$

I have not examined all the implications of equation (C7) but it appears to have (or at least approximate) the important normative property that

$$\sum_{n'=1}^{n'(\max) \gg 1} \sigma^2 P_{n'} = \sum_{n=1}^{N n^{\prime}(\max)} \sigma^2 P_n .$$

Referring to Figure C2, there are N times as many global harmonics (n) contributing power to any part of the segment as segmental harmonics (n'). Thus, in order that the expected total power in the segment be the same as that expected in the segment from the global harmonics, the segmental harmonics must (on average) accumulate the power of N global harmonics.

For example, in the case $n' = 6$, $N = 6$, $\sigma^2 P_n \equiv 1$ the right side of (C7) is 5.42 for $30 \leq n \leq 42$ and does approach 6.00 as $1 \leq n < \infty$. The behaviour of (C7) for various values of n' is shown in Figure C3. Note that the expected power transfer to the segment is almost independent of the segment frequency. Also note that more than 70% of the power in the N global harmonics nearest to the equivalent segment harmonic ($n' = nN$) is transferred to that equivalent harmonic.

Thus the approximate transfer function $\sigma^2 P_{n'} = 6\sigma^2 P_n$ used in the actual data reduction seems to be justified. Indeed, extensive simulations have confirmed this 'scaling' of the segment power spectra.

Figure C4 shows a typical simulation of GEOS 3 (short arc) altimeter data from a random (profile) harmonic field generated from the power law $P_n = 70n^{-1.5}$ meters (with 0.25 random noise added). Six such short (1/6 rev.) arcs were used from six different (full revolution) profiles. Results of harmonic analyses of the short arcs (with ends matching) are shown in Figure C5 (arc 5 is the data in Figure C4). Here, only the averages (rms) of 6 arc frequencies are shown (36 global frequencies) and the general agreement with the (scaled) power law is unmistakeable. At low frequencies ($n < 50$) the average is significantly greater than the point estimates while at high frequencies ($n > 250$) the noise dominates the power.

The arc power averages (from Figure C5) were reduced of their noise estimates and replotted in Figure C6. Also shown in Figure C6 are aggregate averages (means (rms) and estimated errors of the means) for all frequency groups $n > 50$. In spite of the poor noise discrimination all group spectral averages are consistently good predictors of the power law that generated the data. As a set this data represents only one revolution of altimetry.

Comparing with the low frequency results using GEM 8 (Figure C1), it appears that high frequency geoid information is much less variable from pass to pass. But the simulated data used (in Figure C6) was purely harmonic (not geoidal) and did not directly test the ability to recover geopotential variances.

Two further simulations were made to test geopotential recovery with geoidal data on a rotating earth. In both tests a random (100,100) gravity field was used whose degree variances followed Kaula's rule. In the first test 3

C-8

complete one rev. profiles were analysed simulating GEOS-3 geoidal data every 17 seconds. The results of harmonic analyses of these arcs are shown in Figure C7. Again 6 arc-frequency averages are displayed but here since the arcs are global, the discrimination of frequencies is much better. Once again as with the GEM 8 tests, the low frequency results seem weak. (In these simulations however, a rotating earth was used, which should cause more geoidal power to go into very low frequencies (see Appendix E). This particular (small) effect is not seen in Figure C7).

The overall result of this global data test is quite satisfactory. Except for a few groups the theoretical expectation is a good fit to the averages of the data in the 3 arcs. It is interesting that the truncation of the field at $\ell = 100$ is clearly seen in these results. But the arcs here are global and without noise.

A final test was made to simulate most closely the short arc situation with actual GEOS 3 altimetry. Since only residuals of altimetry were analysed, this simulation used a (random) field truncated at the low as well as the high end. Random geopotential harmonics were generated from (13, 0) through (100, 100) according to Kaula's rule. Again, six 1/6 rev. geoid height profiles were calculated (at 5 second intervals) from the field along six separate GEOS 3 orbits. A rotating earth was used and the distribution of arcs was global (within $\pm 65°$ latitude). 'Random' noise was added to each height with a $0.25^2 m^2$ variance. I matched the ends of each profile and performed a standard harmonic analysis of the departure from the matching 'trend line'. The 5 second data permitted

the solution of 100 arc frequencies for each profile which were averaged in groups of six to reduce the influence of random fluctuations of power and noise. The theoretical (expected) 'point' power for these 1/6 rev. arcs (derived from the truncated geopotential variances of Kaula's rule - see Appendix B) is shown in Figure C8. Also shown are the groups of arc averaged power which follow the expected line except beyond n = 100 cy/global rev. where there is no 'signal'. Evidently, though the noise dominated regime is dramatically clear in Figure C8, 6 arc-frequency averages are not sufficient to determine a reliable (white noise) level. The aggregate mean (rms) of the arc data in the groups (each arc mean reduced of its noise estimate) is shown in Figure C9. There, an estimate is also given of the error of the aggregate mean from the arc variation in each group (as in Figure C6). The expected power in this figure is only calculated for the group frequencies. It represents the rms power from the 'point' estimate in Figure C8 over the nearest 36 global frequencies centered on the group frequencies. Except for the poor determination of the noise power ($n > 100$) the group averages agree remarkably well with the expectation from the simplified ('frozen' earth) model.

I conclude that simple averages of harmonic power in short altimeter arcs are sufficient to reveal underlying geopotential variances (in geoidal undulation data). The data should be global in distribution but need be no more than 1 to 2 revolutions (total) to show significant discrimination of high frequency geopotential variances. Determination of data noise at very high frequencies requires

averaging over at least 10 arc frequencies. If only a few revolutions of sea surface data are available and only geoid effects are significant, the simple 'frozen earth' model of the geoidal power is sufficient to interpret sea surface power results.

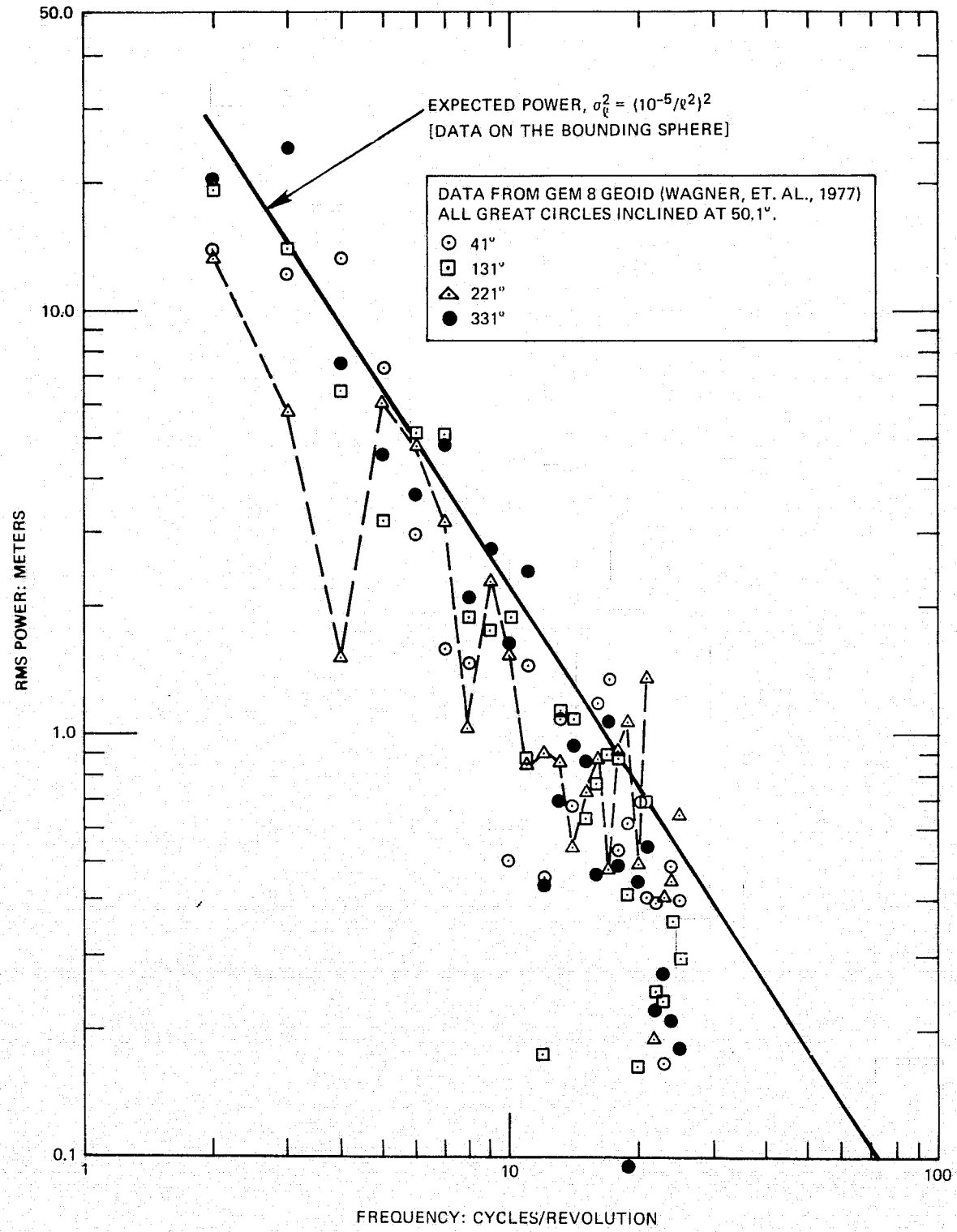

Figure C1. Power in 4 Great Circle Profiles over the GEM 8 GEOID*

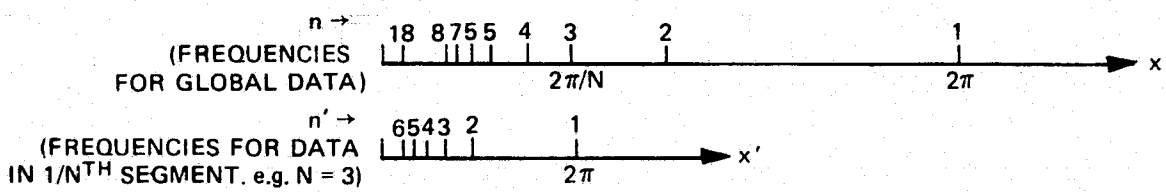

Figure C2. Harmonic Analysis of Non-Periodic Data

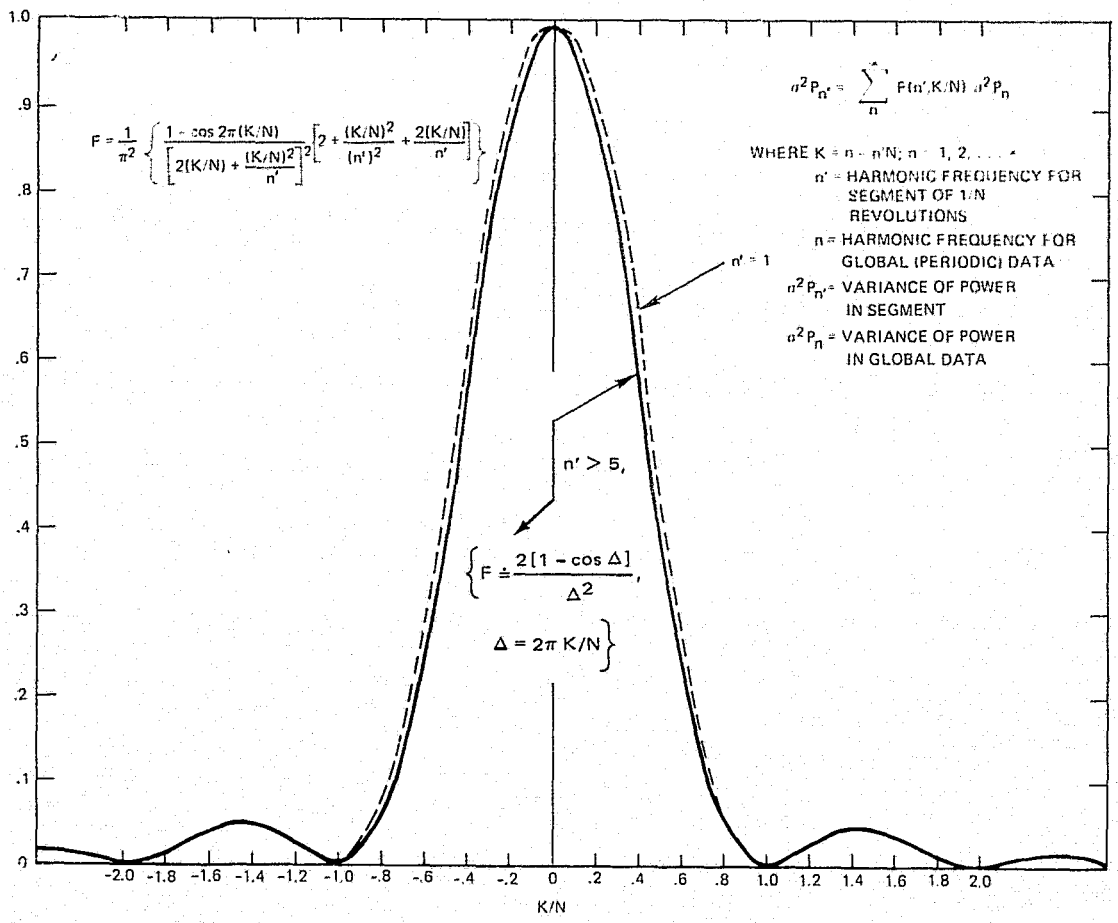

Figure C3. Power Transfer Function for Segments of Periodic Data

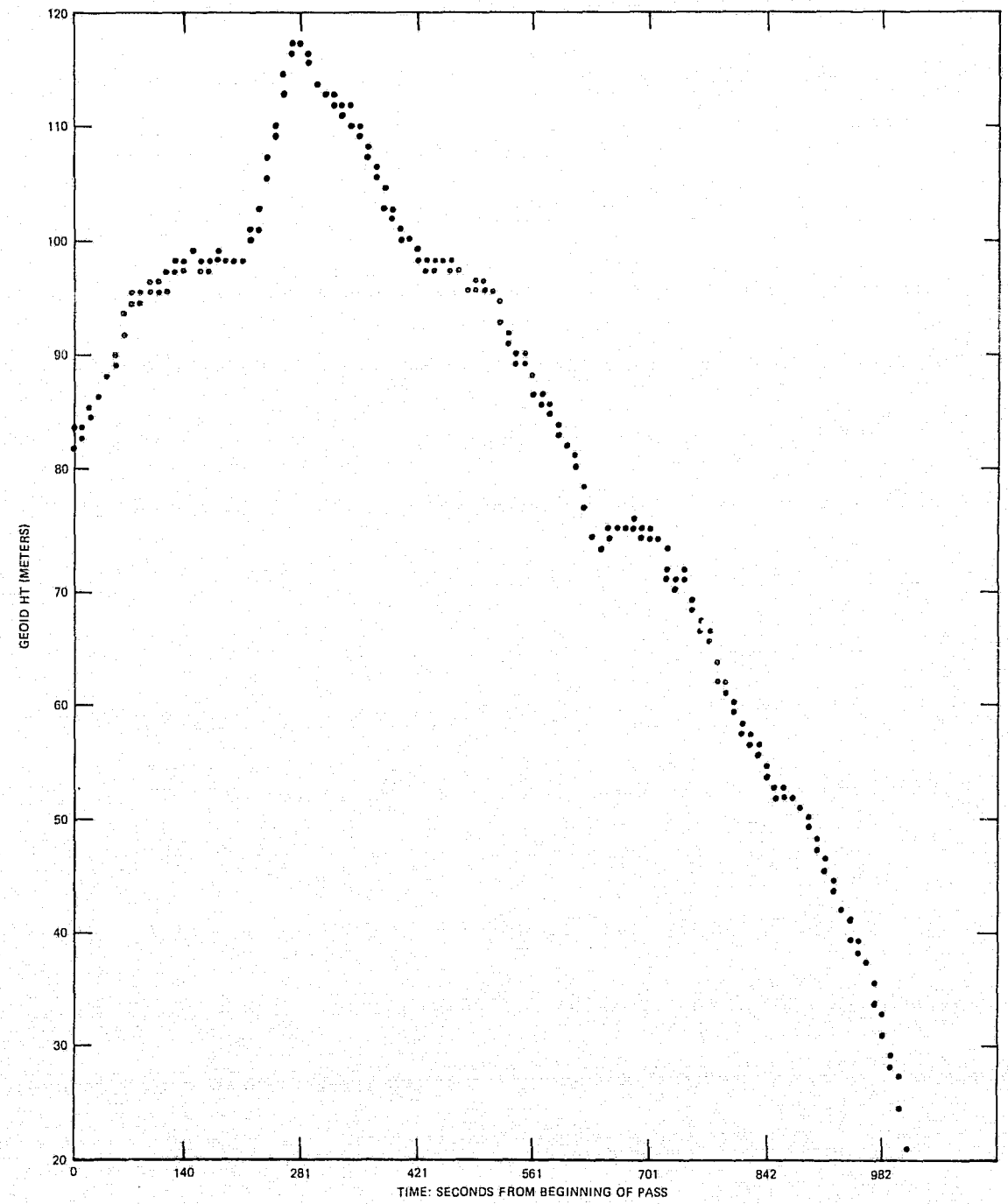

*HEIGHTS WERE GENERATED EVERY 5 SECONDS FOR A FULL GEOS 3 REV. OF 6100 SECONDS (PERIODIC DATA) FROM RANDOM HARMONICS (C_n, S_n) = NORMAL (0, P_n^2) WHERE $P_n^2 = (70n^{-1.5})^2$ m^2., $2 \leq n \leq 600$, [$P_0^2 = (10.7)^2$ m.^{2}. $P_1^2 = (12.5)^2$ m.^{2}]. NOISE WAS THEN ADDED TO EACH DATA: NOISE = NORMAL (0, 0.25^2 m.^{2}). THE ABOVE ARC REPRESENTS THE 5th, 1/6 SEGMENT OF THE GLOBAL DATA.

Figure C4. Simulated Altimetry Geoid Heights for a 1/6 Revolution Arc from a Power Law with Noise*

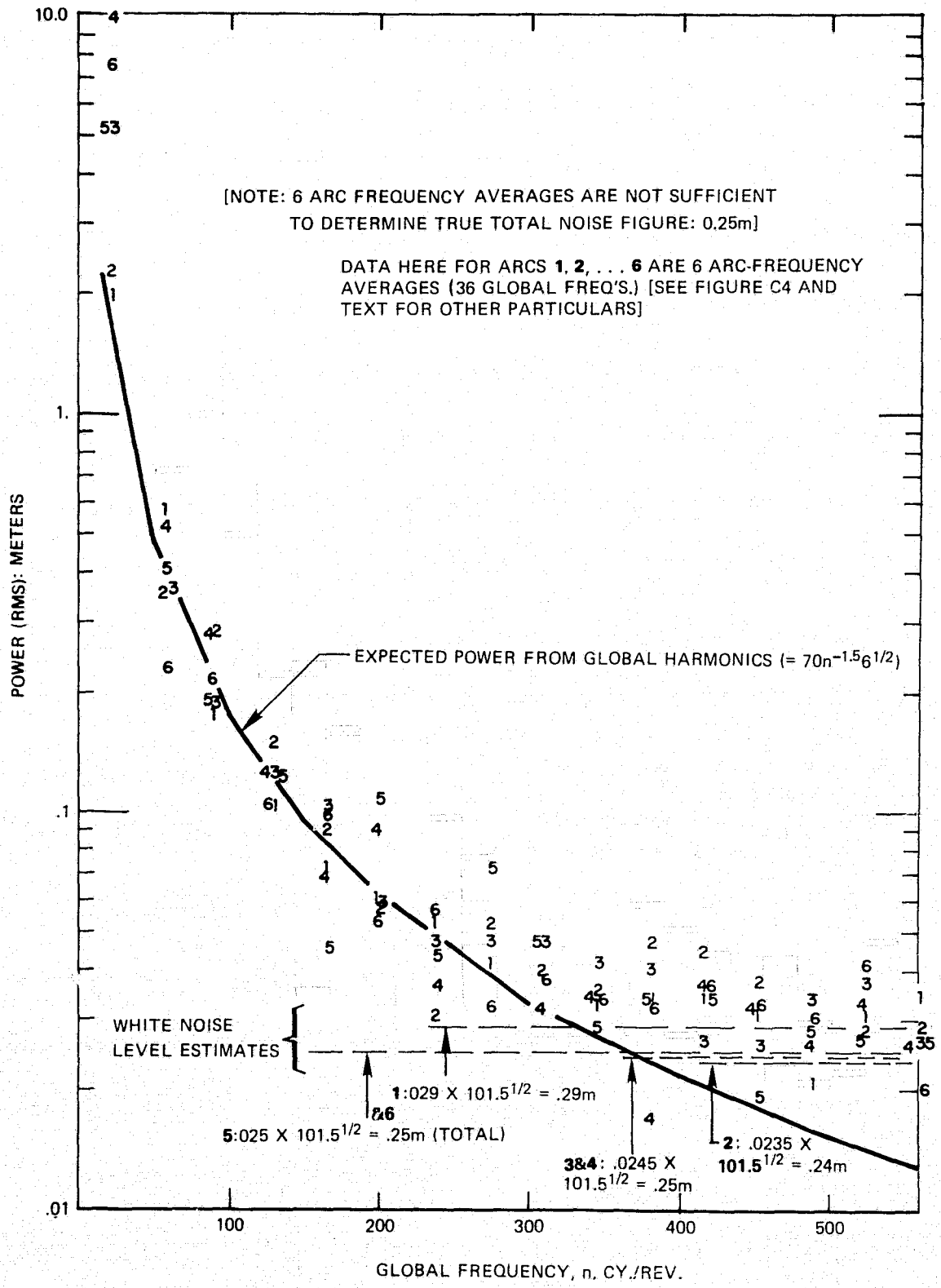

Figure C5. Harmonic Analyses of Six 1/6 Revolution Profiles of Simulated Altimeter Geoid Height Data

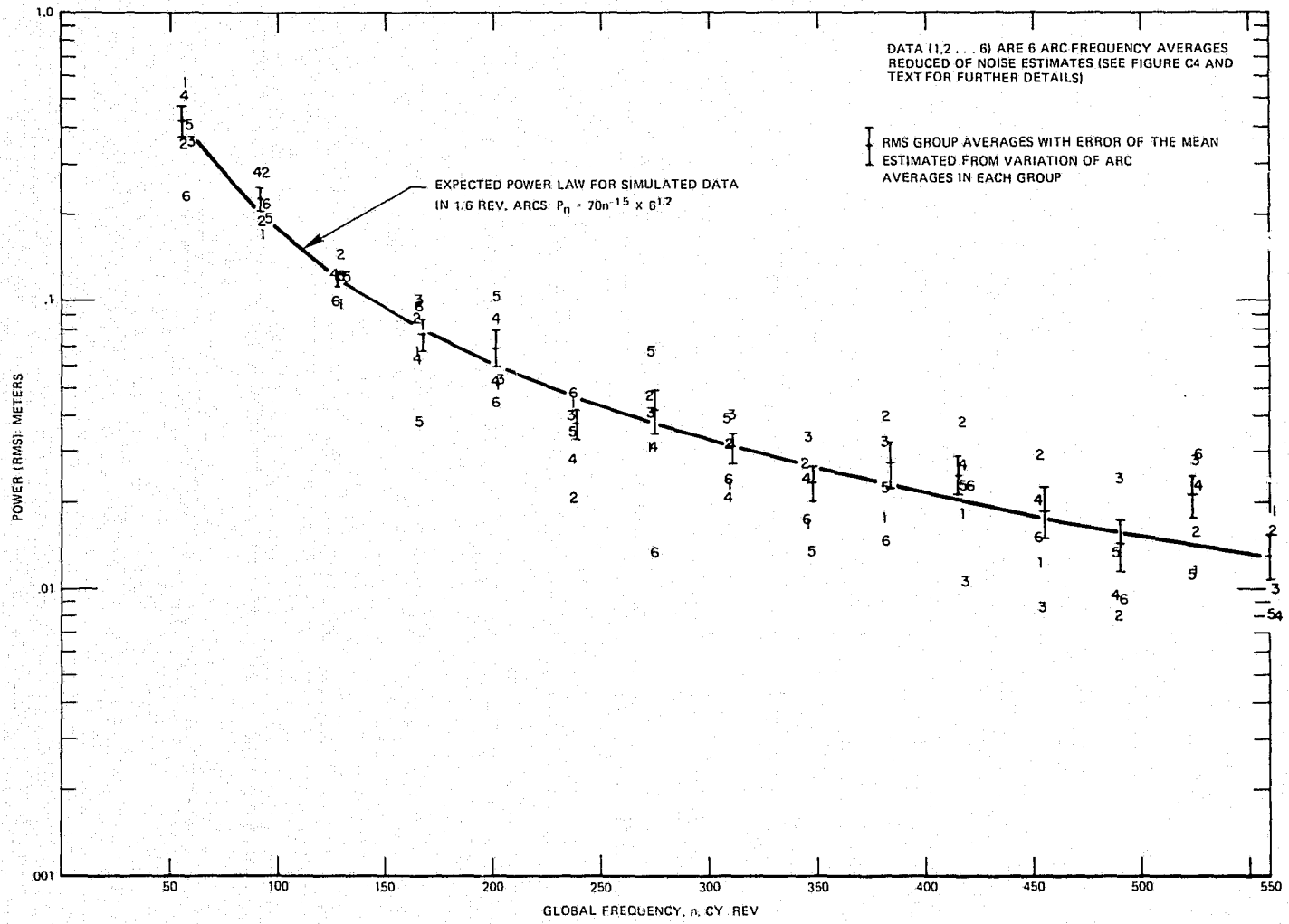

Figure C6. Power Averages from Six 1/6 Rev. Simulated Altimeter Geoid Profiles

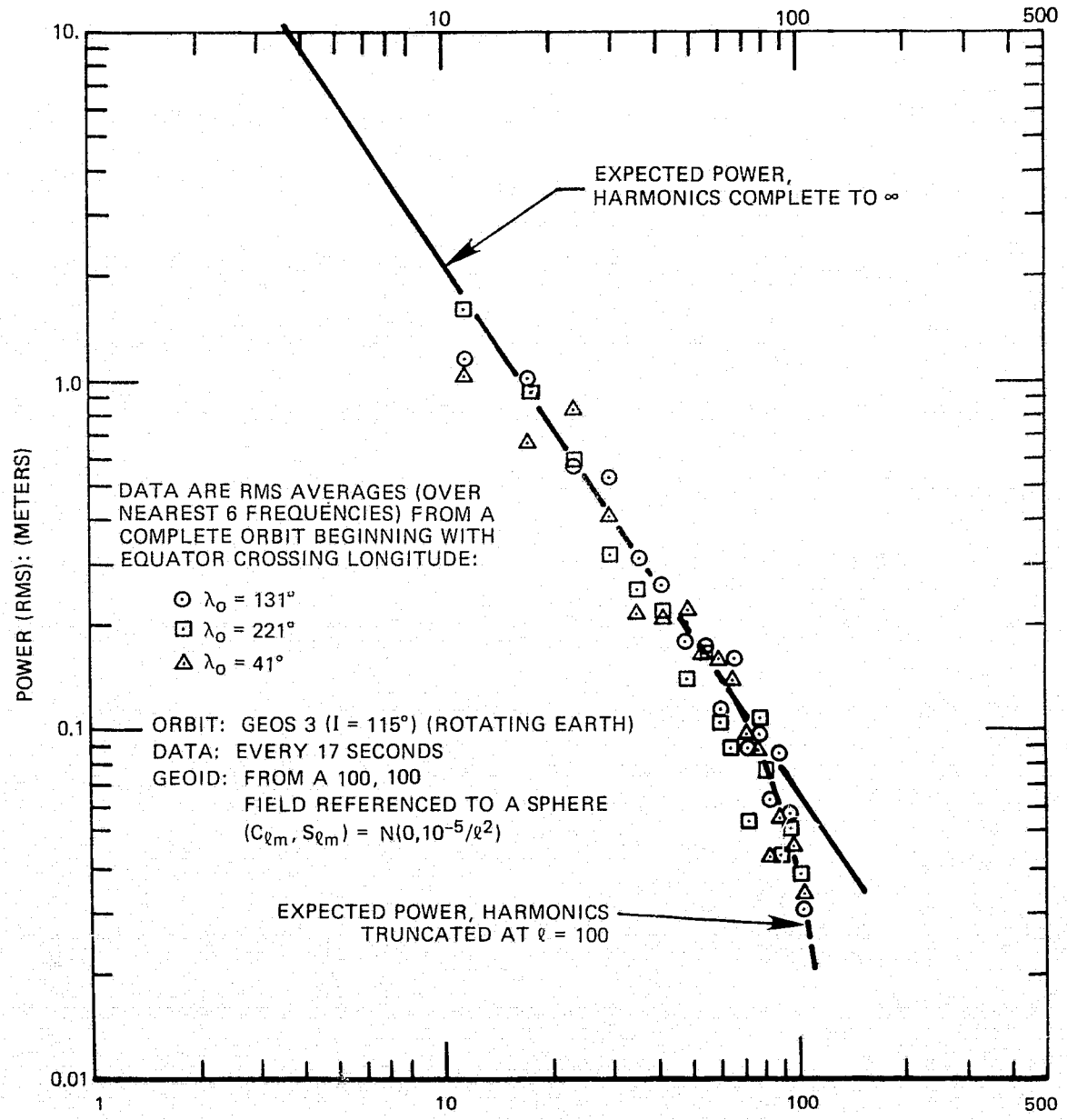

Figure C7. Power Spectra of a Simulated Geoid from Global Altimetry

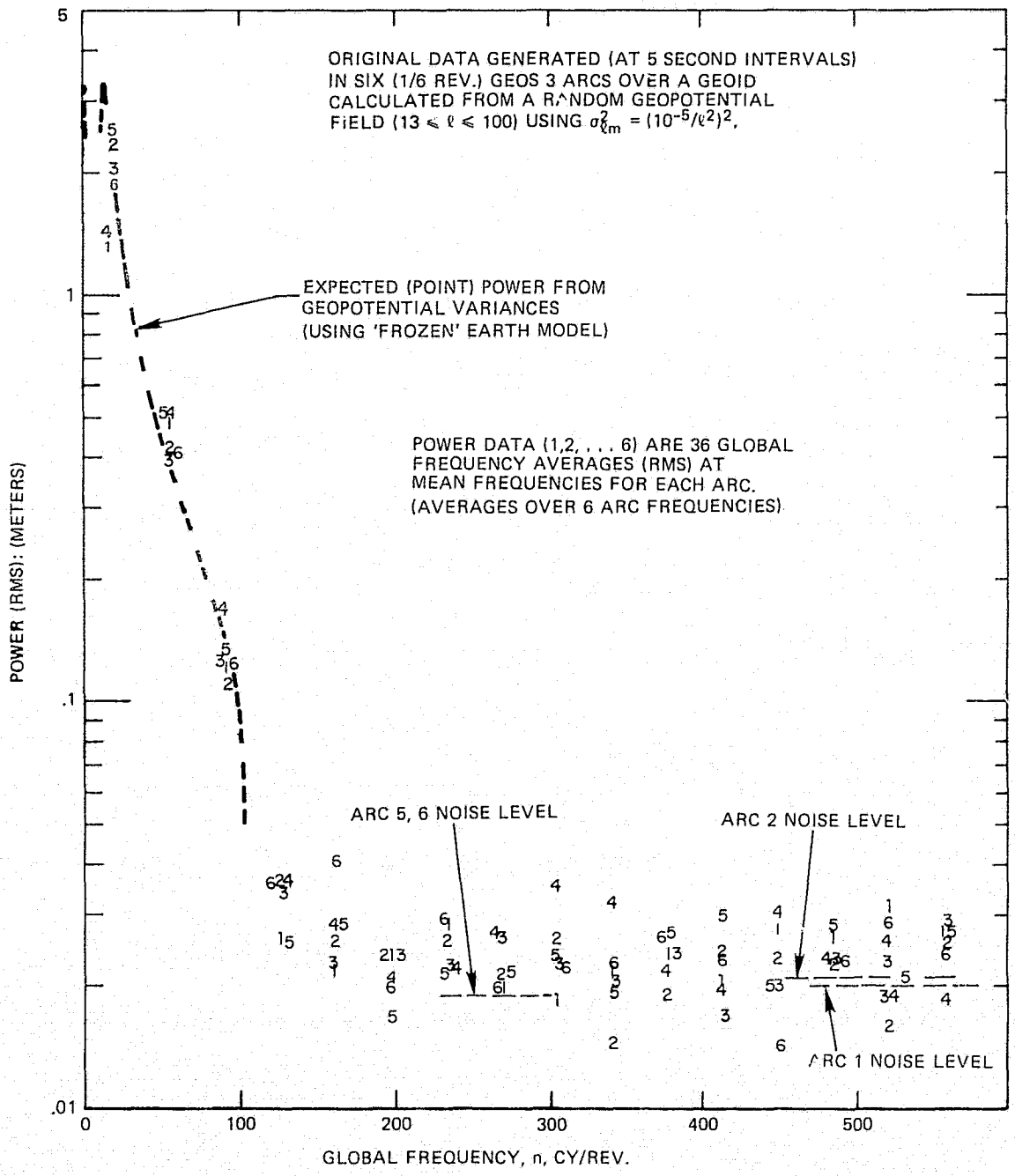

Figure C8. Power Averages and Expectations from Simulated Altimeter Geoid Residuals over a Rotating Earth

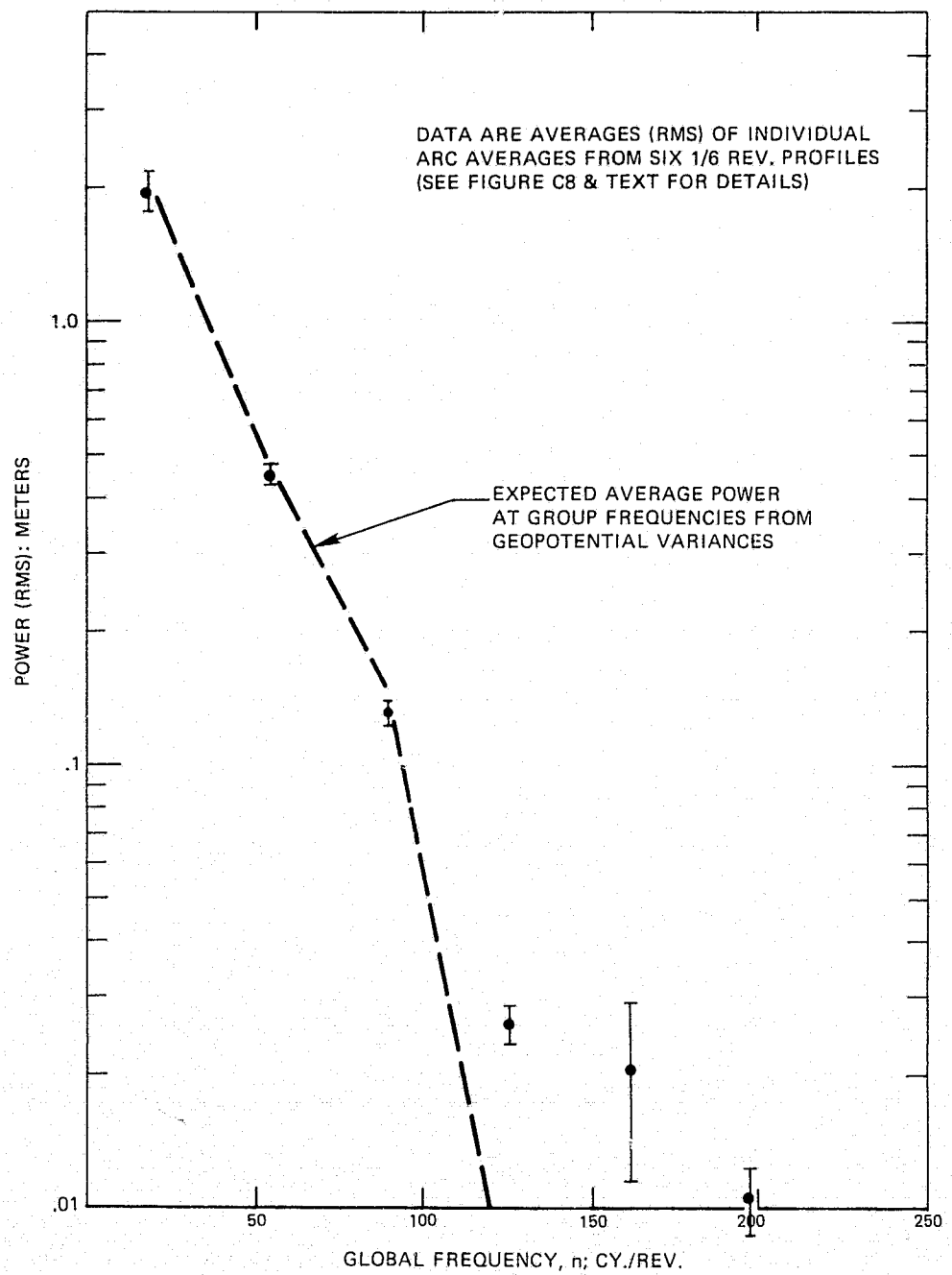

Figure C9. Aggregate Power Averages from Simulated Altimeter Geoid Residuals over a Rotating Earth

APPENDIX D

COMPARISON OF AVERAGE TO POINT POWER FOR THE ALTIMETER GEOID SPECTRUM

Harmonic analysis of short altimeter arcs provides an estimate of global geoid power over a number of frequencies. If there are N arc segments in a revolution, more than 70% of the power at arc frequency n' can be expected to absorb global power at the N global frequencies nearest to n = n'N (see Figure C3). Thus the measured arc power is actually an estimate of average global power. Furthermore, the short arc power itself fluctuates so widely (Figures 4) that it is always advantageous to consider arc averages of power over neighboring frequencies. But in any case, except for a constant power spectrum, the average power (at the mean frequency) will differ from the 'point' power at that frequency. For a declining spectrum the (rms) average (at the mean frequency) will always be greater than the corresponding 'point' power.

I estimated 'point' power from global averages by assuming the global power spectrum behaved as $P_n = 70n^{-1.5}m$. This decline is close to that predicted for Kaula's rule and somewhat faster than actually observed (Figure 6) from altimetry ($n < 220$ cy/rev.). Nevertheless it is a fair first approximation. (A second iteration (using the solution power law) was indifferent to frequencies above 60 cycles and not significantly different for lower frequencies considering the variability of the data.)

I evaluated the relation between point and average power from a simple integral approximation of the power sum:

$$\langle P^2 \rangle = \frac{1}{n_2 - n_1} \sum_{n=n_1}^{n_2} P_n^2 \doteq \frac{1}{n_2 - n_1} \int_{n_1}^{n_2} P_n^2 \, dn$$

$$= \frac{70^2}{2(n_2 - n_1)} \left(n_1^{-2} - n_2^{-2} \right) m^2 , \qquad \text{(D1)}$$

where $P_n^2 = (70n^{-1.5})^2 m^2$.

The evaluation of $[\langle P^2 \rangle]^{1/2} / P_n$ from equation (D1), where $n = (n_1 + n_2)/2$ (for various averaging intervals $n_2 - n_1$) is shown in Figure D1. Note in every case the correction is insignificant (<7%) for mean frequencies greater than twice the averaging interval.

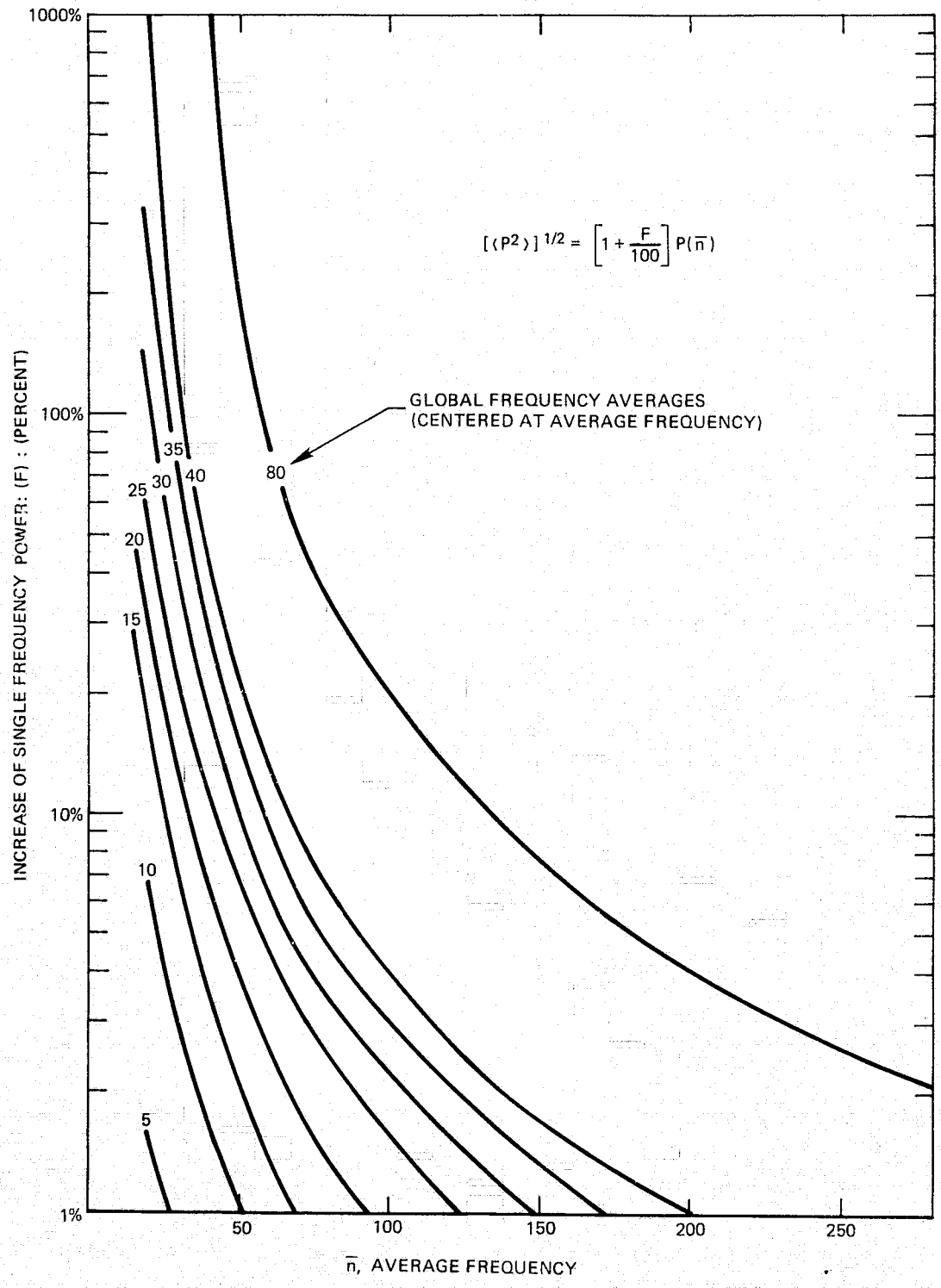

Figure D1. Increase of Power Spectrum for Multiple Frequency Averages

APPENDIX E

THE ALTIMETER GEOID SPECTRUM FOR A ROTATING EARTH

The ground track for a circular orbit satellite is only approximated by a steady progression along a great circle (the frozen earth model). The introduction of a rotating earth greatly increases the complexity of the altimeter-geoid spectrum. But the frozen earth model still provides a remarkably good description for the power averages in the more realistic situation.

Kaula (1966, p. 37) gives the frequencies for a geopotential profile along the track of a satellite as:

$$\dot{\psi} = (\ell - 2p)\,\dot{\omega} + (\ell - 2p + q)\,\dot{M} + m\,(\dot{\Omega} - \dot{\theta}), \tag{E1}$$

where ℓ and m are the degree and order of a potential harmonic, p and q are indeces for functions describing the potential in terms of the inclination and eccentricity of the orbit and $\dot{\omega}$, $\dot{M}$, $\dot{\Omega}$, $\dot{\theta}$ are the rates for the argument of perigee, mean anomaly, node and rotation of the earth. For a circular orbit, $\dot{\omega} + \dot{m}$ = constant (= $\dot{f}$ the satellites true anomaly rate). Furthermore the geopotential power in frequencies where $q \neq 0$ is insignificant. Thus (E1) becomes:

$$\dot{\psi} = \dot{f}(\ell - 2p) + m(\dot{\Omega} - \dot{\theta}), \tag{E2}$$

where, for each geopotential harmonic $0 \leq p \leq \ell$ (i.e. there are $\ell + 1$ frequencies). In the frozen earth model ($\dot{\theta} = 0$, $\dot{\Omega} = 0$) and the frequencies (for each harmonic) are reduced to:

$$n = |\ell - 2p| \text{ cycles/rev.}, \tag{E3}$$

$(\ell + 1)/2$ in number for ℓ odd and $\ell/2$ for ℓ even. Thus there are roughly twice as many frequencies in each harmonic with earth rotation. Furthermore, since the tracks are no longer great circles the frequencies of different harmonics do not coalesce at integer cycles per revolution with expected power independent of inclination. Yet there are broad classes of frequencies around which the line spectra clump. These classes are just those of the secular, short period, m-daily and resonant terms in satellite perturbation theory [e.g. Kaula, 1966 Chapter 3].

As an illustration of both the complexity and regularities of the altimeter-geoid spectrum over a rotating earth consider the case where the satellite makes almost exactly m_r integer revolutions in one day (for GEOS 3 $m_r \doteq 14$). For this resonant orbit $\dot{\psi} = 0 = \dot{f} + m_r(\dot{\Omega} - \dot{\theta})$ for all terms where $\ell - 2p = 1$. The general frequencies for this case are thus:

$$\dot{\psi} = \dot{f}\,[(\ell - 2p) - m/m_r]\,.$$

In terms of the frozen earth model's integer frequencies n, the distinct modified frequencies are:

$$n' = |(\ell - 2p) - m/m_r| \text{ cycles/rev.} \quad \text{(E4a)}$$

$$= n + (m/m_r). \quad \text{(E4B)}$$

[In equation (E4B): $n = |\ell - 2p|$].

Since a field complete through degree ℓ has exactly $\ell + 1$ frequencies n (including n = 0) this field will have $m_r\ell + m + 1$ or $\ell(m_r + 1) + 1$ frequencies n', roughly m_r times the frequencies in the frozen earth model. Actually equation (E4a) shows that of the two terms of (ℓ,m) sharing power at n one [$p = (\ell + n)/2$] shifts its power to a higher frequency $n' = n + m/m_r$ while the other [$p = (\ell - n)/2$] shifts its power to a lower frequency $n' = n - m/m_r$. [Equation (E4b) does not make this distinction]. Note for $m > m_r$ power is shifted more than one integer frequency. If the inclination functions ($F_{\ell mp}$) for large m dominate then the whole spectrum at high frequencies may be shifted by as much as n/m_r. For example in Figure E1 is shown the expected altimeter-geoid power spectrum for all 19th degree harmonics (e.g. a field of just these harmonics) on a rotating earth. The orbit inclination is 50.1° (Skylab), prograde, so that (as expected) power is transferred to lower frequencies ($m_r = 16$ in this figure). The (average) result is that about half of the (frozen earth) power (all at odd integer frequencies) is transferred to the next lowest even frequency. For the retrograde GEOS 3 orbit the shift should be towards higher frequencies. But at n = 100 the maximum shift for GEOS 3 ($m_r = 14$) is only 7 cycles/rev. affecting perhaps half the power. This error (even if systematic) is negligible considering

the current sparse data set. Only in the simulations of global (1 rev.) GEOS 3 data (Figure C7) is there a possibility that this small shift is seen in the high frequency results.

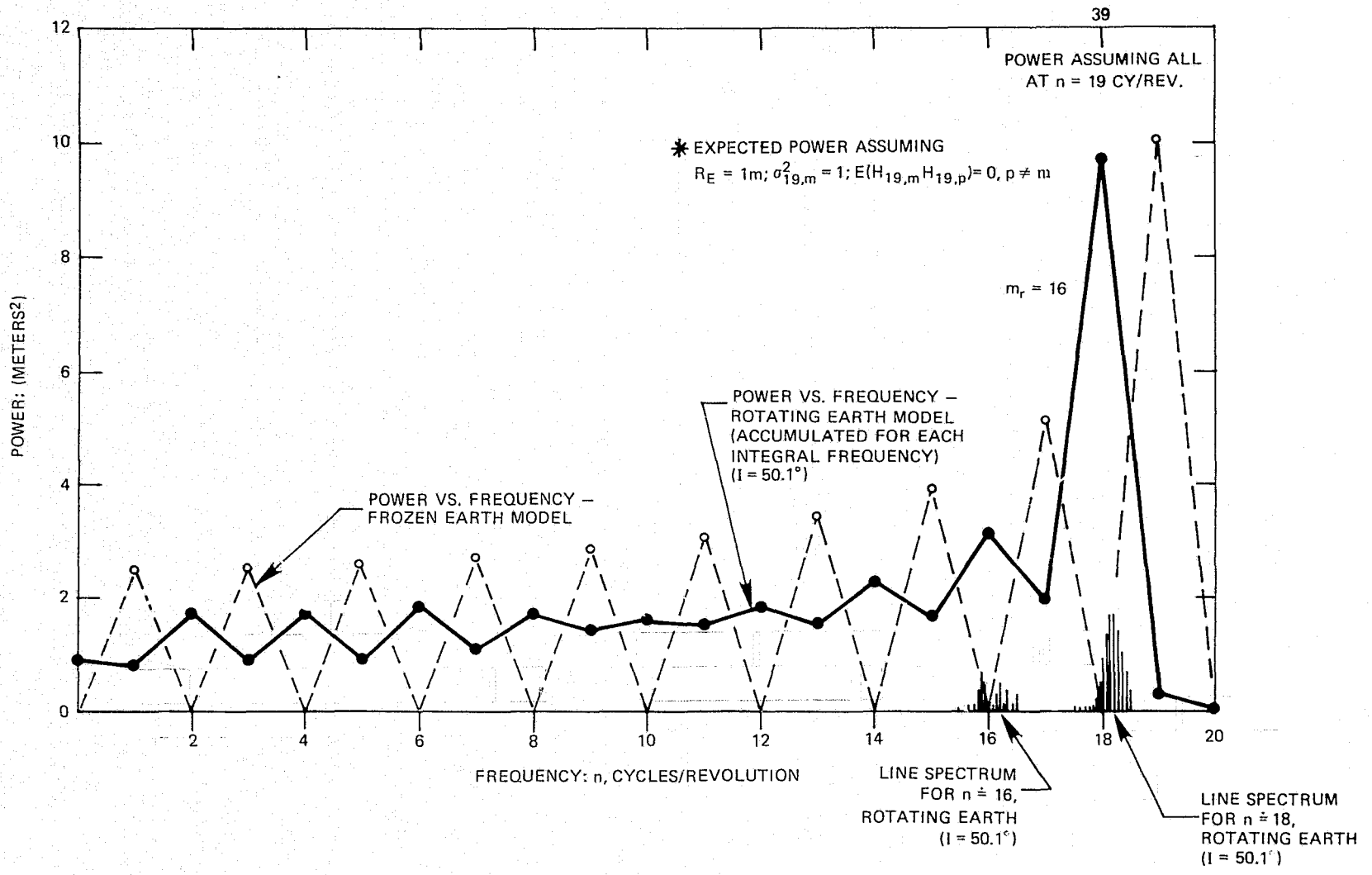

Figure E1. Altimeter Geoid-Power Spectrum for 19th Degree Harmonics*